

Toughened ternary and quaternary polymer alloys of core-shell morphology; correlations among processing, microstructure, micromechanics, and macroscopic mechanical performance in reactive systems

Majid Mehrabi Mazidi^{a,*}, Mir Karim Razavi Aghjeh^{a,**}, Alessandro Pegoretti^b

^a Faculty of Polymer Engineering, Sahand University of Technology, Sahand New Town, Tabriz, 51335-1996, Iran

^b Department of Industrial Engineering and INSTM Research Unit, University of Trento, Trento, 38123, Italy

ARTICLE INFO

Keywords:

Polymer alloy
Reactive processing
Core-shell morphology
Dispersion state
Micromechanics
Toughness

ABSTRACT

Polymer alloys are increasingly being used in engineering applications. These multicomponent polymeric systems are one of the fastest growing segments of today's plastics industry. This review examines the state-of-the-art and recent developments in the field of high performance reactively toughened ternary and quaternary polymeric alloys of encapsulated (core-shell) morphology. These alloys consist of a functionalized elastomeric polymer that functions as both dispersant and impact modifier for the resulting multiphase system. The chemical reaction of the impact modifier during melt processing gives rise to its interfacial localization and development of a core-shell structure for dispersed components. It is well-established that the dispersed composite nano/micro-domains in these blends provide a superior stiffness-toughness balance with improved processability at lower rubber contents compared with traditional toughened binary blends containing homogeneous rubbery domains. The thermodynamic and kinetic issues governing the development of an encapsulated morphology are presented. The impacts of processing conditions, microstructural (molecular, architectural, rheological, and physical) characteristics of blend components, and various blending parameters on the formation and evolution of core-shell nano/micro-morphology are reviewed thoroughly in conjunction with their subsequent influences on the macroscopic mechanical response of the blends. Special focus is on detailed discussion of the involved nano- and micro-mechanics of deformations associated with different phase structures, interphase adhesions, and dispersion states of core-shell nano/micro-structures during both high-speed impact and quasi-static fracture mechanics tests. The use of volume-strain measurements for determining the relative contribution of various dilatational and non-dilatational nano/micro-deformations accompanying the failure process during macroscopic mechanical loadings is examined profoundly. The theoretical models proposed for prediction of modulus and strength of multiphase systems comprising core-shell structured domains as well as the design criteria deduced from these models to develop high-performance materials of high impact resistance with low rigidity loss are highlighted. Finally, future research perspectives and possible directions for further progress in this field are outlined.

1. An introduction to polymer blending; opportunities and challenges

Melt blending of polymers has long been recognized as the most economic and versatile route to generate polymeric materials with targeted properties [1–4]. Utilizing this concept provides the opportunity

to improve existing properties or develop new properties to meet specific needs, reduce material's cost with little or no loss of properties, improve processability, fulfill the demands of industries by surpassing the polymerization step, and offers a means for recycling of industrial and/or municipal plastics wastes [2–6]. Historically, polymer blends, also known as polyblends or polymer alloys, were initially developed to

* Corresponding author.

** Corresponding author.

E-mail addresses: m_mehrabi@sut.ac.ir (M.M. Mazidi), karimrazavi@sut.ac.ir (M.K. Razavi Aghjeh).

<https://doi.org/10.1016/j.polymer.2023.126186>

Received 16 March 2023; Received in revised form 2 July 2023; Accepted 7 July 2023

Available online 10 July 2023

0032-3861/© 2023 Elsevier Ltd. All rights reserved.

improve the impact strength of rigid polymers [2–6]. Since then, there has been a growing need for developing newer polymeric materials having a more complete set of several desired properties including stiffness, strength, toughness, thermal and corrosion resistance, chemical resistance, fire and flame retardancy, paintability and etc. With this respect, polymer blending has played a crucial role in developing materials with such a diverse set of functional properties. In addition, the design flexibility offered by blending approach makes it very attractive to consider for producing tailored polymeric materials [3–7]. These are why the polymer blends and alloys have received much attention from both academia and industries over the past decades, and currently these multiphase polymeric systems are one of the fastest growing segments of today's plastics industry [3–6].

Owing to negligible entropy and positive enthalpy of mixing, most polymer pairs are immiscible, that is, do not mix on the molecular or segmental scale, from the thermodynamics point of view [3–7]. Majority of immiscible polymer blends are incompatible in that their blending gives materials exhibiting poor phase adhesion across the interface region and, hence, inferior mechanical properties with respect to the parent components. Nonetheless, the great proportion of commercially useful blends are immiscible, and their outstanding performance stems from their heterogeneous microstructure [3,5–7]. Unusual property synergisms can be achieved when immiscible polymers are properly blended together to form multiphase polymer systems where the discrete microparticles of minor component are dispersed in the matrix of major component.

The overall performance of the polymer blends is strongly dependent on the phase morphology of the resulting blend which, in turn, is determined by the concentration of components, their rheological properties, interfacial interactions, and the processing conditions employed for blend preparation [2,4,6,8]. Considering the polymer blending, engineering the interfacial region between the components, the development of particular phase morphology and its stabilization through accurate control of various microstructural parameters affecting the morphology for a specific end-use application remain as major challenges. Proper control of blend morphology and good adhesion between the phases are of crucial importance in order to achieve good ultimate performance, especially mechanical integrity [2,4,6,8].

2. Toughened semicrystalline-matrix blends of core-shell morphology and their importance

The technical and commercial success of high impact polystyrene (HIPS) and acrylonitrile-butadiene-styrene (ABS), which were first developed over 60 years ago, has led to a widespread and intensive programme of research on the use of rubbers as toughening agents, and there is now an impressive list of rubber-toughened polymers, including both thermoplastics (amorphous and semi-crystalline) and thermosetting resins [9–18]. This is because toughness is an important selection criterion when using a material for structural applications. In all of these materials, the aim has been to increase the fracture resistance whilst, at the same time, preserving the desirable properties of the parent polymer, notably stiffness, strength, processability, and appearance [9–15]. Nonetheless, some reductions in modulus, strength, and creep resistance are inevitable upon rubber toughening, but the overall result has been an improvement in the balance of properties [9–14]. The simultaneous use of a rigid (organic or inorganic) phase and a soft rubbery phase was then proposed as an effective method to alleviate the negative aspects associated with rubber modification. This approach has been the subject of vast research during the past decades [19–30]. In particular, the melt blending of a rigid polymeric component in combination with a soft rubbery one as modifiers for extending the properties of semicrystalline thermoplastic resins, as the base polymer, over a wider temperature range has received a great deal of attention. This is because the semicrystalline polymers benefit from good stiffness, strength, chemical resistance, and thermal stability which make them suitable for

widespread engineering applications [2,4,6,8,10–14]. Although semicrystalline polymers usually exhibit a ductile mode of failure under normal testing conditions at room temperature, at low temperatures and/or under high speed dynamic mechanical loadings and triaxial stress states, especially in thick sections and in the presence of a sharp notch, they undergo a brittle fracture [4,6,9–14]. This catastrophic deformation behavior severely limits the application of semicrystalline polymers where a high degree of toughness is required.

For most applications, in particular when special properties are in focus, mechanical properties cannot be neglected. Any specific application fails, if there is a premature mechanical deformation or failure. In fact, there are many applications, which demand good mechanical behavior or an outstanding combination of mechanical properties (e.g., stiffness, strength, and toughness) [2,4,6,8–15].

In ternary blends comprising a soft rubbery component along with a stiff polymeric phase as modifiers, the ultimate performance is controlled by the phase morphology and dispersion state of the modifier polymers in the matrix. Depending on the location of modifier components with respect to each other in the matrix of a ternary blend, different macroscopic behaviors could be expected under the external mechanical loadings. This should be taken into consideration when designing multiphase systems with acceptable performance for load bearing structural applications. Among the different phase morphologies developed during melt blending, the encapsulated one, also known as core-shell or composite-droplet morphology, in which one of the modifier components is engulfed by the other one dispersed in the matrix, has gained a great deal of attention, as this type of morphology mimics the traditional core-shell impact modifiers being frequently used as modifiers in commercial high-performance amorphous thermoplastic resins [19–30]. A core-shell morphology, which consists of a rigid core and a soft shell, rather than pure low modulus (rubbery) modifiers, has been used to impart a substantial toughening to the matrix while keeping rigidity reasonably high. The results reported in the literature indicate that the developed multiphase systems with core-shell morphology show promising balance of stiffness and toughness, and indeed some of these blend systems have already been successfully in use for engineering applications [1,2,4,6,8–16]. Similarly with the well-known rubber-toughened binary blends, the mechanical properties and macroscopic behavior of these ternary blends of core-shell morphology are strongly dependent on the size and size distribution of dispersed composite droplets, the dispersion state of core-shell domains in the matrix, interfacial interactions between core and shell as well as the shell and surrounding matrix phase, degree of encapsulation of core-forming polymer by shell forming polymer phase, shell thickness, shell strength, internal structure of core-shell domains, and the mechanical properties (stiffness, strength and impact resistance) of both core-forming and shell-forming polymers. As mentioned earlier, the phase morphology by itself is determined by the processing conditions, composition of modifier components, rheology and viscoelastic properties of modifier polymers constituting the resulting blend.

Accordingly, the present review tries to provide the state-of-the-art and an up-to-date knowledge about the progress has been made on the subject over the past five decades, with a particular emphasis on the reactive blend systems having core-shell structured morphology, that is, the development of a core-shell structure for modifier domains in the blend is controlled by the chemical reactions taking place between these minor (dispersed) components during the melt blending process. Attempt was made to discuss in-detail the role of various aforementioned microstructural parameters on the (nano- and micro) morphology, dispersion and distribution state of core-shell structures and, above all, their impact on the ultimate performance of the resultant blend with focus on the macroscopic mechanical properties, fracture toughness (energy) and failure modes, under both the high speed dynamic and quasi-static stress-fields. With this regard, special emphasis was placed on the nano- and microscopic processes (nano- and micro-mechanical deformations, activation and development of various

energy-dissipation mechanisms, crack nucleation and crack propagation resistance) responsible for the mechanical characteristics and macroscopic behavior of corresponding systems. A close processing, nano- and micro-structure (morphology), nano- and micro-deformation, macroscopic mechanical performance (behavior) correlation was established for systems under investigation. These correlations and the underlying mechanisms accounting for property improvements and high-performance characteristics are of crucial importance and can be used as criteria for further modifying the existing polymers' structures in order to produce new materials with improved or tailored properties.

Since this work deals with the toughened reactive blends with a core-shell phase morphology, the fundamental issues related to the development of such morphology are briefly discussed at first. Then, the concept of toughness and rubber toughening along with the associated underlying micromechanisms is qualitatively reviewed. After that, the subject of reactively toughened ternary and quaternary alloys of core-shell morphologies will be presented in detail in various aspects defined in the title and mentioned earlier.

3. Core-shell morphology development; thermodynamic and kinetic aspects

The first report on ternary polymer blends dates back to 1980s by Hobbs et al. [19] concerning the morphology of blends consisting of three or more polymeric components. They observed that in some ternary systems one of the minor components formed a layer around the other component but in other systems the two minor components separately dispersed in the matrix of the major component [19]. Another type of morphology, in which one of the dispersed phases was partially covered by another dispersed phase, has also been reported for ternary blends [20–30]. Thus, the most common morphologies of ternary blends can be classified as: (a) two separately dispersed phases, (b) core-shell (encapsulated) structures (or composite droplet), and (c) partial encapsulation (stack formation). These morphologies are schematically illustrated in Fig. 1.

In these multicomponent systems, the phase morphology is generally

determined by the following factors: material characteristics (interfacial tension between the components and rheological characteristics of the blend constituents), blend composition, and processing parameters (mixing time, mixing temperature and the deformation flow field). In other words, the morphology of polymer blends is controlled by both the thermodynamic and kinetic factors [19–30]. In fact, the internal structure within a composite droplet for ternary systems can exhibit different types of morphologies (Fig. 1b): “multi-core structure” or the presence of shell sub-inclusions in the core of the composite droplets [30–37]. The spreading coefficient and minimal free energy surface models have been used extensively to predict the morphology of ternary and quaternary blends through knowing the interfacial tension (α) values between the components [19–30]. Hobbs et al. [19] used the spreading coefficient concept and rewrote Harkin's equation to predict the morphology of ternary blends, in which two distinct minor phases are dispersed in a major matrix phase. In a ternary blend of three polymers A, B and C (supposing A is the matrix) the spreading coefficient, λ_{CB} , is defined as:

$$\lambda_{CB} = \alpha_{BA} - \alpha_{CA} - \alpha_{BC} \quad (1)$$

where λ_{ij} is the spreading coefficient of *i* component over *j* component and α_{ij} is the interfacial tension between *i* and *j* components. For B to be encapsulated by C, λ_{CB} must be positive. In the case when both λ_{CB} and λ_{BC} are negative, B and C will tend to form separated phases in A phase. According to the signs of the spreading coefficient, for a given matrix, different types of morphologies can be obtained (see Fig. 1). Hobbs et al. [19] tested their model successfully for several ternary and quaternary blends. In order for equation (1) to be useful in characterizing multi-phase blends, it is necessary to know the interfacial tensions for the various polymer pairs with considerable accuracy. For this purpose, the surface tension of respective polymers must be measured. To carry out the calculation, these values must be further broken down into dispersive and polar contributions. The best approximation appears to be given by the harmonic mean equation [38,39]:

$$\gamma_{ij} = \gamma_i + \gamma_j - 4 \left[\frac{\gamma_i^d \gamma_j^d}{\gamma_i^d + \gamma_j^d} + \frac{\gamma_i^p \gamma_j^p}{\gamma_i^p + \gamma_j^p} \right] \quad (2)$$

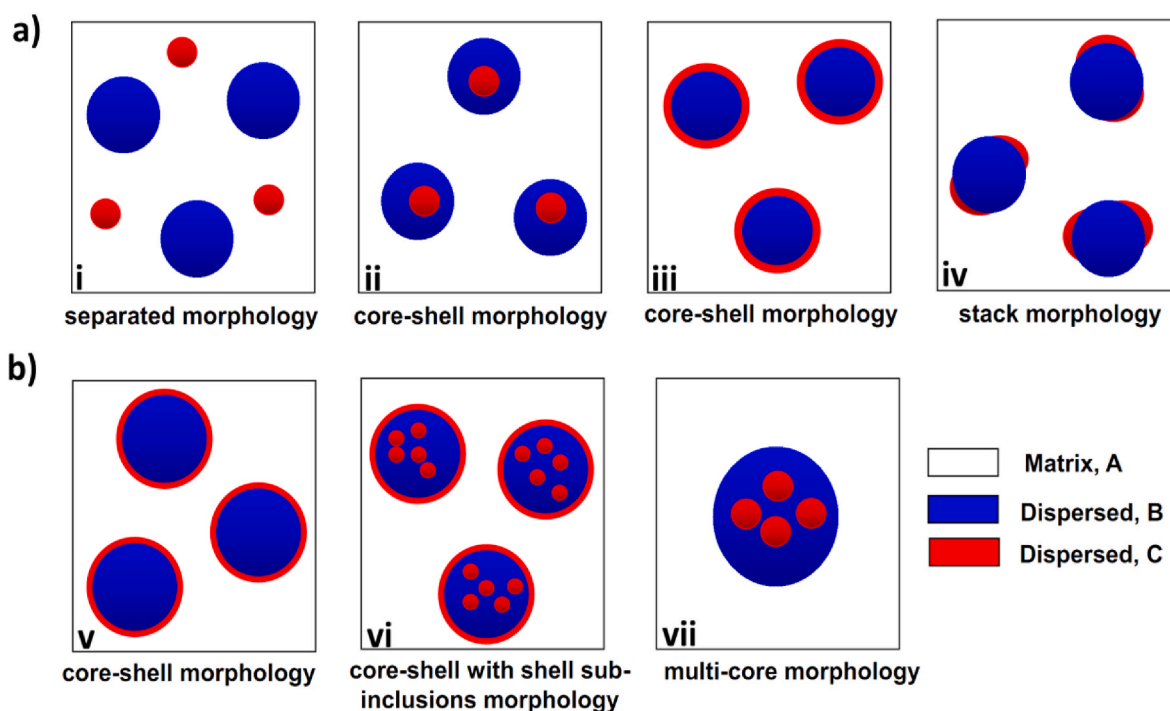


Fig. 1. (a) Typical morphologies of the ternary polymer blends, (b) potential morphologies of a composite droplet in the matrix. Considering the spreading coefficient values, for (i) $\lambda_{AB} > 0$ or $\lambda_{AC} > 0$, $\lambda_{BC} < 0$, $\lambda_{CB} < 0$; (ii) $\lambda_{BC} > 0$, $\lambda_{CB} < 0$; (iii) $\lambda_{BC} < 0$, $\lambda_{CB} > 0$; and (iv) $\lambda_{BC} < 0$, $\lambda_{CB} < 0$, $\lambda_{AB} < 0$ or $\lambda_{AC} < 0$ [19–25,30–36].

where γ^d and γ^p are the dispersive and polar terms. Since melt blending is necessarily carried out at elevated temperatures, the use of equation (1) is justified only if the interfacial tensions are determined at the processing temperature. Thus, the values determined from equation (2) must be extrapolated to a common melt temperature.

Guo et al. [26,27] developed a new phenomenological model, called the minimum free energy model. The authors derived an expression for the free energy of mixing of a multiphase blend, function of the interfacial area, and interfacial tension between each two components of the blend. The most stable morphology corresponds to the minimal free energy of mixing of the different morphologies shown in Fig. 1. For any type of morphology, the free energy of mixing can be written as:

$$G = \sum_i n_i \mu_i + \sum_{i \neq j} A_{ij} \alpha_{ij} \quad (3)$$

where μ_i is the chemical potential of i , n_i is the number of moles of i , A_{ij} is the interfacial area between components i and j and α_{ij} is the interfacial tension between components i and j . The first term of equation (3) is equal for all types of morphologies, but the second term differs from one morphology to another. Guo et al. [26,27] evaluated the second term of equation for cases (a-c) of Fig. 1 as:

$$\left(\sum A_i \sigma_{ij} \right)_{B+C} = (4\pi)^{\frac{1}{3}} \left[n_B^{\frac{1}{3}} x^{\frac{2}{3}} \sigma_{AB} + n_C^{\frac{1}{3}} \sigma_{AC} \right] (3V_C)^{\frac{2}{3}} \quad (4a)$$

$$\left(\sum A_i \sigma_{ij} \right)_{B/C} = (4\pi)^{\frac{1}{3}} \left[n_B^{\frac{1}{3}} (1+x)^{\frac{2}{3}} \sigma_{AB} + n_C^{\frac{1}{3}} \sigma_{BC} \right] (3V_C)^{\frac{2}{3}} \quad (4b)$$

$$\left(\sum A_i \sigma_{ij} \right)_{C/B} = (4\pi)^{\frac{1}{3}} \left[n_B^{\frac{1}{3}} x^{\frac{2}{3}} \sigma_{BC} + n_C^{\frac{1}{3}} (1+x)^{\frac{2}{3}} \sigma_{AC} \right] (3V_C)^{\frac{2}{3}} \quad (4c)$$

where $x = V_B/V_C$, V_i is the volume fraction of phase i , n_B and n_C are the particles numbers of B and C phases. The lowest value of $\sum A_{ij} \alpha_{ij}$ will correspond to the lowest value of Gibbs energy of mixing, which can be considered as the most stable morphology. Guo et al. [26,27] assumed that $n_B = n_C$ and calculated the interfacial energy for each phase structure in a simplified form as follows:

$$(RIE)_{B+C} = \left(\sum A_i \gamma_{ij} \right)_{B+C} / k = x^{\frac{2}{3}} \gamma_{AB} + \gamma_{AC} \quad (5a)$$

$$(RIE)_{B/C} = \left(\sum A_i \gamma_{ij} \right)_{B/C} / k = (1+x)^{\frac{2}{3}} \gamma_{AB} + \gamma_{BC} \quad (5b)$$

$$(RIE)_{C/B} = \left(\sum A_i \gamma_{ij} \right)_{C/B} / k = x^{\frac{2}{3}} \gamma_{BC} + (1+x)^{\frac{2}{3}} \gamma_{AC} \quad (5c)$$

$$k = (4\pi)^{\frac{1}{3}} n_C^{\frac{1}{3}} (3V_C)^{\frac{2}{3}}, x = \frac{V_B}{V_C}$$

where $(RIE)_{B/C}$ denotes the relative interfacial energy for the separately dispersed morphology of two minor components, $(RIE)_{B/C}$ denotes the morphology in which the B phase encapsulates C, and $(RIE)_{B/C}$ denotes the morphology in which the C phase encapsulates B.

Both the spreading coefficient and minimal free energy surface models have been used extensively to predict the morphology of ternary and quaternary blends. As mentioned above, the rheological properties of polymers can affect the resultant morphology in ternary blends [12–17]. The conclusions regarding the effect of viscosity ratio are still, however, controversial. While some authors observed that the component of lower viscosity will encapsulate the component of higher viscosity [28], some observed a contrary behavior [29], and some others did not notice any influence of viscosity ratio on the type of morphology [30,31].

Reignier et al. [31] showed that in order to study the influence of viscosity ratio on the morphology of multiphase systems, the viscosity ratio should be estimated at a constant shear stress rather than at a

constant shear rate, because the shear stress, rather than the shear rate, is continuous at the interface between the dispersed phase and the matrix phase. The authors [31] also showed the influence of elasticity on the morphology obtained in ternary blends. Following Van Oene's work [32], the authors developed a conceptual model to predict the encapsulation effects in composite droplet type systems based on a dynamic interfacial tension. Van Oene [32] demonstrated that, under conditions of dynamic flow, the elasticity differences between the components of a blend can alter the interfacial tension (called dynamic interfacial tension), and this tension can be quite different from the interfacial tension in the absence of flow. Reignier et al. [31] introduced the dynamic interfacial tension term into the minimum free energy theory by Guo et al. [26,27] replacing the static interfacial tension, obtaining the following equations:

$$\left(\sum A_i \sigma_{ij} \right)_{B+C} = 4\pi R_i^2 \left[\sigma_{BA} + \frac{R_i}{6} (N_{1,B} - N_{1,A}) \right] + 4\pi R_i^2 \left[\sigma_{CA} + \frac{R_i}{6} (N_{1,C} - N_{1,A}) \right] \quad (6a)$$

$$\left(\sum A_i \sigma_{ij} \right)_{B/C} = 4\pi R_c^2 \left[\sigma_{BA} + \frac{R_c}{6} (N_{1,B} - N_{1,A}) \right] + 4\pi R_i^2 \left[\sigma_{CB} + \frac{R_i}{6} (N_{1,C} - N_{1,B}) \right] \quad (6b)$$

$$\left(\sum A_i \sigma_{ij} \right)_{C/B} = 4\pi R_c^2 \left[\sigma_{CA} + \frac{R_c}{6} (N_{1,C} - N_{1,A}) \right] + 4\pi R_i^2 \left[\sigma_{BC} + \frac{R_i}{6} (N_{1,B} - N_{1,C}) \right] \quad (6c)$$

where N_i is the first normal stress difference for the phases A, B, and C, R_i and R_e are the internal and the external radius of the core-shell droplets, and σ_{ij} is the interfacial tension between the components i and j .

The formation of core-shell structure is usually related to the minimization of surface free energy of polymer blends [19–25]. In fact, in a typical core-shell morphology, the interfacial energies between the shell forming polymer and the other components (matrix phase and core-forming phase) are lower than the interfacial energy between the matrix and the core-forming polymer which, in turn, lead the shell-forming polymer to act as an interfacial layer between the core and the matrix phases [19–30].

The prediction and control of phase morphology in multicomponent polymeric systems are of vital importance for optimization of desired properties as there is a close interconnection between the phase morphology and ultimate characteristics, especially the macroscopic mechanical performance. The detailed discussion about the morphology development in ternary blends and the controlling factors is beyond the scope of this paper and can be found in the literature [20–37].

4. Toughened ternary blends of core-shell morphology; reactive and non-reactive processing

Most of semicrystalline and amorphous thermoplastic polymers, both commodity and engineering types, such as polyolefins, polyamides, polyesters, polycarbonates, etc. suffer from notch-sensitivity and fail in brittle manner under impact loadings, especially at low temperatures [2, 4,6,8–15]. The (binary) blends of these polymers with each other show interesting properties, making them promising candidates for structural applications. However, the resulting blends, even when they are properly compatibilized, also exhibit low resistance to crack propagation under severe (triaxial) loading and/or external conditions [2,4,6,8–15]. Consequently, there is a necessity for improving the toughness of these blends via further incorporation of a suitable impact modifier. Indeed, both compatibilization and impact modification should be taken into account when a desirable balance of the properties is to be achieved [2,

4,6,8–15]. In many cases it is preferable to select an impact modifier that, at the same time, can also function as interfacial agent between the blend components. This would reduce the number of components and complexity of the resulting blend system [2,3,6,12–15].

In the case of binary blends composed of a polar and a non-polar thermoplastic resin, functionalized species are frequently used to promote compatibilization as well as impact modification of the blend [1–6, 12–15,40–49]. These graft copolymers are usually constituted of a soft elastomer, thermoplastic elastomer, polyolefin elastomer, or a plasticizer as the main chain which is grafted (or functionalized) with a polar group such as maleic anhydride (MA), acrylic acid (AA), or glycidyl methacrylate (GMA). During the melt blending process, the polar group on the modifier usually covalently reacts with the (functional groups or linkages of) polar component of the blend whilst the main chain of modifier usually physically interacts with the macromolecular chains of non-polar component of the blend (Fig. 2). Thus, during the so called reactive processing, a graft copolymer is formed in-situ at the interfacial region between the components in the blend in the form of an interfacial layer (shell forming phase), acting as interfacial agent (compatibilizer) between the non-polar and polar phases with the subsequent effects of reducing the interfacial tension, increasing the interfacial adhesion and stabilization of phase morphology, in addition to its toughening effect [1–6,12–15,40–49]. Consequently, an encapsulated (core-shell or composite droplet) phase morphology of modifier components would develop during the fabrication process of these reactive blends. For instance, the mechanism of core-shell morphology formation resulted from imide coupling of succinic anhydride groups of the compatibilizer, introduced by MA grafting, and amine groups, e.g., amine end groups of PA6 is depicted in Fig. 2 [1–6,12–15,40–49].

Horiuchi et al. [24] studied the morphology development of ternary PA6/PC/SEBS and PA6/PC/PS immiscible blends, with PA6 as the continuous matrix phase in both blends. Maleinated SEBS (SEBS-g-MA) or maleinated PS (PS-g-MA) was incorporated with its unmodified polymer (un-SEBS and un-PS, respectively) at various ratios into the blends of PA6/PC. The blends of PA6/PC/un-SEBS and PA6/PC/un-PS (68/23/9) showed a similar phase formation in which the two dispersed polymers were stuck together in a PA6 matrix (Fig. 3). The use of the maleinated polymers instead of their unmodified polymers in the blends of PA6/PC changed the phase formation drastically [24]. The maleinated polymers reacted with amine end groups of PA6 at the interface during the melt mixing. Through this interfacial reaction, the domains of the maleinated polymers were dispersed in the PA6 matrix at about 100 nm in diameter, and at the same time the maleinated polymers encapsulated the PC domains. In fact, the interfacial reaction induced the change of the formation of the domains composed of two dispersed phases [24]. That is, the interfacial reaction changed the formation from “stack formation”, where the two dispersed polymers are stuck together, to “capsule formation”, where the PC domains are

encapsulated by the other phase (Fig. 3) [24]. Through the discussion in terms of the equation proposed by Hobbs et al. [19] and the experiments using Neumann’s concept, the driving force of this morphology development is assumed to be the reduction of the interfacial tension by the interfacial reaction between PA6 and the maleinated polymers. Moreover, when both the unmodified and its maleinated polymers are incorporated together in a variety of ratios, the encapsulation by SEBS onto the PC domains gradually becomes incomplete as the ratio of the unmodified SEBS increases, whereas the encapsulation by PS of the PC is complete even when un-PS and PS-g-MA are incorporated together (Fig. 3). This may come from the difference of degree of the reduction of interfacial tensions as a function of the interfacial reactivity that can be changed by varying the ratio of the maleinated polymer to its unmodified polymer [24].

As discussed above, in multiphase blends, other factors including melt viscosity (viscosity ratio), blend composition, processing parameters, melt elasticity, and interfacial tension at dynamic flow profoundly affect the final morphology of the resulting blend. For instance, Saeb et al. [53] studied type of morphology in ternary blends of HDPE/PA-6/EVOH using phenomenological models of spreading coefficient (SC), relative interfacial energy (RIE), and dynamic interfacial energy (DIE). Scanning electron microscopy showed core-shell type morphology, in which PA-6 cores engulfed by EVOH domains. This microstructure was successfully predicted by the SC and RIE models, whereas an unexpected dispersion of EVOH and PA-6 domains was foreseen by the DIE model [53]. Also, a quantitative study performed on morphological features to corroborate particle size alteration influenced by temperature and dispersed phase content. In particular, the contribution of elasticity ratio was determined on the size of dispersed drops, in addition to contribution of interfacial tension and viscosity ratio. It was found that the elasticity ratio of dispersed to matrix phase significantly changed by temperature and composition of dispersed phase. Therefore, the authors conclude that the elasticity contributes in particle size alteration more than interfacial tension and viscosity ratio [53]. Moini Jazani et al. [54] examined the role of viscosity ratio of core-shell forming polymers in PP/PC/SEBS/SEBS-g-MA blends by using three different PCs of different melt viscosities. Changes in blend morphology from PC/SEBS core-shell particles partially surrounded by SEBS-g-MAH to inverse SEBS/PC core-shell particles in PP matrix were observed upon reducing the viscosity ratio of PC to SEBS (Fig. 4). It was found that the viscosity ratio completely controls the size of the core-shell droplets and governs the type, population, and shape of the dispersed domains [54]. The blend containing highly viscous PC was found to have various dispersed domains with a broad size distribution. On the other hand, a finely dispersed morphology involving SEBS and PC droplets along with SEBS-PC core-shell inclusions was seen for the blend composed of the least viscous PC [54].

In the case of non-reactive ternary blends having core-shell

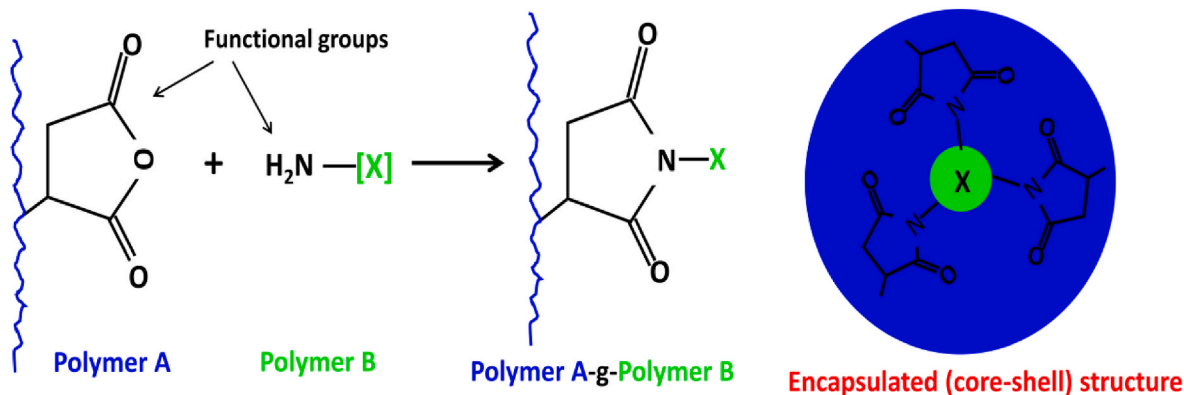


Fig. 2. Chemical reaction between the succinic anhydride group grafted on the compatibilizer (polymer A) and amine end group of a polyamide (nylon) (polymer B), and the formation of an encapsulated (core-shell) structure. (Redrawn after Ide and Hasegawa) [50–52].

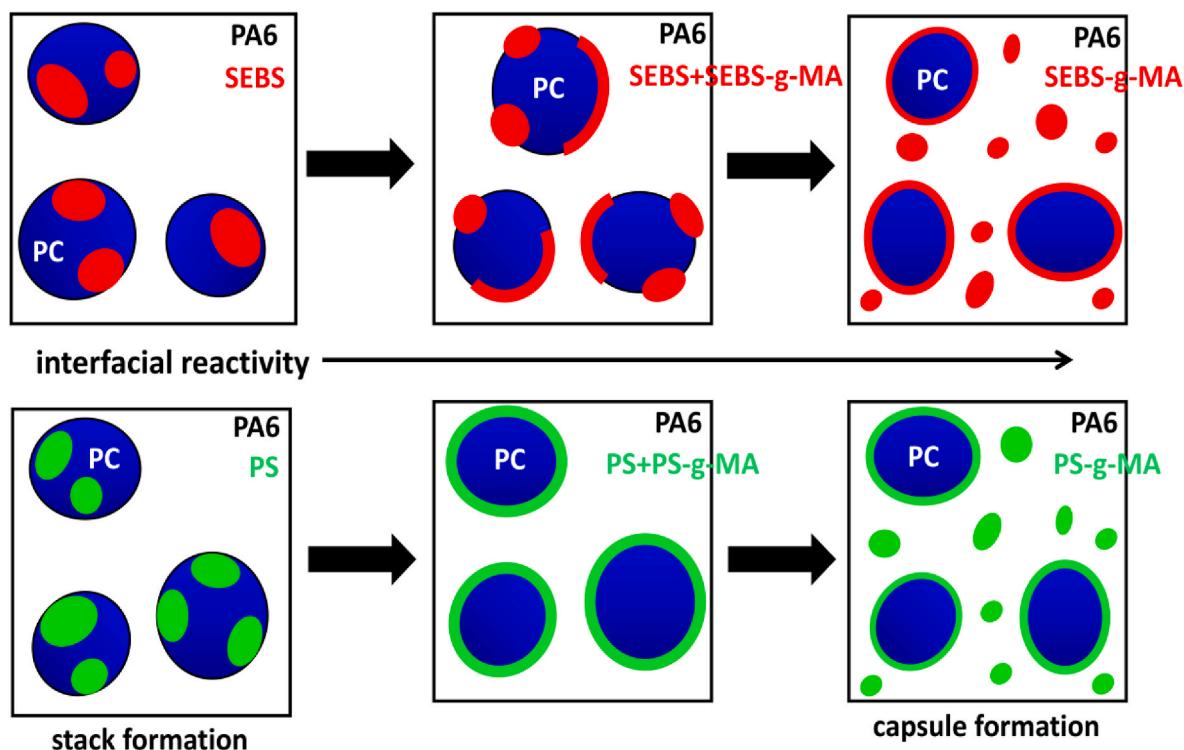


Fig. 3. Schematic illustrations to explain the morphology development by varying the ratio of the unmodified polymer to its maleinated polymer: (a) PA6/PC/SEBS blend system; (b) PA6/PC/PS blend system [24]. (reproduced from Horiuchi et al. [24], with kind permission of American Chemical Society).

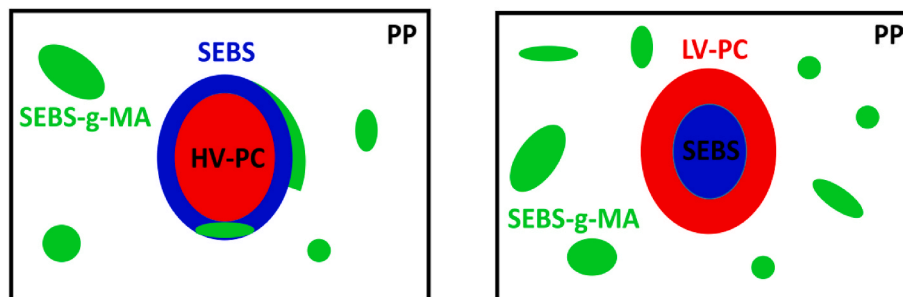


Fig. 4. schematic representation of morphology development in PP/PC/SEBS/SEBS-g-MA blend as a function viscosity ratio of PC to SEBS polymers. HV-PC and LV-PC denote to high viscosity and low viscosity PCs, respectively. (reproduced from Moini Jazani et al. [54], with kind permission of Springer).

morphology, discussed in the next part of this work, the formation of composite dispersed structures is primarily controlled by the interfacial energy gradients as well as physical macromolecular interactions between the blend's components. These investigations are reviewed in literature [24–33] and are not in line with the scope of the present work.

Therefore, in the vast majority of the toughened semicrystalline-matrix ternary blends (both reactive and non-reactive systems) reported in the literature, and discussed in this review and the next part of this work, a soft elastomeric phase usually constitutes the shell-forming polymer, while the core polymer is usually a thermoplastic in character, with much higher stiffness than the shell polymer.

5. The importance of nano- and micro-mechanical processes operating in multiphase blends

The steady improvement of properties in general and better matching of specific properties to more demanding applications are continuous goals of polymer research. Desirable mechanical properties are essential for nearly all applications of polymers in daily life [2,4,8,9,12–14]. The improvement of the mechanical properties necessitates a

better understanding of the multiple dependency of molecular structure, morphology and processing conditions, on ultimate mechanical properties, that is, good knowledge of processing-structure-property correlations [4,6,8,10–14,55,56]. The bridge between microstructure (morphology) and the macroscopic mechanical properties is the micro-mechanical processes or mechanisms occurring during loading at nanoscopic and microscopic levels: the so-called field of nano- and micro-mechanics [56]. The knowledge of these mechanisms is a key for successful development of new materials and further improvement in the properties of already in use polymers.

Electron microscopy investigations can provide important information about the different structural details contributing to the durability and mechanical response of the blend systems [1,4,6,8,55,56]. Of particular interest is the study of micromechanical processes of deformation and fracture. Corresponding to the different structural details in polymers, there is a great variety of micromechanical processes possible in a polymeric material under load [2,4,8,10,55,56]. They include changes of individual macromolecular segments (on nm scale) up to macroscopic fracture (on μm and mm scales). Thus, numerous techniques are necessary for studying these processes, with those revealing

information on the morphology as well as on micromechanical processes are particularly advantageous, since they make it possible to readily establish a structure-property correlation in polymers and their combinations [56–60].

In the case of toughened binary blend systems the involved nano- and micro-mechanical deformation processes operating in the corresponding systems have been well explored and currently there is an in-depth knowledge about the underlying mechanisms responsible for the property improvements [9–15,55–58]. Obviously, the current knowledge on the role of modifier domains in these binary blends would pave the way for gaining more insight into the role of individual components in activation of various microscopic deformation processes in toughened ternary and quaternary systems. Admittedly, this information could provide a basis for further tailoring the microstructure and, thereby, to alter the microscopic deformations in order to fine tune the specific macroscopic mechanical behavior in demand. Accordingly, the following sections will provide some basic and fundamental information concerning the toughness and rubber toughening, and the underlying micromechanisms operative in the rubber-toughened binary blends as well as their role in the initiation and development of various energy absorption and dissipation processes. More detailed information on the rubber toughening and toughened binary blends can be found in the excellent textbooks and reported monographs [9–15,55–58].

6. Toughness and rubber-toughening

Toughness is a measure of energy absorption and dissipation during loading [10,12,15,56,57,61,62]. Toughness is among the most complicated mechanical properties, which is actually difficult to control as it is greatly influenced not only by many morphological and microstructural parameters but also by external variables [10,12,15,57]. Many plastics are susceptible to brittle fracture [57,61], because the energy absorbing processes, such as crazing or shear yielding mechanisms, operating in these polymers are highly localized and confined to a very small volume of material (mostly around the crack tip) even though these mechanisms involve large plastic strains and considerable local energy absorption by the material [10,57]. As a result, the total amount of plastic energy absorbed and dissipated by the material under loading is low. In order to increase the toughness of thermoplastic resins, the various energy dissipating mechanisms have to be activated over a sufficiently large volume of material and, on the other hand, their propagation and growth must be controlled to prevent crack nucleation and premature crack propagation [10,12,15,57]. The most efficient approach is to initiate localized energy absorbing mechanisms but from many sites, rather than a few isolated ones, so that a much greater volume of the polymer is involved. This multiple-deformation mechanism has been most successfully achieved by the incorporation of a second rubbery phase in the form of dispersed particles in the matrix polymer [10,12,15,56,57]. The resulting material has a significantly higher fracture resistance than the parent polymer: impact strength, elongation at break, work to break and fracture toughness (energy) are all increased several-fold. There is an inevitable reduction in modulus, strength, and creep resistance; transparency is usually lost and melt viscosity is increased, but these losses are far outweighed by the gains in fracture resistance. The rubber-toughened polymer has a better balance of properties than the parent polymer, and is therefore a commercially successful product despite its higher price [10,12,15,56,57].

The fracture process of the toughened polymer is markedly postponed and the crack propagation resistance is substantially enhanced as a result of extensive plastic deformation, usually with the same mechanism as the pristine parent polymer, prior to failure. This transition from brittle to ductile response results from the reduction of the overall plastic resistance of the matrix material below the brittle fracture strength upon the modification process [10,12,15,57,61,62]. Optimum particle size to achieve a satisfactory toughness for a rigid thermoplastic resin depends primarily on the inherent fracture mechanism of the host

polymer (matrix), but is commonly within the range of 0.1–5 μm [10,12,15,57]. As a general rule, brittle glassy matrices that tend to craze benefit more from large rubber particles, typically between 2 and 5 μm . On the other hand, matrices that can absorb energy via plastic drawing and shear yielding have been effectively toughened with relatively smaller particles, with the diameter of 0.3–0.5 μm or less [10,12,15,57]. Very fine particles, as, e.g., those smaller than 0.05 μm may not take part in toughening process since they need higher stress to cavitate [62–65]. The immiscibility and phase segregation are very important for effective toughening as a rubber dissolving in the matrix acts merely as a plasticizer, reducing the glass transition temperature and thereby severely affects the stiffness with only limited improvement of toughness. The well-dispersed elastomer with a suitable particle size makes it possible a large volume of the matrix to participate in the process of plastic deformation, leading to a considerable amount of energy absorption and/or dissipation [10,15,57,61,62].

A number of quite different mechanisms of such toughening have been proposed in the past, all of which relied on a dispersion of elastomer particles within a glassy or semicrystalline matrix, including energy absorption directly by rubber particles [66,67], energy dissipation upon rubber cavitation, or debonding at rubber-matrix interface [68–70], matrix crazing [69–73] or shear yielding [74] or a combination of both [69–73]. The early hypothesis attributed toughness enhancement to dissipation of energy in the elastomeric phase either directly or by the effect of bridging cracks by rubber particles [66,67]. The amount of energy absorbed on impact was attributed to the sum of the energy to fracture the rigid matrix and the work to break the elastomeric particles encountered on the crack path. This hypothesis was dismissed soon since it was estimated that the total energy associated with the rubber deformation and break can account for only a small fraction of the observed enhanced impact energy [75]. Consequently, this mechanism can play only a minor role in toughening of rigid polymers. Rubber toughening is a well-established concept and considered as the most effective method for improving the fracture toughness of thermoplastic polymers, composites, nanocomposites, adhesives, paints as well as the thermosetting resins [76,77]. Recently Wang et al. [77] has reviewed the use of rubber toughening method in a wide variety of plastic resins.

Here, the main energy dissipating mechanisms responsible for enhanced crack resistance of rubber-toughened binary blends will be reviewed briefly at first, as these micro-mechanical processes will form a basis for better understanding of descriptions on various microscopic deformations and toughening micro-mechanisms involved in the multiphase blends with core-shell morphologies discussed in the subsequent sections.

7. A qualitative overview on toughening mechanisms in rubber-toughened binary blends

7.1. Multiple crazing

Crazes are crack-like sharply localized bands of plastically deformed material, initiated at points of high stress concentrations such as surface scratches, flaws, cracks, dust particles, or other heterogeneities [10,12,15,57]. Crazes are usually formed in planes normal to the direction of maximum (tensile) principal stress and consisted of highly oriented polymer fibrils of approximately 5–15 nm in diameter, stretched out in the direction of loading, and separated by elongated nanovoids [10,12,15]. In contrast to a crack, a craze is capable of transferring an applied load. Crazes are, however, frequently the precursors of brittle fracture since during the applied stress the most elongated fibrils inside the craze will break as the craze gradually grows in length and width. As a result of this fibrillar breakdown, microcracks are usually nucleated in the center of craze [10,55–57]. Crazing requires the presence of dilatational component of stress tensor and may be inhibited by hydrostatic pressure. On the other hand, it is generally promoted by the presence of a triaxial tensile stress [9,10,57]. Such a stress state develops ahead of

large flaws or notches in relatively thick specimens (plane-strain conditions). Thus, the presence of sharp cracks, notches, or defects in thick specimens is favorable to craze initiation, susceptible to brittle fracture.

In the late 1960s Schmitt [78] and Kesskulla [79,80] proposed that the rubber particles can not only deflect or terminate cracks but can also act as stress concentrators, which efficiently initiate crazes in their very surroundings. The role of rubber particles as stress concentrators, able to initiate extensive crazing, turned out crucial for toughening of the matrix. Bucknall proposed the mechanism of toughening by the so-called multiple crazing [9,10,75], which became the basis of many toughening approaches developed later (Fig. 5).

It has been established and widely accepted that the deformation process involving crazing is initiated at the surface of numerous elastomer particles, simultaneously in many sites of the matrix [9,10,75,81]. Bucknall and co-workers [9,10,69,75] have proposed that the rubber particles have two separate but equally important functions. Firstly, under an applied tensile stress, crazes are initiated at points of maximum triaxial stress concentrations, which are usually near the equators of the rubber particles. The crazes then grow approximately normal to the maximum applied stress, although deviations may occur because of interactions between the particles' stress fields. Secondly, the rubber particles are craze terminators, preventing the growth of very large

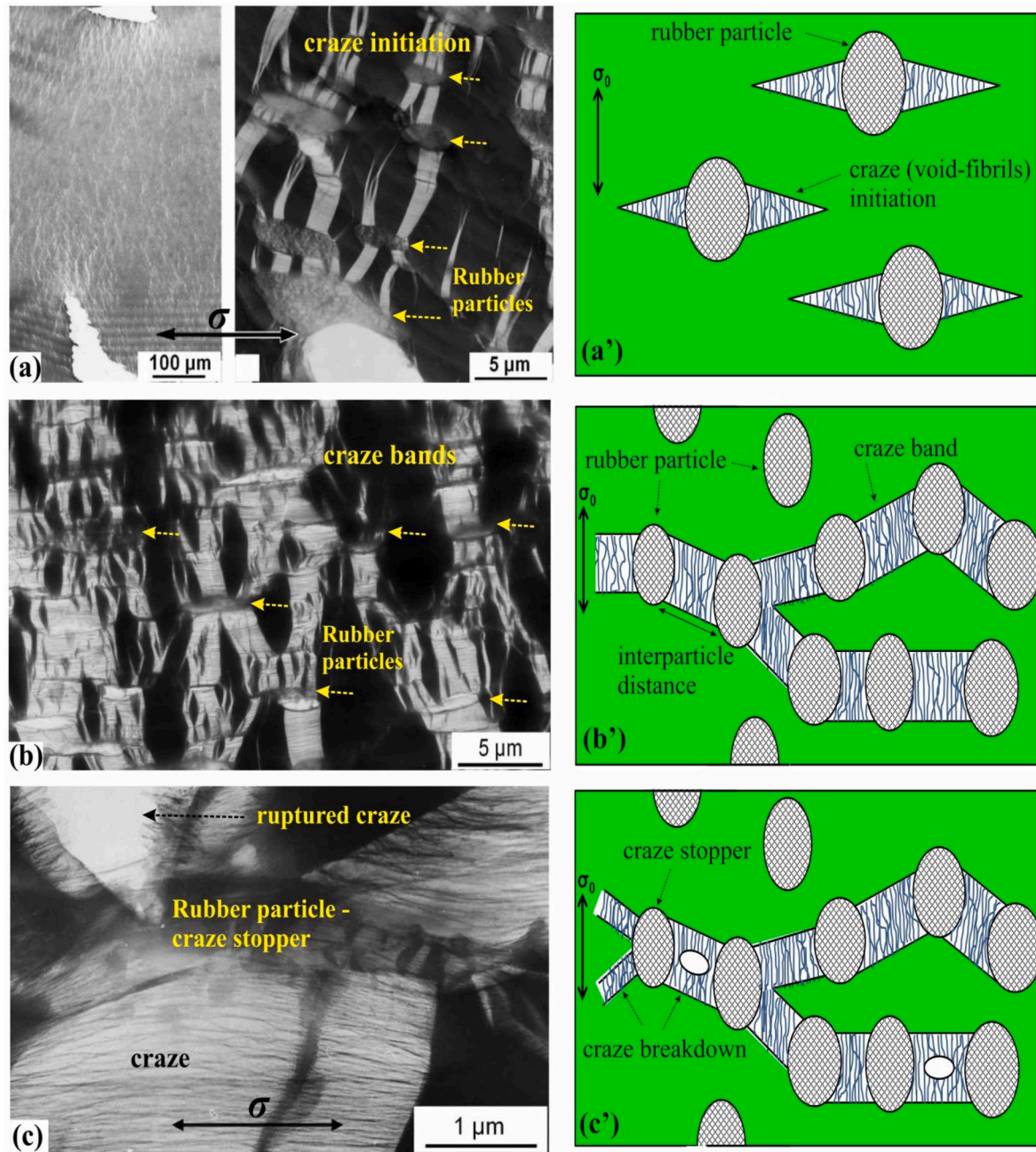


Fig. 5. (left column) TEM micrographs showing (multiple) crazing process in HIPS at different magnifications. (a) overview of deformation area; area in front of a crack tip with rubber particles (grey) in a matrix (black) with crazes (bright); (b) broad crazes and craze bands between rubber particles; and (c) ruptured craze with crack stop in a rubber particle (deformation direction horizontal). (reproduced from Michler, with kind permission of Springer-Verlag Berlin Heidelberg) [55,56]. (right column) Schematic representation showing three-stage mechanism of multiple crazing: (a') stress concentration and craze initiation at rubber particles; (b') superposition of stress fields (small interparticle distance, high rubber volume content) and formation of broad craze bands; and (c') limitation of crack length and stopping at rubber particles. (Redrawn after Michler, with kind permission of Springer-Verlag Berlin Heidelberg) [55,56].

crazes (Fig. 5). Poor termination means that large crazes are produced which could act as sites for premature crack initiation and growth. Thus, the result is that a large number of small crazes are generated in the toughened polymer, in contrast with the small number of large crazes formed in the same polymer in the absence of rubber particles [10,12,15,57]. The multiple crazing triggered throughout a comparatively large volume of rubber-modified material accounts for the high energy absorption in fracture tests and the extensive stress-whitening during the deformation and failure. Bucknall [10,69–75] has suggested that in order to be effective as craze terminators the rubber particles must be of suitable size having adequate adhesion to the surrounding matrix.

7.2. Shear yielding

Bucknall [69,75] depicted shear yielding as the process by which most of the ductile polymeric materials accommodate high strains. Shear yielding involves a displacement of matter during the deformation (molecules sliding past each other). Contrary to crazing, shear yielding is strongly temperature dependent. The initial evidence for the importance of shear yielding mechanism in multiphase polymers came from mechanical property and optical microscopy studies. These studies revealed that in uniaxial tensile tests necking, drawing and orientation-hardening, indicating shear yield deformations, occurred and that the matrix had undergone localized plastic deformation around virtually every rubber particle. The detailed micromechanisms of the shear yield mechanism in rubber-toughened polymers have been identified by Haaf et al. [82], and Donald and Kramer [83] and their studies offer the most convincing explanation for the observed phenomena. They concluded that the dispersed rubber phase initiated microshear bands at an angle of 55–64° to the direction of the applied stress, depending upon the particle size of the modifier in the blends. Haaf et al. [82] also found that cavities were initiated in the rubber particles and were aligned along the shear bands. This cavitation of the rubber particles obviously explains the stress whitening. The observation of cavitation in some rubber-toughened polymers, apart from accounting for the stress whitening, also enabled an additional explanation for the enhanced shear yielding of the matrix to be proposed. The presence of many closely packed particles which can cavitate enables the local build-up of hydrostatic tension produced by localised (constant volume) shear processes to be relieved. Thus, possibly soon after the development of some initial shear yielding, the constrained conditions are relieved and even relatively thick bulk specimens may behave as if the matrix were everywhere under plane-stress conditions. The shear yield deformations occur more readily under a biaxial rather than a triaxial stress state and cavitation of the rubber particles therefore favors local shear yield deformations [57]. However, if the matrix does not readily shear but like styrenic matrices is far more prone to crazing then this mechanism is not available and cavitation and voiding of the rubber particles can be damaging [57].

7.3. Simultaneous shear yielding and crazing

Many toughened polymers may exhibit both shear yielding and crazing, and both these mechanisms have been observed. As a general rule, the mechanism which is dominant in the toughened polymer will simply reflect the main mechanism which is operative in the matrix when it is unmodified [10,57]. However, microstructural features of the toughened polymer, such as particle size and interparticle distance, and external variables such as rate and temperature of test, mode of loading (stress state) as well as the specimen geometry will affect the balance of the mechanisms. The simultaneous initiation of shear bands and crazes led Bucknall and co-workers [10,84,85] to suggest that in addition to increasing the energy absorption, shear bands may act as effective craze terminators for growing crazes. Hence, in those polymers where shear banding occurs in addition to crazing then the need for the presence of relatively large rubber particles to function as craze terminators is

removed. Shear yielding will be the dominant toughening mechanism as compared with crazing when the yield initiation stress is simply lower than the craze initiation stress. Henkee and Kramer [86] demonstrated that the entanglement density, ν_e , is a critical parameter which determines whether a polymer will tend to deform by crazing or by shear yielding. A low entanglement density favors crazing, while above a critical value of entanglement density (roughly $\nu_e \approx 0.15 \text{ mmol/cm}^3$ (Wu [87]) there is a change from crazing to shear yielding. On the other hand, the flexibility of chains in thermoplastic polymers seems also to be likely an important parameter for this crazing/shear yielding transition, because below the temperature of secondary relaxation processes, the pseudoductile polymers usually become brittle despite the fact that entanglement density does not change at this temperature [55–58]. Consequently, the entanglement density, ν_e , can be considered as the primary parameter which controls the crazing behavior, whereas the chain stiffness parameter, C_∞ , is predominant in controlling the shear yielding behavior [55–58].

7.4. Rubber particle cavitation

It is well-established that rubber particles' cavitation plays a decisive role in toughening [56,66,69–73,88,89]. Although cavitation itself involves little energy absorption, it facilitates, sometimes massive, deformation of the matrix, which appears the primary source of the energy absorption. In the middle of thick sample or in front of the crack tip or pre-notches in impact specimens, the stress state is triaxial (plane-strain condition), making plastic deformation more difficult than the biaxial stress (plane-stress condition) and favors brittle fracture as the surrounding stressed material resists the lateral contraction which is needed to maintain a constant volume on deformation. The rubber particles respond to a high level of triaxial stresses produced by near plane-strain conditions with internal cavitation or sometimes with debonding from the surrounding matrix, if the rubber-matrix interfacial adhesion is low, both of which create voids either inside rubber particles or at their interfaces, respectively (Fig. 6). Upon formation of voids, the constraints imposed on the matrix are locally removed, and the triaxiality of the stress is relieved, at least partially, around each cavitated elastomer particle ahead the notch or the running crack [10,57,90]. Due to a notable reduction of constraints, the stress state around these particles, especially within thin matrix ligaments between neighboring cavitated particles, can be converted from a triaxial to an early biaxial one. Thus, the primary impact of cavitation is usually an enhancement of shear yielding mechanism in the matrix [69,91]. Formation of cavities gives rise to local decrease in the hydrostatic stress component followed by a corresponding increase in the deviatoric (shear) component, and a higher stress concentration factor [91]. Another important consequence of cavitation is conversion of the material from a continuous solid to the porous (cellular) structure, which demonstrates modified sensitivity to the mean stress on yielding. Thus, the matrix can yield easier, even at the plane-strain conditions ahead of the notch.

To get the maximum toughness, two conditions must be satisfied: a widespread cavitation ahead of the crack tip and extensive involvement of the matrix in plastic deformation. Moreover, the ability of the rubber phase to undergo strain-hardening mechanism under the loading is very important. To achieve this, the rubber should be strongly bonded to the matrix and to any internal sub-inclusions, when particles have heterogeneous morphology. The participation of the elastomer phase in strain hardening allows for higher load transfer onto cavitated particle and thereby better stabilization of deformation. This suggests that the formation of voids through internal cavitation, especially multiple voiding accompanied by the formation of fibrils inside particle, is more efficient in toughening than particle debonding.

Similarly to multiple crazing, cavitation is also accompanied by stress whitening of the deformation zone [91,95]. The stress needed to nucleate a void inside an elastomer particle is a function of the cohesive energy density of that elastomer, chain entanglements (MW), degree of

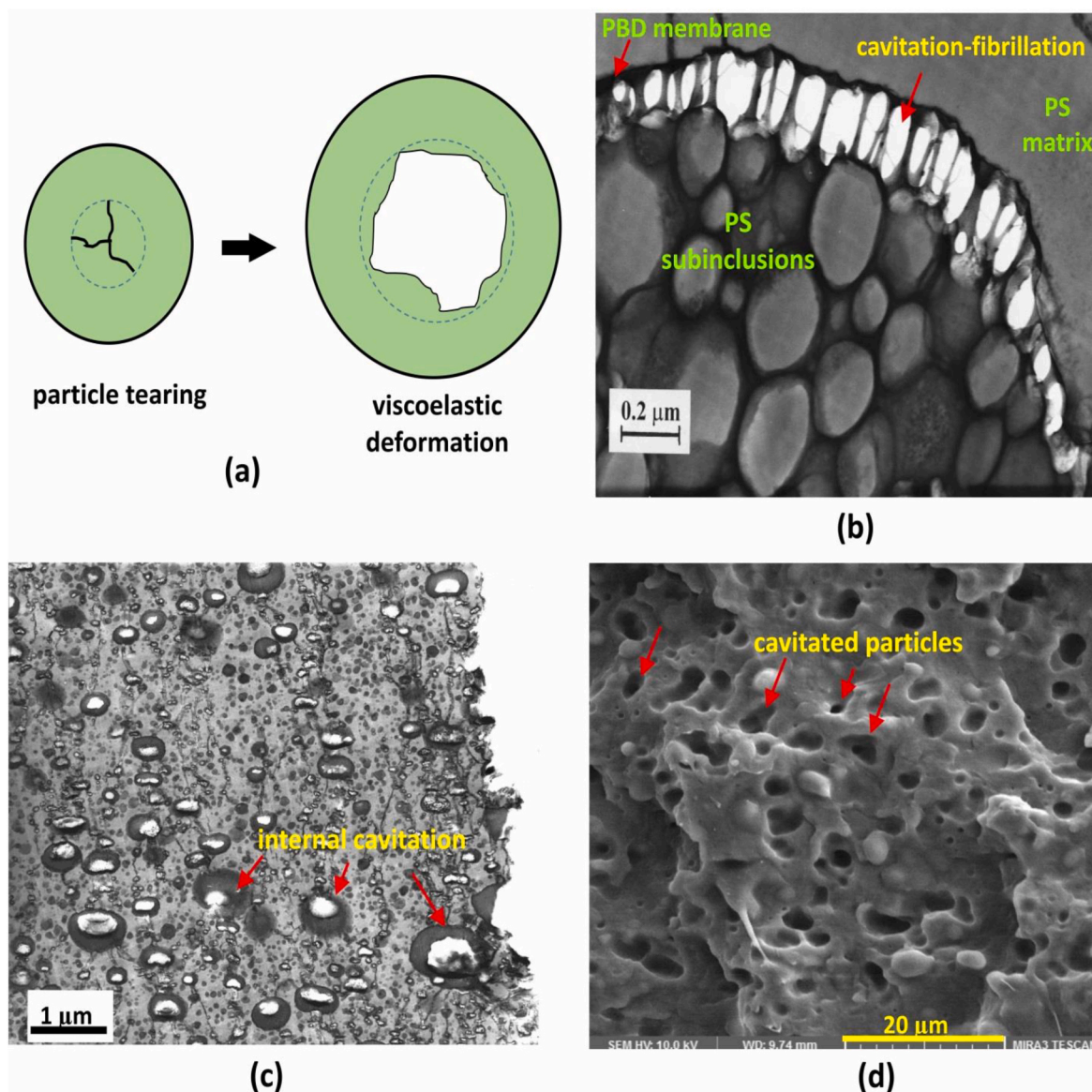


Fig. 6. (a) cavitation of rubber particle according to the Fond-model demonstrating that the required cavitation energy consisted of two terms, a first for tetrahedral tearing of nucleus and a second for its viscoelastic deformation up to the opening of the void (remade after Fond [18], with kind permission of Springer Nature). (b-d) micrographs showing the typical rubber particle cavitation in HIPS (TEM image in b), ABS under quasi-static SEN test (TEM image in c), and PP/EPDM under Izod impact test (SEM image in d) multiphase systems (reproduced from Bucknall [58], Jar et al. [92], and Mehrabi Mazidi [93,94], with kind permission of John Wiley & Sons, Inc.).

cross-linking of the rubber phase, particle size, its elastic modulus and poisson's ratio, and presence of any inhomogeneities inside the elastomer particle (as, e.g., precavities, small crystallites, or foreign impurities) [96–99]. Any defect or heterogeneity, if present inside the elastomer particle, can result in a significant reduction of the cavitation stress of that particle. Even for particles as small as 0.2 μm in diameter, the energy barrier for cavitation is quite low [92,100,101].

7.5. Dilatational bands' formation

The mechanism for rubber toughening in non-crazing polymers has been explained by several researchers [101,102,103] who demonstrated that rubber particles can activate dilatation yielding in the deformed zone close to the fractured surface. They concluded that yielding in the blend sample occurs through the formation of dilatation bands, containing cavitated rubber particles, which allows the original voids to expand as plastic flow develops in the band and to relieve the

dilatational stress. There is broad evidence that rubber particle cavitation in several different polymers is indeed concentrated within band-like zones of high shear strain [102,104–106]. Similar cavitated yield zones have been reported in the literature concerning metals, where they have been referred to as “dilatation bands.” Such dilatation bands form because when an element of material is restrained in two dimensions, the only modes of deformation compatible with the imposed constraints are simple shear parallel to the plane and volume dilatation normal to it. The presence of both results in formation of a dilatation band, as illustrated in Fig. 7. The inclination angle eventually falls to zero when the void volume fraction reaches 0.53 [99]. This rotation of the band plane reduces resistance to crack tip opening; at the crack tip plane, $\Psi = 0$, yielding occurs entirely in response to tensile stresses applied normal to the bands, which in that respect may resemble crazes.

Since almost all of reactively toughened multiphase systems discussed in this review are composed of semi-crystalline polymer matrices,

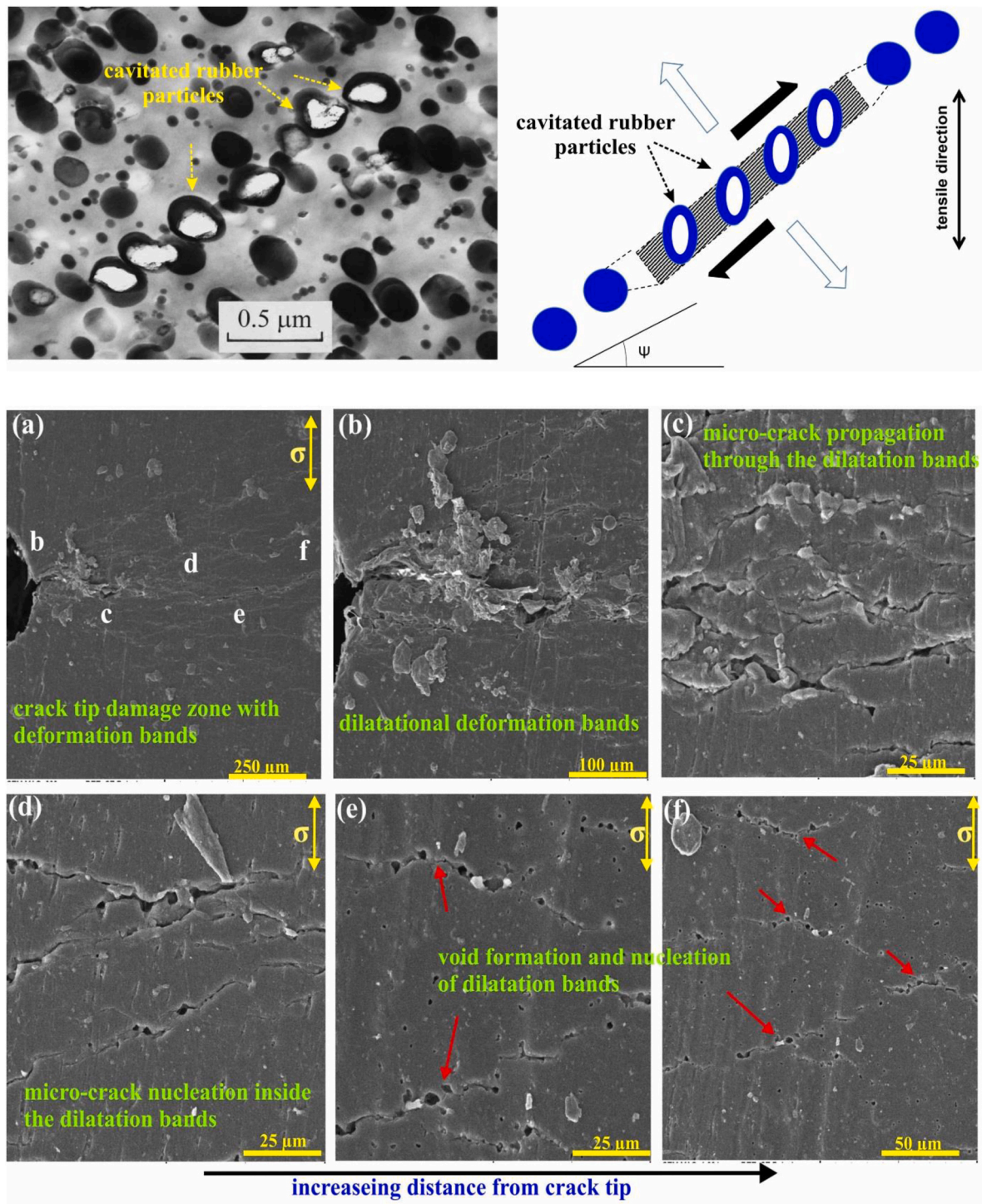


Fig. 7. (top) A dilatational shear band in rubber-toughened PA6 developed under Charpy impact test (left). The PBD rubber particles were stained with OsO₄ before sectioning. Schematic diagram of a dilatational shear band (right). [Remade after Bucknall [101,106], with kind permission of Wiley-VCH GmbH]. (below) SEM micrographs of crack-tip damage zone for PP/EPDM blend developed under quasi-static fracture tests showing localized plastic deformation, nucleation of dilatation shear bands of cavitated particles and locally yielded surrounding matrix, and micro-crack initiation and subsequent propagation through deformation bands (the deformation direction is vertical). (Reproduced from Mehrabi Mazidi) [93].

the critical parameters contributing to toughness improvement and the fundamental steps involved in the energy absorption mechanisms in these thermoplastics are briefly discussed in the following section.

8. Rubber toughening of semi-crystalline polymers

Semicrystalline polymers are usually ductile. However, at lower

temperatures (below the glass transition temperature) and under impact loadings they fail in a brittle mode [10,12,15,57,107–113]. In semi-crystalline polymers with shear yielding as the dominant mechanism of energy dissipation, the critical parameter is the interparticle distance, ID, or the thickness of matrix ligament in-between the dispersed particles [12,15,56,109–115]. According to Wu [114,115], the blends are tough for interparticle distances smaller than a critical value, ID_c, and

brittle, if the distances are larger than ID_c . There is a brittle-ductile transition at a constant critical interparticle distance, ID_c . The ID_c was found to be independent of particle size and rubber volume fraction, but depend on the type of polymer matrix. The ID_c in semicrystalline polymers is not a fixed value but depends on testing conditions; it increases with temperature and decreases with the applied strain rate [116–120]. Intense plastic yielding starts in the matrix strands between the particles, if they are thinner than a critical value (in a similar manner with the macroscopic brittle-ductile transition from a plane strain state to a plane stress one) [114–117]. There is a need for cavitation of rubber particles to enable local yielding of the adjacent matrix ligaments. As with the multiple-crazing mechanism discussed above, a three-stage mechanism of multiple shear yielding can be defined (Fig. 8) [13,15,56].

Stage I. *stress concentration and void formation*; under external loadings, stress concentration around the rubber particles initiates cavitation (nano-void formation) inside the particles. In places of a maximum shear

stress component weak shear bands form between the particles at an angle of roughly 45° to the load direction. Stage II. *Induced shear deformation and superposition effect*; owing to high local stress concentrations shear processes are initiated in the matrix ligaments in-between the particles (or voids). Shear deformation proceeds at numerous adjacent matrix bridges simultaneously, thus taking place in fairly large volume of material. Stage III. *Strain hardening and crack stop*; Strain hardening of the yield zones with a process of stretching of the rubber phase to very high strains. Rubber particles cause crack tip blunting and consequently crack stop, preventing premature crack propagation and fracture (Fig. 8, lower part).

It has already been shown that [121–123] the toughening mechanisms involved in different blend systems are drastically influenced by the phase structure and dispersion state of the various modifier particles, which in turn lead to different micromechanical deformation processes. This is because the different morphology types of modifier particles

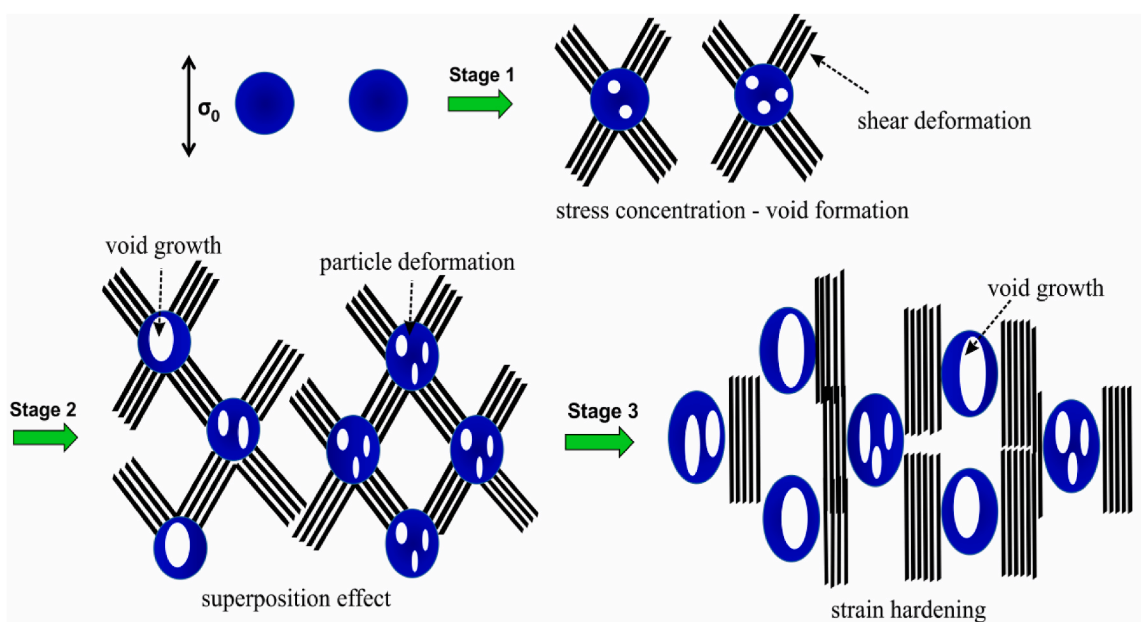
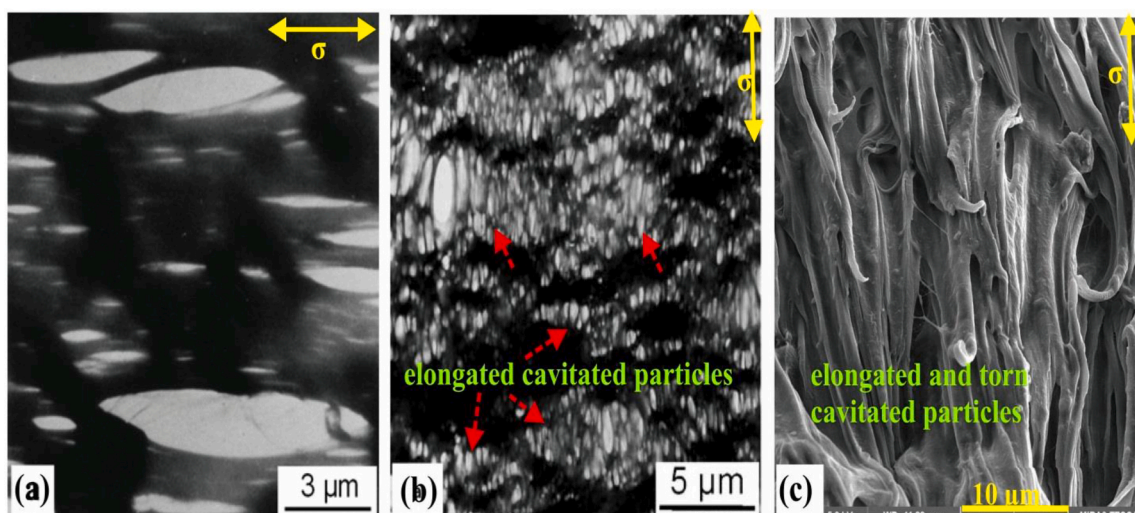


Fig. 8. (a-c) deformed toughened semicrystalline polymers showing micro-void formation inside plastically elongated rubber particles and matrix plastic deformation for PP/EPDM (TEM image in a) and PA66/butyl acrylate (TEM image in b), and highly elongated and torn cavitated rubber particles in PP/EPDM blend (SEM image in c) [56,93]. (below) A three-stage mechanism of multiple shear yielding in toughened semi-crystalline polymers. Stage I. stress concentration and void formation; Stage II. Induced shear deformation and superposition effect; Stage III. Strain hardening and crack stop (Remade after Kinloch, Riew, and Michler [13,15, 56], with kind permission of American Chemical Society and Hanser Verlag).

greatly affects the local stress fields, which play a major role in process of void formation and shear yielding of the matrix material. In heterogeneous polymer systems toughened by one kind of modifier particles, different morphologies can be identified depending on the concentration of rubbery phase and the processing conditions [123–130]. These morphologies can be classified as discrete, inter-mediate and percolation structures. The discrete morphology exhibits individual particles that are well separated in the matrix, whereas the percolation structure, also called the co-continuous [123–126] or interconnected [127] structure, appears to consist of rubbery networks. An inter-mediate morphology is something between discrete and percolating morphology. Many studies indicate that blends containing interconnected particles give much better toughness compared to those containing discrete particles, probably due to the bridging effect of interconnected rubber particles which facilitates the shear yielding and/or further growth of the shear bands from the crack tip, and thus more energy is consumed before fracture [125–130].

In the following sections, the reactive alloys of core-shell morphologies are reviewed and discussed comprehensively from the processing-structure-property perspectives. The historical development of reactively compatibilized alloys is presented at first. Then the influence of various blending parameters as well as the characteristics of polymeric components constituting the blends is closely examined.

9. Semicrystalline-matrix reactive blends of core-shell morphology; historical background

The concept of utilizing reactive (monomeric) species in order to obtain more homogeneous blends of two antagonistically incompatible polymers, such as blends of PA6 with either PP or PS, was first introduced by Ide and Hasegawa [50–52]. These researchers prepared MA-grafted PP (by solution grafting) and PS copolymerized with MAA (by suspension polymerization) at first and then used these interpolymers, as exactly termed in their paper, as mixing promoters for blends of PA6 with PP and PS, respectively. They found that in the presence of a certain amount of the prepared interpolymers, marked dispersibility of the polymer blend could be obtained, probably by the formation of a certain graft polymer between some carboxylic group such as MA or MAA and external amino groups of PA6 [52]. In fact, in the resultant blends the interpolymers formed an interfacial phase between the blends components, which encapsulated the dispersed domains. Polymer blends into which such interpolymers were introduced as the third component had better physical properties than only mechanically blended polymers without such interpolymers [52]. This concept was then further employed by using other reactive groups/monomers for developing numerous grafted (functionalized) and copolymerized polymers in the industry as well as on the commercial scale. Compared with non-reactive melt mixing, the reactive processing rendered faster size reduction, finer particle size, better morphology stability and a much thicker interface [131].

One of the applications of these copolymers is in multicomponent polymeric systems which they function as interfacial agent (compatibilizer), promoting the homogeneity and better mixing quality between the blend constituents. In some cases, when the backbone of these copolymers is soft and rubbery in character, the toughening effect may also be obtained in the resulting blend system, in addition to their emulsifying action.

The impact of type and molecular structure of the compatibilizer/impact modifier on the morphology development and stiffness-toughness balance in the blends of core-shell morphology is discussed at first. Then the influence of other parameters is reviewed in separate sections.

9.1. Effect of molecular architecture and content of shell-forming polymer

The molecular architecture of shell-forming polymer plays a key role

in the morphology, dispersion state, and interfacial characteristics of the resulting reactive ternary blend. In addition, the physical properties and macromolecular relaxations of shell-forming (rubbery) phase are directly influenced by its chemical architecture. All of these factors strongly affect the mechanical performance of reactively toughened ternary blends of core-shell morphology. For example, Holsti-Miettinen et al. [132] studied the effect of four compatibilizers including PP-g-MA, EBA-g-FA, SEBS-g-MA and EAE-GMA at two concentrations (5 and 10%) on the properties of PA6/iPP blends. The SEBS-g-MA had most significant effect on the morphology, mechanical properties (tensile ductility and impact strength), and melt rheology of the resulting blends among the different modifiers, and the blends containing SEBS-g-MA exhibited excellent mechanical properties, especially at high PA6/iPP ratios [132]. At 10 wt% of compatibilizer, the finest dispersion was achieved with SEBS-g-MAH as the compatibilizer with the particle size of less than 0.5 μm and hardly distinguishable separate domains. The impact strength was found to be dependent on both the compatibilizer type and PA6/iPP composition. The compatibilizers EBA-g-FA, PP-g-MAH, and EAE-GMA behaved qualitatively similarly, in that all produced better impact strength at higher PA concentrations. Compatibilizer SEBS-g-MAH behaved totally differently; it increased the toughness at both low and high PA concentrations. Interestingly, the improvement of impact strength was more pronounced in a blend where the PA weight fraction was 0.8, than in pure polyamide with the same amount of SEBS-g-MAH, reflecting the importance of presence of dispersed polypropylene domains in improving the impact toughness of PA6 matrix [132]. For PA/PP (80/20) blend, the apparent melt viscosity increased with compatibilization. At 10 wt% of compatibilizer, the viscosity was highest with compatibilizer SEBS-g-MAH, which further indicated better chemical compatibilization [132]. The compatibilization effect of SEBS-g-MA was based on the reaction between the amine end group of PA6 and the anhydride group in SEBS-g-MA along with the compatibility between olefinic midblocks of SEBS with iPP. According to these results, the authors proposed that compatibilizer SEBS-g-MAH may be partly located at the interphase as a compatibilizer but also partly incorporated as a rubbery impact modifier in the resin [132].

Rosch and coworkers performed extensive research works on the modified PP/PA6 blends [133–137]. To study the role of molecular architecture, Mulhaupt et al. [133] evaluated various anhydride-terminated isotactic- and atactic-oligopropenes of NAMWs ranging between 1000 and 10,000 g/mol as blend compatibilizers for PP/PA6 (70/30) blend. They found that the PA6 dispersion in the PP continuous phase is not affected by blend compatibilizer stereo-regularities. In terms of dispersion state quality, a critical molecular weight of the propene polymers, $1150 < M_{n,crit} < 5500$ g/mol, was found above which the average size of the PA6 microphases was reduced with increasing volume fractions of the modified propene polymers. Below this critical molecular weight the succinic anhydride-terminated oligopropenes, both isotactic and atactic samples, were inefficient as dispersing agents. In terms of mechanical properties, stiffness, yield stress and NCIS increased with increasing stereoregularities and molecular weights [133]. Rosch et al. [134–137] compared the performance of SEBS-g-MA, EPM-g-MA, EPM and PP-g-MA (at 2.5 and 20 wt%) as compatibilizers for PP/PA6 (70/30) blend. Different morphological textures were developed via reactive processing depending on the compatibilizer molecular architecture and volume fraction (Fig. 9d); (1) with EPM, the blends containing simultaneously dispersed spherical PA6 and irregularly shaped EPM were obtained, which the size of PA6 and EPM particles was, respectively, controlled via PP-g-MA and EPM volume fractions, allowing independent variation of PA6 and EPM sizes, (2) with EPM-g-MA, PA6 particles containing EPM subinclusions, were dispersed in PP by means of PP-g-MA addition when PA6 and EPM-g-MA were compounded prior to PP/PA6 blend formation, (3) for blends containing EPM-g-MA and SEBS-g-MA, the imide-coupling at the PP-PA6 interface, surface-tension gradient and immiscibility between PP, PA6 and rubber led to the accumulation of the

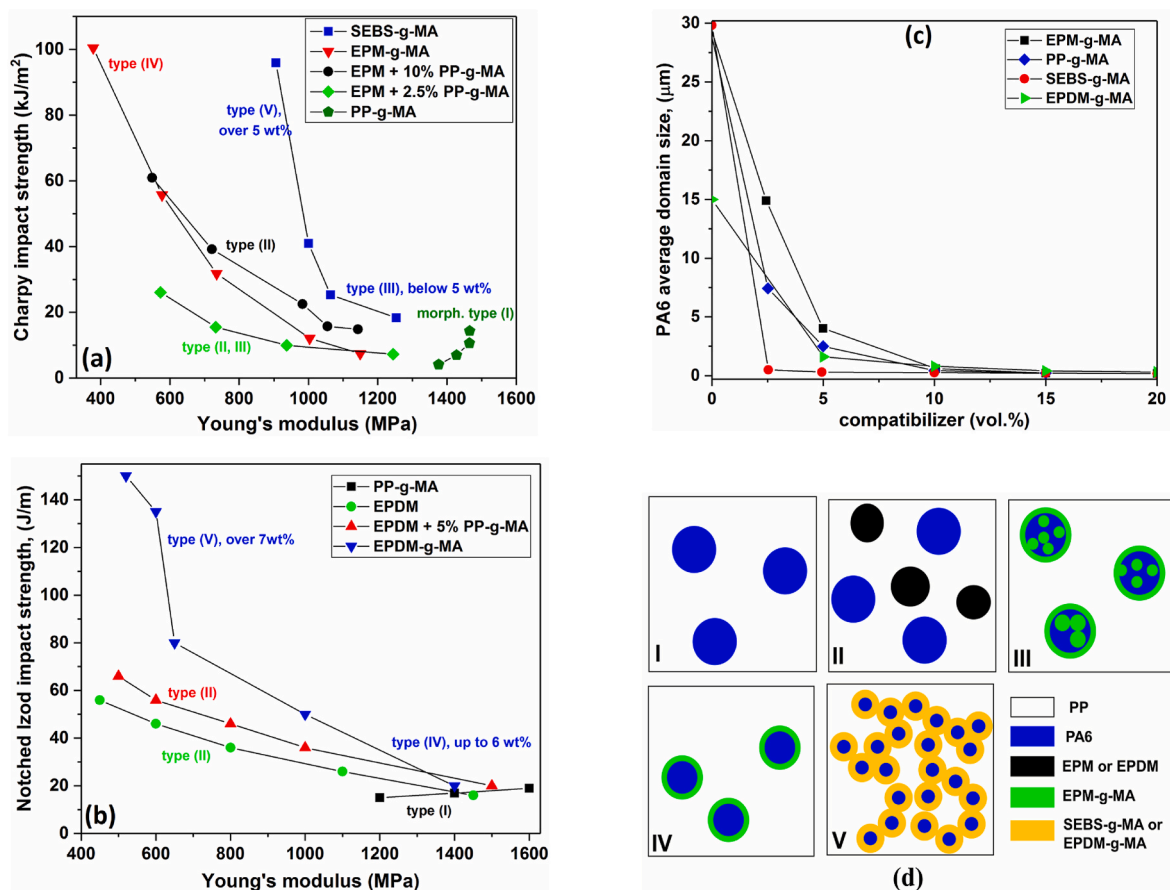


Fig. 9. Microstructure and mechanical performance of PP/PA6 (70/30) blends as a function of compatibilizer's molecular architecture and content (morphology type in (d)). (a,b) toughness-stiffness balance trend with blend morphology, (c) PA6 dispersion in PP matrix, and (d) morphology development (redrawn after Rosch et al. [134–137] and Mehrabi Mazidi [93], with kind permission of Wiley-VCH GmbH).

rubber at the PA6 microparticle surface, which resulted in microparticles with a PA6 core and a rubber shell. MA-grafted rubbers acted as polymeric dispersing agent, which improved PA6 dispersion in the PP matrix, and (4) with SEBS-g-MA and at concentrations exceeding 5 vol %, percolation of the colloidal core-shell particles, consisting of PA6 nanoparticle core and SEBS shell, occurred, which in turn led to the formation of a cocontinuous phase [134].

Interestingly, even at small SEBS volume fractions, cocontinuous phases of PP and SEBS-PA6 were detected in the PP matrix. The SEBS-g-MA compatibilizers brought about the formation of irregularly shaped honey-comb type microphases. Typically, the polyamide microparticles were embedded in SEBS-g-MA shells and agglomerated to form clusters of such core-shell particles [134]. Such core-shell type dispersed particles were formed when non-reactive rubber was replaced by reactive rubber, i.e. MA-grafted rubber. In fact, less than 1 wt% MA grafting of the rubbers was sufficient to accumulate the rubber quantitatively at the PA6/PP interface [134]. Considering the influence of various compatibilizers on average particle size of PA6 dispersed phase, SEBS-g-MA proved to be the most effective dispersing agent as compared with both PP-g-MA and EPM-g-MA (see Fig. 9c). Whilst more than 10 vol% of both PP-g-MA and EPM-g-MA compatibilizers were required to reduce the PA6 particle size below 1 μm, about 2.5 vol% SEBS-g-MA was sufficient to obtain PA6 nanoparticles in the range of 100 nm [134]. With increasing SEBS-g-MA content and decreasing average core-shell particle size, percolation of clusters produced a cocontinuous phase of agglomerated core-shell nanoparticles [134]. The best stiffness-toughness balance was observed for PP/PA6 blends modified with SEBS-g-MA, most likely due to the unusual morphological feature of PP/PA6/SEBS-g-MA blend, which was followed by EPM + PP-g-MA,

EPM-g-MA, and PP-g-MA (Fig. 9a). At greater than 15 vol% SEBS-g-MA, crack propagation during pendulum impact was stopped, and intense stress-whitening was observed near crack tip. The dependence of yield stress of the ternary blends on the type of rubbery phase was in the following order: SEBS-g-MA > EPM-g-MA > EPM, indicating excellent interfacial adhesion between the SEBS shell and PP matrix, which provided efficient transfer of mechanical stresses from the PP matrix onto the dispersed structures [134]. The SEBS-modified blend gave higher stiffness than the EPM-modified blend as a result of much higher elastic modulus of SEBS compared with that of the EPM. Such SEBS-g-MA compatibilized PP/PA6 blends demonstrated extraordinarily high impact strength (exceeding 90 kJ/m²) with high strength and stiffness to meet the demands of engineering applications [134].

In comparison to PP/EPM blends, incorporation of PA microphases caused severely reduced toughness. With decreasing PA6 particle size, performance of PP/PA6/EPM was approaching that of PP/EPM without added PA6. These researchers claimed that PP/PA6/EPM blend with separated morphology and compatibilized with PP-g-MA cannot provide suitable stiffness-toughness balance [134–137]. Although the morphology developed by EPDM-g-MA compatibilizer in PA/PP blend was similar to that of SEBS-g-MA (Fig. 9d), the stiffness-toughness balance achieved for resulting core-shell system was inferior in the presence of the former interfacial agent as compared with the latter one (Fig. 9b). Gonzalez-Montiel et al. [138] concluded that unfunctionalized rubbers, such as EPR and SEBS, had a limited use as impact modifiers for nylon 6/PP-g-MA blends. The use of maleated polypropylene does not help to disperse either of these non-reactive rubbers in the nylon 6 phase; therefore, the rubber was found to locate within the polypropylene domains. Such morphology leads to blends with low

toughness at room temperature and high ductile-brittle transition temperatures [138]. Use of maleic anhydride grafted polypropylene (PP-g-MA) in nylon 6/PP blends modified with maleated rubbers improves the degree of dispersion of the PP phase and strengthens the nylon 6/PP interface, i.e. PP-g-MA serves as a compatibilizer. The ductile-brittle transition temperatures of toughened blends containing PP-g-MA were found to be lower than those of blends with unfunctionalized polypropylene for any given nylon 6/PP ratio [138]. Blends with nylon 6/PP-g-MA ratios above 80/20 showed ductile-brittle transition temperatures equivalent to toughened nylon 6 without any polypropylene [138]. The authors further pointed out that the mixtures of functionalized (PP-g-MA) and unfunctionalized polypropylene (PP) can provide varying degrees of heterogeneity. The degree of heterogeneity affects the low temperature toughness of rubber-modified nylon 6/PP blends where the polypropylene phase is co-continuous or continuous [138]. A fine degree of dispersion of the PP-g-MA in the PP/PP-g-MA mixture improves the low temperature toughness, while mixtures with a larger or broader distribution of PP-g-MA domain sizes lead to blends with poor impact strength [138]. In another work, Gonzalez-Montiel et al. [139] used two types of MA-grafted elastomers,

EPR and SEBS, and found that both function as impact modifiers and compatibilizers for PA6/PP blends. The SEBS-g-MA appeared to be more effective compatibilizer. The Izod impact strength greatly improved by addition of 20 wt% of the maleated rubbers. The two rubbers were equally effective for increasing room temperature toughness. Addition of the maleated rubbers to nylon 6/PP blends reduced both the yield stress and modulus, as expected. Lower DBTTs were obtained when EPR-g-MA rubber was used, owing to its lower T_g and lower modulus at low temperatures compared to SEBS-g-MA rubber. TEM photomicrographs revealed that in PA6-rich blends, the SEBS rubber formed a relatively uniform layer at the interface between the nylon 6 and PP in addition to the particles of rubber dispersed in the nylon 6 phase, whereas EPR rubber formed a relatively thick, non-uniform layer around the PP domains [139]. The size of the polypropylene domains decreased as the amount of EPR-g-MA and SEBS-g-MA in the blends increased. The rubber content, PA6/PP ratio and MW of the components strongly influenced the morphology and toughness of the resulting blends. Low DBTTs were obtained for blends in which any combination of the above parameters yielded morphology where nylon 6 was the matrix phase with polypropylene and rubber finely dispersed in it, provided the

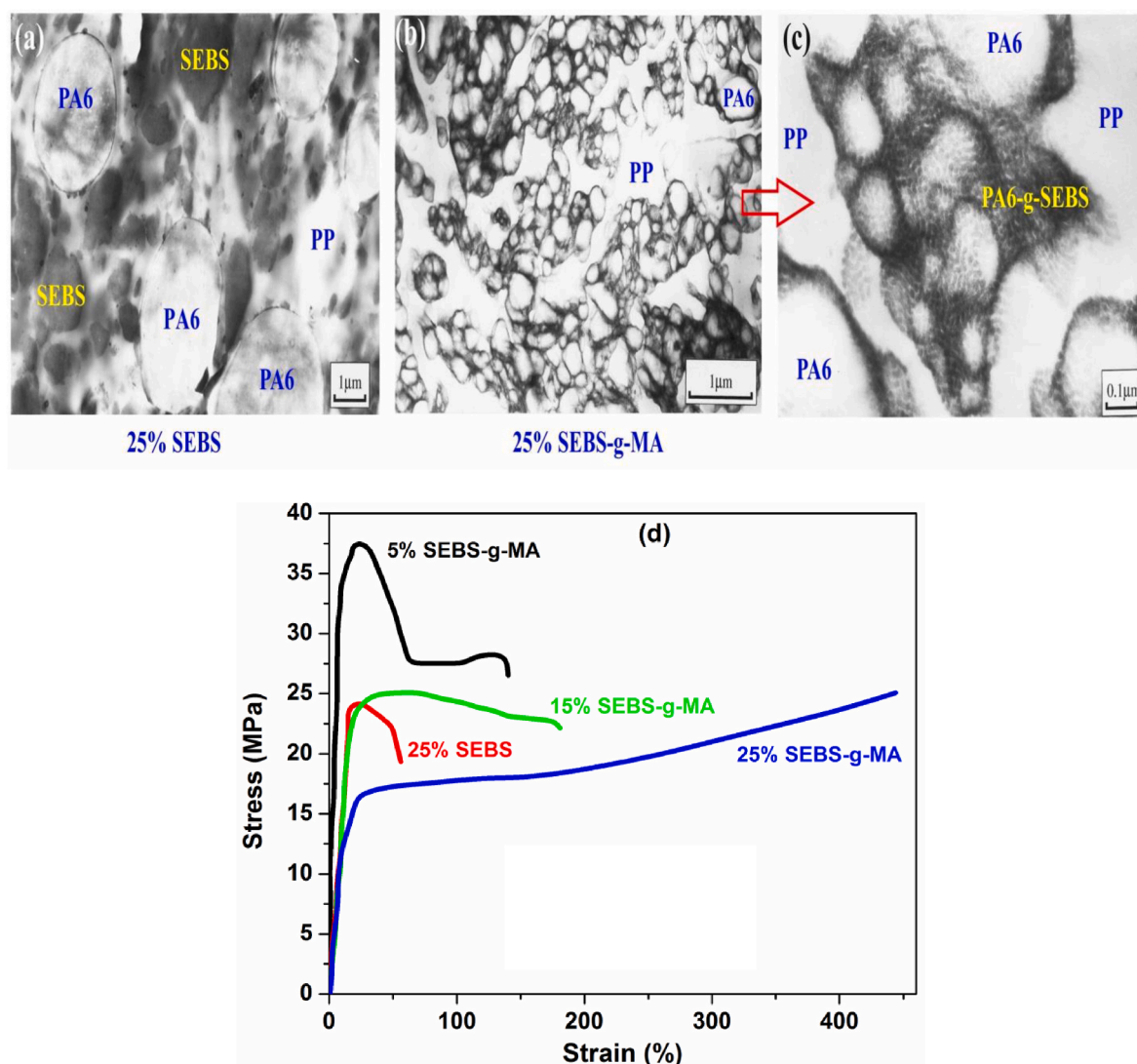


Fig. 10. TEM micrographs of PA6/PP (50/50) blends containing 25 wt% of either SEBS (a) or SEBS-g-MA (b, c). The samples were stained by ruthenium tetroxide. The polyamide domains are completely encapsulated by grafted SEBS-g-MA and form extended agglomerates joined together by the compatibilizing phase in (b, c). The dark dots in (c) represent PS microdomains in the self-assembling interphase polymer (reproduced from Ohlsson [141], with kind permission of Elsevier Science Ltd). (d) Tensile stress-strain curves at room temperature, comparing the properties of PP-PA6 blends compatibilized by 25% SEBS, or 5%, 15% and 25% of SEBS-g-MA (redrawn after Ohlsson [141], with kind permission of Elsevier Science Ltd).

component molecular weights were high enough to provide adequate intrinsic ductility [139]. Horiuchi et al. [140] studied the effect of SEBS and SEBS-g-MA on the morphology and interface of the incompatible PA6/PC blends. TEM observations showed that in PA6-rich blends the SEBS-g-MA was located at the domain boundary of PA6 and PC to encapsulate the PC droplets and also existed in the PA6 matrix at about 50 nm in diameter, whereas the SEBS was attached to PC particles but did not surround the domains. The SEBS-g-MA localized on the interface worked as a coupling agent to improve the interfacial adhesion between the PA6 and PC. However, significant reduction of the dispersed particles was not achieved by the addition of SEBS-g-MA, probably because the SEBS-g-MA phase is not miscible enough with PC to penetrate into the PC phase [140]. In the PC rich blends, SEBS-g-MA was occluded in PA6 domains and existed on the interface between PA6 and PC as well, while with unmodified SEBS the dispersed SEBS and PA6 phases formed separated dispersions in PC matrix. These types of phase morphologies were also predicted through using the spreading coefficient concept [140]. Ohlsson et al. [141,142] studied the effect of SEBS and SEBS-g-MA on the morphology and properties of blends containing equal amounts of PP and PA (PA6 or PA66). The morphological studies showed that even at high concentrations (25 wt%) most of the SEBS phase domains were separately dispersed in the polypropylene matrix, and only a small fraction was located at the PP-PA interface (Fig. 10a). In the PP-PA6 blend, with 25% by weight of SEBS, most polyamide domains had diameters in the range 1–5 μm . On the other hand, SEBS-g-MA functioned as an effective compatibilizer through showing a strong tendency to develop a distinct interphase (with interphase-layer thickness of about 15 nm), separating the polyamide domains from the PP matrix (Fig. 10b). The total surface area of the polyamide phase domains increased in proportion to the SEBS-g-MA concentration, indicating that the thickness of the interphase layer was almost constant and independent of compatibilizer concentration. At high concentrations of SEBS-g-MA (25 wt%), the PA6 phase domains formed large aggregates, held together by a thermoplastic elastomer interphase network (Fig. 10b and c). The PA-grafted thermoplastic elastomer formed under melt mixing conditions is an effective compatibilizer for PP-PA blends. The compatibilizing effect is not only due to the high affinity of the polyamide grafts for polyamide, but also to the rather high affinity of ungrafted EB midblocks for PP. In addition the presence of polystyrene endblocks, confer self-assembling properties to the compatibilizing polymer. The average PA6 domain size for blends containing 5 wt% and 25 wt% of SEBS-g-MA was estimated to be 360 nm and 110 nm, respectively. In addition, the authors found that the effect of SEBS-MA on the morphology of PP-PA66 blends was about the same as that for PP-PA6 blends, although the domain sizes were somewhat different [141,142].

The large difference in morphology observed for blends containing SEBS and SEBS-g-MA was also reflected in their uniaxial tensile behavior. Addition of SEBS to PP-PA6 blends led to limited improvement of tensile ductility (Fig. 10d), caused by the presence of rubbery SEBS domains in the PP phase [141,142]. With blends containing SEBS-g-MA, at 5 wt% rubbery phase the blend deformed by yielding and necking. The deformation behavior of the blend with 25 wt% of SEBS-g-MA was similar to that of PP-SEBS blends with a bicontinuous structure, i.e. a typical yield point was absent, and the sample deformed and fractured in a more or less rubber-like fashion (Fig. 10d), supported the suggestion that the blend contains an almost continuous network of agglomerated PA-6 domains, enclosed in a rubbery interphase of partially grafted SEBS-g-MA [141,142]. The melt flow properties of this blend also suggested that similar agglomerates are also present in the melt. The deformation behavior and elongation at fracture of blend having 15 wt% SEBS-g-MA was intermediate between those of blends with 5 and 25 wt% of SEBS-g-MA (Fig. 10d) [141].

The literature survey demonstrated above clearly points out that an excellent control of phase morphology and dispersion state of modifier phases towards superior toughness-stiffness balance can be obtained

through variation of molecular architecture of reactive compatibilizer serving as interfacial layer between the core polymer and surrounding matrix.

Blend composition is one of the parameters that has been studied extensively in the literature. In the following section, this subject is reviewed thoroughly.

9.2. Effect of blend composition

It is well-known that the morphology and properties of multicomponent polymer systems are dependent on the proportion of blend components. Thus, Gonzalez Montiel et al. [138] found that the mechanical properties of the PA6/PP blends toughened by 20 wt% of SEBS-g-MA and EPR-g-MA depend strongly on the blend ratio. The impact strength showed a maximum at about 20–25% polypropylene for both rubbers. There was no maximum or minimum in the yield stress or modulus corresponding to the maximum observed for the Izod impact strength for compositions containing 0–25% polypropylene. Beyond 50% polypropylene, where the polypropylene becomes the continuous phase, the impact strength was lower. The yield stress and Young's modulus of the blends gradually decreased as the PP content in the blend was increased, and the trend was the same for both rubbers. Toughened blends showed much lower yield stress and elastic modulus than the unmodified PA6/PP blend [138]. The DBTT of blends toughened by EPR-g-MA rubber increased in a continuous manner as polypropylene was added (Fig. 11). On the other hand, for blends modified with SEBS-g-MA, the DBTT decreased at first as polypropylene was incorporated, reached a minimum at about 10% PP, and then went up gradually with further addition of PP. The co-continuous region is reached at a lower weight percentage of PP when SEBS-g-MA rubber was used. The dispersed PP particles were smaller for the blends containing SEBS-g-MA than for the blends containing EPR-g-MA, suggesting that the SEBS-g-MA rubber was a more effective compatibilizer than EPR-g-MA.

The lower DBTTs for blends containing EPR-g-MA followed from the fact that this rubber is the better impact modifier for nylon 6, which, no doubt stems from the differences in the modulus versus temperature characteristics of the two rubbers [138]. Low DBTTs were obtained in the region where the nylon 6 is the continuous phase, no matter which rubber was used. Departure from this morphology towards co-continuity or phase inversion resulted in an increased DBTT (Fig. 11). Thus, in order to achieve toughness in PA6/PP blends, it is desirable to have the rubber and the PP as dispersed components in the nylon 6 matrix. This

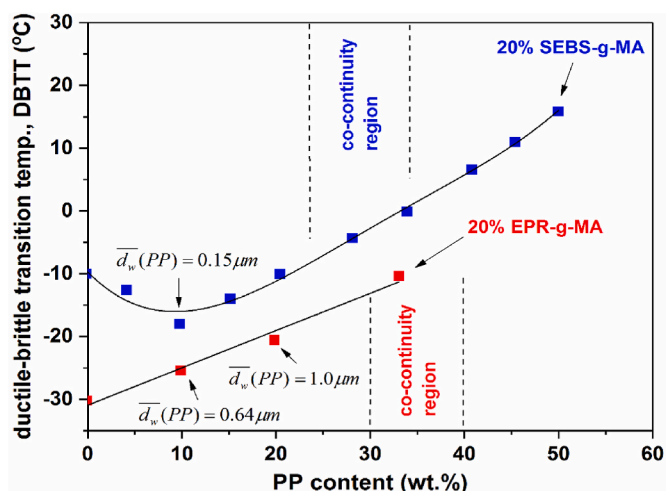


Fig. 11. Ductile-brittle transition temperature (DBTT) as a function of the percentage of polypropylene relative to nylon 6 on a rubber-free basis for PP/PA6 blends modified with 20% EPR-g-MA or SEBS-g-MA (d_w is the weight average PP particle diameter) (redrawn after Gonzalez Montiel [138], with kind permission of Elsevier Science Ltd).

observation agrees well with the relative toughenabilities of nylon 6 and PP. Toughened nylon 6 shows higher impact strength values than toughened PP [143–145]. Also, the DBTTs of toughened nylon 6 are generally much lower than those reported for toughened PP [146,147]. Rubber-modified blends with co-continuous nylon 6 and PP phases showed good toughness at room temperature but had poorer low temperature toughness than blends with lower amounts of PP in the form of dispersed particles [138]. Blends where PP is the continuous phase were not tough at room temperature. In fact, the 50/50 nylon 6/PP blend containing 20% EPR-g-MA did not appear to become tough at any temperature [138].

Kim et al. [148,149] studied the morphology development and mechanical properties of PP/PA6/SEBS-g-MA (70-x/30/x) blends containing 2.5–20 vol% of rubbery phase. The modifier particles showed core-shell structures, with PA6 inclusions engulfed by a single rubbery shell which seemed to be effectively adhered to the PP matrix as well as the PA6 inclusions. With increasing volume fraction of SEBS-g-MA in the blend, the finely separated discrete structures formed clusters, and eventually turned into island-like structures (percolation structures) at higher SEBS-g-MA loadings (Fig. 12).

With increasing SEBS-g-MA volume fraction, Young's modulus and yield stress slightly decreased but impact strength increased significantly [148,149]. These blends exhibited an interesting combination of stiffness, strength, and improved toughness. In samples containing more than 15 vol% of SEBS-g-MA, the cracks did not propagate through the specimen during impact testing but remained inside a certain area, and intensive stress-whitening was developed near the crack tip [148,149]. In blends with non-break impact fracture behavior, the particle percolation morphology was responsible for superior fracture toughness but at the cost of lower yield stress compared to the morphology of discrete dispersed particles [148,149].

Yu et al. [150] prepared super-tough nylon 6 by using PEO-g-MA rubber/semicrystalline polyolefin blend (60/40 wt ratio) as an impact modifier. The obtained results indicated that the modifier mixture, comprising a semicrystalline polyolefin core and a polyethylene-octane

rubber shell, not only provided a better processability of extruding and pelletizing with a lower cost, but also offered superior toughening effect in comparison with the pure PEO-g-MA rubber. The incorporation of impact modifier greatly improved the NIIS. With an increase in the impact modifier content, a transition from brittle to tough occurred; the elongation at break of the nylon 6 blend increased whereas the tensile strength, flexural modulus and flexural strength gradually decreased [150]. The massive shear yielding of the PA6 matrix was found as the main mechanism of the impact energy dissipation. In addition, the influence of melt viscosity of nylon 6 on toughening effectiveness was also investigated. High melt viscosity of matrix was found to be advantageous to the improvement of NIIS. This is because the matrix viscosity influences the size of the dispersed phase. High viscosity of nylon 6 matrix promoted the finer dispersion (size reduction) of impact modifier, which subsequently improved its toughening efficiency in the resulting blend [150].

Wilkinson et al. [151] examined the structure and properties of blends based on 70 wt% of PP with 30 wt% dispersed phase(s) (PA6: SEBS or PA6:SEBS-g-MA). The three-component PP/PA6/SEBS 70/15/15 blend, containing non-reactive SEBS, exhibited two independently dispersed phases; PA6 phase with a size-scale of 1–5 μm and SEBS phase with a size-scale of $\leq 0.5 \mu\text{m}$ [151].

The use of reactive SEBS-g-MA resulted in the formation of dispersed structures consisting of PA6 particles encapsulated by SEBS layer. Varying the PA6:SEBS-g-MA weight ratio in the dispersed phase allowed to manipulation of the dispersed phase structure, from discrete core-shell PA6/SEBS particles at low SEBS-g-MA fractions to larger, more complex agglomerated PA6/SEBS structures at higher SEBS-g-MA contents (Fig. 12, lower part) [151]. The dispersed discrete core-shell particles resulted in an increase in NCIS of greater than an order of magnitude compared to the PP matrix, and almost equivalent tensile properties. The larger agglomerated structures, in the form of more extended dispersions in the matrix, also generated very large increases in impact strength, of up to thirty-fold, but at the expense of significant reductions in tensile modulus and yield stress [151]. The morphological

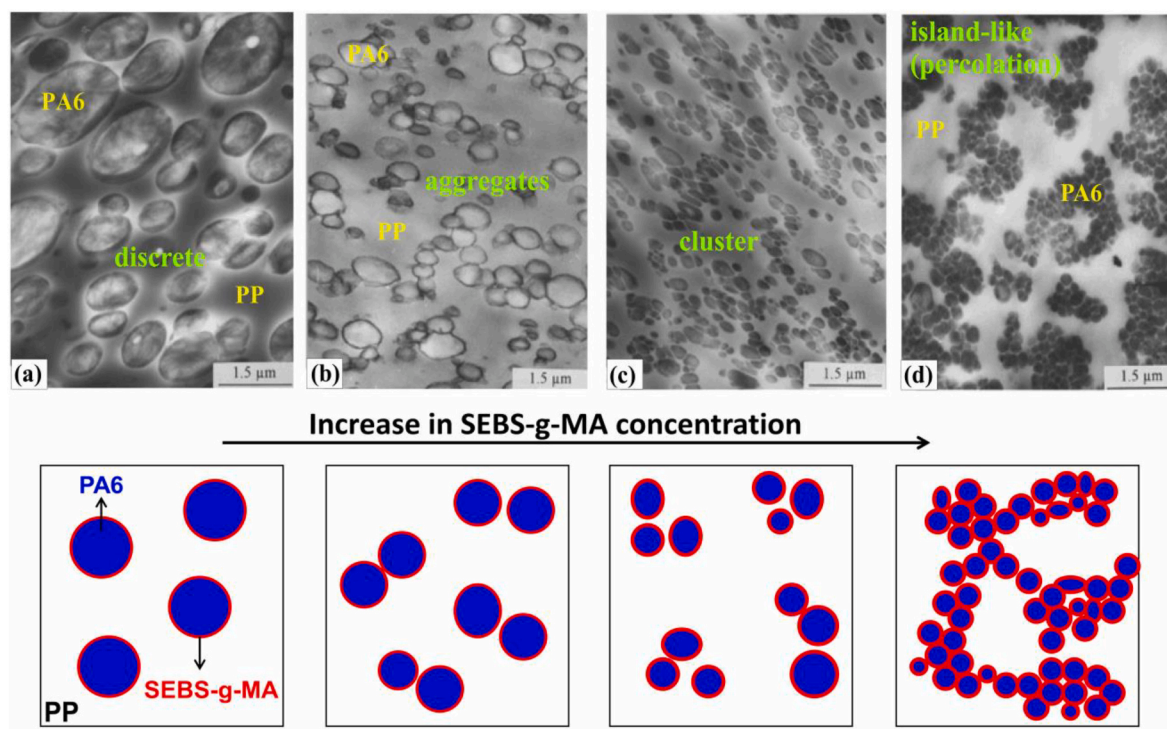


Fig. 12. (Top) TEM micrographs of PP/PA6/SEBS-g-MA (70-x/30/x) blend morphology with varying volume fraction of SEBS-g-MA. (a) 2.5, (b) 5, (c) 10, and (d) 20 vol.-%. (below) Schematic representation of formation of phase morphology as a function of SEBS-g-MA content. (reproduced from Kim et al. [149], with kind permission of Elsevier Science Ltd).

features and the dispersion states of the modifier polymers with blend composition observed by Wilkinson et al. [151] is similar to what reported by Rosch et al. [134–137], Ohlsson et al. [141], and Kim et al. [148,149]. In terms of the impact of specific type of dispersion state on the mechanical properties of the resultant blends, the obtained results by different researchers [133,134,137,141,148,149] concurrently demonstrate the highly beneficial effect of percolated (large agglomerates of modifier polymers throughout the matrix phase) phase morphology on the impact toughness of the multiphase systems with core-shell morphology. Tucker et al. [152] used a special version of a factorial design known as extreme vertices to study the mechanical and morphological properties of PP/PA6 blends compatibilized with PP-g-MA and SEBS-g-MA. The use of PP-g-MA enhanced the yield stress, modulus, toughness and impact strength while the use of SEBS-g-MA increased tensile strain and impact strength with a decrease of yield stress [152]. The effect of nylon/compatibilizer ratio was found critical for the optimization of PP/nylon compatibilized blends irrespective of nylon amount over the range of compositions studied. The effect was observed in response surfaces of yield stress and modulus for PP-g-MA compatibilized blends, and toughness for SEBS-g-MA compatibilized blends [152]. Zeng et al. [153] studied the morphology and mechanical properties of PP/PA6 (70/30) blend containing 15 wt% of either POE-g-MA or PP-g-MA. A core-shell morphology was detected for blend modified by POE-g-MA. Its Izod impact strength was four times that of pure PP matrix, whilst the tensile strength and Young's modulus were almost unchanged. The greatest tensile strength was obtained for PP/PA6/PP-g-MA blend, but its Izod impact strength was reduced in comparison with the pure PP matrix [153].

Bai et al. [154] prepared a series of PP/PA6/POE-g-MA blends, with weight fraction of PA6 from 0 to 40% and the weight fraction of POE half that of PA6. Morphological analysis by TEM revealed the POE modifier both as a thin interlayer (less than 100 nm thickness) at the PP/PA6 interface, and as a few isolated particles in the matrix [154]. The elastic modulus and yield stress in tension were nearly constant for PP and blends, and the NIIS increased very much with alloying content. For blends with low alloying content (both PA6 and POE-g-MA), the POE interlayer was very thin and PA6 particles were mostly spherical; the crack propagated easily across the section and left a smooth fractured surface. By contrast, for blends with high alloying content, the POE interlayer was thick and PA6 particles were highly elongated [154]. Ou et al. [155] studied the effect of a TPE-g-MA on the morphology and properties of PP/PA6 blends. At 15 wt % TPE-g-MA, the toughness greatly improved with only slight reduction of the tensile strength and modulus of PP/PA6 blends. The TPE-g-MA/PA6 ratio influenced the interfacial structure and adhesion between the components. TPE-g-MA was located at the interface of PP and PA6 in the ternary blends [155].

Krache et al. [156] investigated the interconnection between the viscoelastic properties and morphology in binary and ternary blends of PE, PP and PA6,6 with SEBS and SEBS-g-MAH as compatibilizers. The rheological measurements confirmed the increased interaction between the separate polymers containing SEBS-g-MAH as a compatibilizer, likely due to the formation of new covalent bonds through an amine-anhydride reaction [156]. For the blends with the compatibilizer very pronounced transition from a Newtonian flow to a pseudoplastic flow was observed at low frequencies [156]. Liu et al. [157] studied the morphology development in PP/PA6 (70/30) blend modified by POE and POE-g-MA thermoplastic elastomers. The PP/PA6/POE blends exhibited poor interfacial adhesion between the dispersed phase and matrix according to SEM analysis. However, the use of POE-g-MA induced a finer dispersion and promoted interfacial adhesion. For PP/PA6/POE-g-MA blends a core-shell structure consisting of PA6 particles encapsulated by an interlayer was formed in PP matrix. With increasing of POE-g-MA concentration, the dispersed core-shell particles morphology was found to transform from discrete acorn-type particles to agglomerates with increasing degree of encapsulation. Here, the evolution of phase morphology with POE-g-MA is similar to the results

reported by other researchers on the same blend system but toughened by SEBS-g-MA [133–137,141,148,149].

In another report, Liu et al. [158] investigated the effect of EVA-g-MA concentration on the mechanical properties and morphology of PP/PA6 blends. The addition of EVA-g-MA improved the compatibility between PP and PA6, and resulted in a finer dispersion of dispersed PA6 phase. The 18 wt% critical concentration was defined as the interface saturation concentration, beyond which the interface is saturated by the modifier. Upon incorporation of EVA-g-MA up to 18 wt %, the compatibilized blend exhibited lower yield stress with broadening of the yield peak, accompanied by necking during elongation [158]. With further increasing of EVA-g-MA to 30 wt %, the yield point diminished, and the strain hardening stage appeared. Elongation at break exhibited 41-fold increase as compared with the uncompatibilized PP/PA6 blend. In this case, the stress-strain behavior of the sample was in a more or less rubber-like manner, suggesting that the blend may contain an almost continuous network of agglomerated PA6 domains, enclosed in a rubbery interphase of partially grafted EVA-g-MA. In addition, the addition of EVA-g-MA gradually decreased both strength and moduli of PP/PA6 blend, and markedly improved the impact toughness, especially when EVA-g-MA concentration exceeds 24 wt%. Fractograph micrographs revealed the activation of matrix shear yielding at 18 wt% EVA-g-MA. Further increasing of EVA-g-MA concentration to 30 wt %, intensified and extended the matrix yielding and elongated matrix ligaments was occurred [158]. Ke et al. [159] proposed a facile method for preparing supertough PA6 with low rubber content. A low molecular weight functionalized rubber, PB-g-MAH was first grafted onto a LDPE molecule backbone via reactive extrusion with DCP as an initiator at 200 °C. The weight composition of LDPE/PB-g-MAH/DCP was 95/5/0.1. Then, rubber modified LDPE (LDPE-g-PB-g-MAH) was melt-mixed with PA6 at 230 °C. The resulting blend yielded a core-shell structure with a LDPE core and an elastic PB shell in PA6 matrix identified by TEM analysis. The impact energies of blend toughened by LDPE-g-PB-g-MAH were much higher than blend toughened by LDPE-g-MAH and POE-g-MAH at identical PA contents (Fig. 13). These results led to the conclusion that the thin rubber layer around the LDPE core was much more effective than pure LDPE or POE particles to initiate matrix yielding and dissipate impact energy. Typical AFM micrographs of cryo-fractured surfaces of these three toughened blends revealed interface debonding, internal cavitation of rubber particles during fracture, and fibril formation at the debonded interface between the core-shell particles and matrix for blends containing LDPE-g-MAH, POE-g-MAH, and LDPE-g-PB-g-MAH modifiers, respectively (Fig. 13) [159].

Ke et al. [159] claimed that in blends containing LDPE-g-MAH and POE-g-MAH, interface debonding and internal cavitation indicate that no stresses can be transferred effectively between particles and matrix. However, in blend modified with LDPE-g-PB-g-MAH, stresses can be transferred via the fibrils at the interface, and the macromolecular chains of PA6 connected with these fibrils will be highly elongated during the deformation of the specimen (Fig. 13). Relative to neat PA6, considering both elastic modulus and notched impact toughness properties, blend with a core-shell toughener, i.e., rigid core and soft rubber shell, was the best among the three blend systems studied. For blend with 90 wt % PA and 10 wt % core-shell toughener, there was only a 10% loss in modulus but a 10-fold increase in impact toughness compared to neat PA6.

Yan et al. [160] prepared PA6/SEBS-g-MA/PS (containing 15 wt% of the total minor components) blends via anionic polymerization of ϵ -CL by reactive extrusion. The TEM images showed that a core-shell structure with PS core and SEBS shell was formed in the PA6 matrix. Both the elongation at break and NIIS of PA6/SEBS/PS (85/10/5) blends were improved by 700% and more than 200%, respectively, with slight loss of tensile (4.5%) and flexural strength (14.7%) as compared with that of pure PA6 [160]. Increase in SEBS-g-MA content in the ternary blends led to a steady increase in tensile strength, flexural strength and elongation at

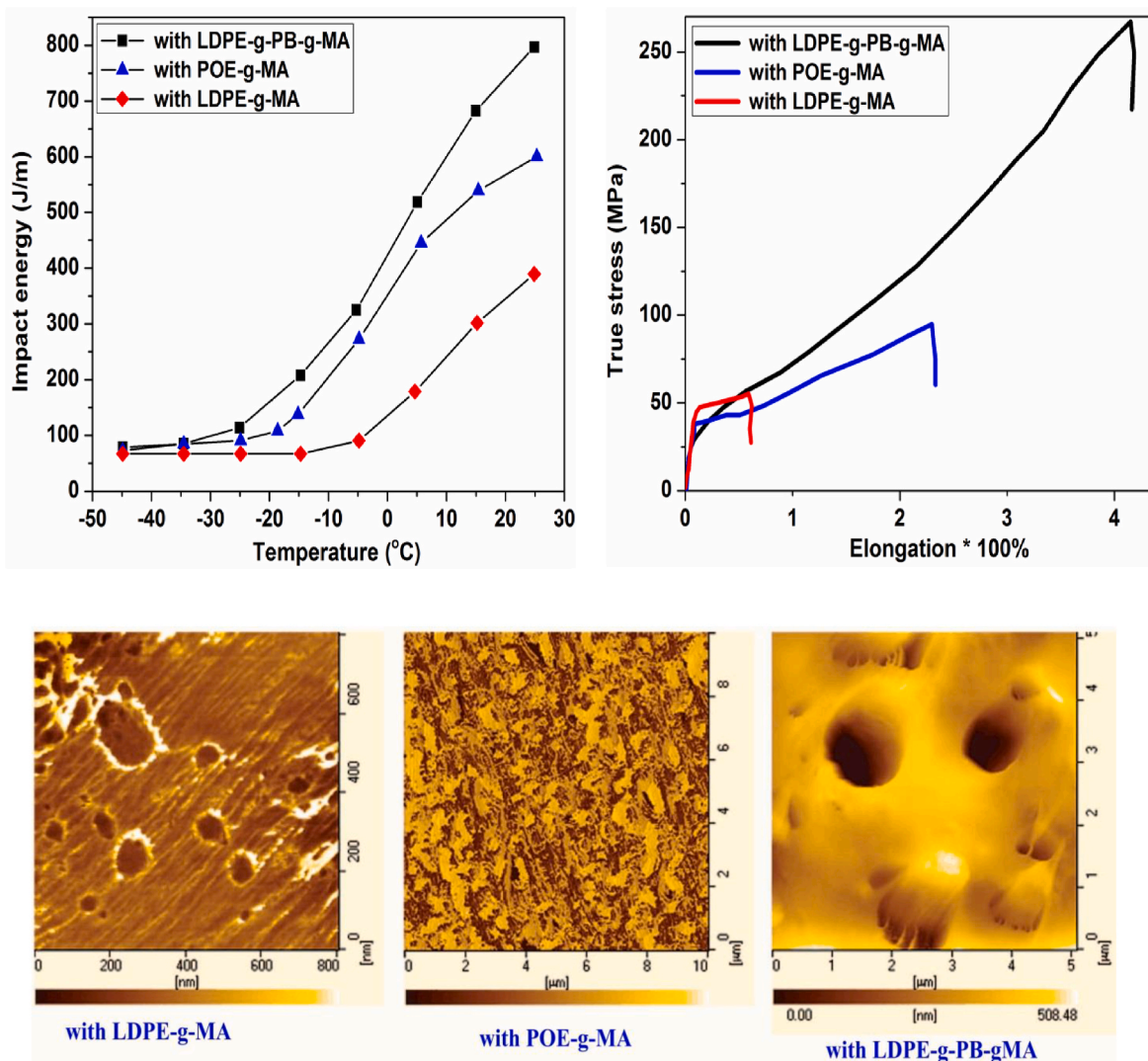


Fig. 13. (top) Impact energies versus temperature (PA6 content 80 wt %), and true stress-engineering elongation curves (PA6 content 70 wt %) of different toughened PA6 blends. (below) AFM micrographs of cryo-fractured surface of different blends (PA6 content 80 wt %) containing different tougheners (reproduced from Ke et al. [159], with kind permission of American Chemical Society).

break [160]. Ma et al. [161] studied the toughening of PA6 with β -nucleated thermoplastic vulcanizates (TPVs) based on PP/EPDM-g-MAH blends. The PA6 blends toughened with β -TPVs exhibited significantly enhanced toughness, balanced mechanical and thermal properties compared with PA6 toughened by TPV without β -NA or only by EPDM-g-MAH. The introduction of β -NA in TPVs greatly enhanced the impact strength of PA6. With increasing β -NA content, the impact strength of the toughened blends continuously increased. The results showed that using much less EPDM-g-MAH and a certain content of β -NA can produce significant toughening effect for PA6, which is beneficial for lowering the cost of the toughened system. The migration of β -NA from PP to PA6/PP and PP/EPDM-g-MAH interfaces improved the interfacial adhesion and gave rise to more uniform dispersion as well as smaller size of the dispersed phase; moreover, the core-shell structure comprised of rubber particles enveloped by PP on the surface, brought about easier and stronger interference of the stress field of EPDM phase [161]. Zhang et al. [162] examined the morphology and properties of fully bio-based ternary blends of PLA, PHBV, and PBS. A good balance of stiffness and toughness was attained for ternary blends with PHBV as matrix. The PHBV/PLA/PBS 60/30/10 blend showed a typical core-shell morphology with optimum mechanical performance and thermal resistance [162]. In another work, Zhang et al. [163] prepared super-tough

PLA/EMA-GMA/PEBA (70/20/10) blend with a NIIS of 500 J/m and a unique multiphase stacked structure, that is, showing morphology of partial encapsulation of EMA-GMA by PEBS in the PLA matrix. Synergistic effect of good interfacial adhesion and interfacial cavitation promoted massive shear yielding of the matrix material which in turn contributed to the marked toughening effect [163]. Rastin et al. [164] studied the effect of amount of HDPE-g-MA (ranging from 0.5 to 6 wt%) on the properties of HDPE/EVOH/PA6 blends. Smaller composite droplets with narrower size distributions were attained by gradual incorporation of compatibilizer. The authors found that the core-shell type morphology remains unchanged by addition of 0.5–6 wt% of HDPE-g-MAH to the ternary blends. Upon the incorporation of 1.5 wt% HDPE-g-MAH to binary blends, there was about 2.5- and six-folds increase, respectively, in the impact strength of 75/25 HDPE/EVOH and HDPE/PA6 systems compared with their corresponding non-compatibilized blends. Beyond this concentration of compatibilizer, the impact strength of HDPE/PA6 further enhanced significantly, while HDPE/EVOH did not break [164]. Wu et al. [165] found that the addition of 25 wt% SEBS-g-MA significantly increased the NIIS of PPO/PA6 (30/70) blend. The compatibilization by styrene-maleic anhydride copolymer with 8 wt % of maleic anhydride further enhanced the impact strength. Li et al. [166] prepared PP grafted with MA and St

monomers, PP-g-(MA-co-St), as a multiphase compatibilizer which exhibited an effective interfacial agent in PP/PA6/SEBS (70/15/15) blend. With increasing the compatibilizer, the morphology evolved from the individual PA6 particle encapsulated by SEBS to several smaller-size PA6 particles partially encapsulated by SEBS phase, then to the tiny PA6 particles and some larger-size SEBS agglomerates predominantly dispersed separately in PP matrix (Fig. 14). The morphology development predicted by spreading coefficients was in agreement with that observed by SEM [166].

Mechanical properties increased markedly with compatibilizer content at first and then decreased relatively sharply at higher loadings of the compatibilizer. The highest level of mechanical properties was obtained at 15 wt% compatibilizer, which led to 23%, 132%, 647% and 220% increase of yield stress, stress at break, strain at break and impact failure energy, respectively [166]. In another work, Wu et al. [167] studied the role of weight ratio and content of PPO/PS on the morphology and mechanical behaviors of PA6/SEBS-g-MA/(PPO/PS) blends. The core-shell particles formed by PPO/PS (core) and SEBS-g-MA (shell) played a key role in toughening of resulting blends. The notched Izod impact strength firstly increased and then decreased with the increase of PPO/PS contents. As the PPO/PS weight ratio increased, on the one hand, the entanglement density of PPO/PS improved, on the other hand, the PPO/PS phase transformed from continuous to sea-island structure [167]. The changes in tensile properties were not as large as the impact strength. The HDT gradually

improved with the increase of the PPO/PS weight ratio. PS improved the distribution of the core-shell particles due to its low viscosity, and PPO guaranteed the entanglement density of the PPO/PS phase, and the optimal mechanical properties were achieved at PPO:PS 3:1 wt ratio [167]. Wang et al. [168] studied the toughening effect of PA6/PBT core-shell particles in HDPE matrix. The authors claimed that at 20 wt% of the total modifier contents, HDPE/PBT/PA6 ternary blends showed higher impact resistance than the HDPE/PBT and HDPE/PA6 binary blends, due to the formation of core-shell morphology. The ternary blend with 1:1 PBT/PA6 weight ratio exhibited the highest impact strength, which was two-times of that of neat HDPE, due to its more perfect core-shell morphology. Zolali and Favis [169] reports significant improvements in the compatibilization and toughening of a co-continuous PLA/PA11 blend through the assembly of partially wet droplets at the interface. All the polymers examined by the Zolali and Favis [169] developed a partial wetting morphology but with different compatibilization and toughening efficiencies. EMA-GMA was the most effective compatibilizer; however, the best mechanical results obtained for the ternary PLA/EMA/PA11 blend. PLA/EMA/PA11 (45/10/45) shows a 4-fold increase in the notched Izod impact strength (73 J/m) and a high elongation at break ($\approx 250\%$). The stress-field overlap through an interconnected network path created by the partially wet droplets at the interface enhanced the shear yielding and consequently the toughening of the ternary systems [169]. In another work, Zolali and Favis [170] showed that all the PCL, EMA, EMA-GMA rubbery polymers

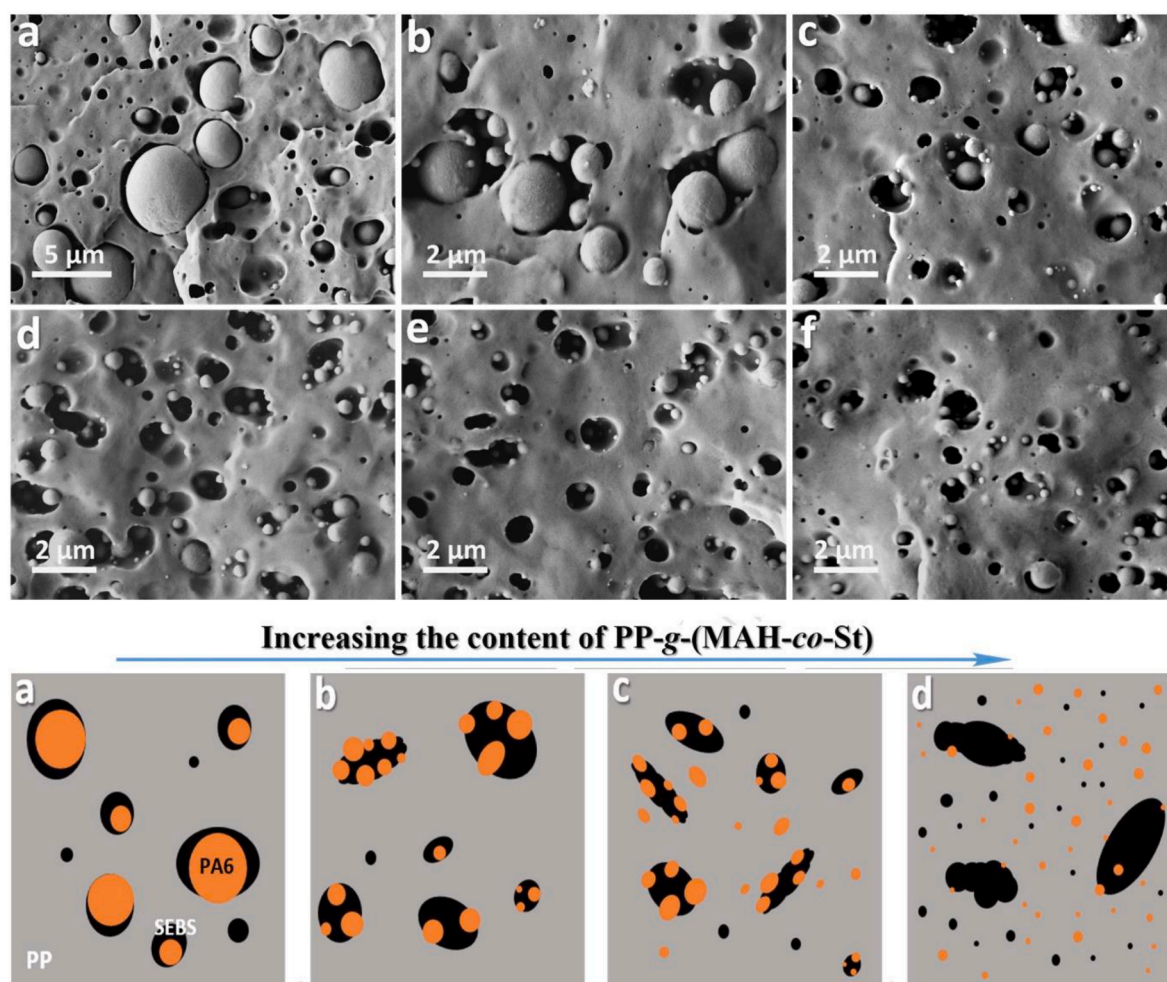


Fig. 14. SEM micrographs (top) and schematic representation of morphology evolution (bellow) for PP/PA6/SEBS (70/15/15) blend compatibilized by PP-g-(MA-co-St) at different levels. (a) 0 wt%, (b) 1 wt%, (c) 2 wt%, (d) 5 wt%, (e) 10 wt%, and (f) 15 wt% The samples were etched in THF to remove SEBS phase (reproduced from Li and Xie [166], with kind permission of Elsevier Science Ltd).

percolate at the interface between the components in a co-continuous PLA/LLDPE blend; however, different toughening and compatibilization effect was identified for these rubbery modifiers. EMA-GMA produced the highest compatibilization effect with the consequence of the greatest increase in the impact strength of the resulting ternary blend. For PLA/LLDPE/rubber (45/45/10) blends the values of NIIS for blends containing PCL, EMA, and EMA-GMA were 100, 359 and 515 J/m, respectively. Accordingly, the importance of both tricontinuous morphology and strong interfacial interactions were highlighted in obtaining high toughness materials [170].

Zhu et al. [171] modified HDPE by the development of 20 wt% of PA6/HDPE-g-MA core-shell particles. With the formation of the core-shell structure, the mechanical properties of HDPE, including tensile strength, elastic modulus, and the impact strength were enhanced. The presence of core-shell particles increased the impact strength of HDPE by 300% probably due to function of core-shell domains as micro-crack stoppers, and deviators as well as the dissipation of impact energy by plastic drawing of HDPE shell (Fig. 15). The impact strength of HDPE/HDPE-g-MA (80/20) was greater than that of PE/HDPE-g-MA/PA6 (80/10/10 or 80/15/5) blends [171].

Wang et al. [172] employed a multi-flow vibration injection molding technology (MFVIM) to convert the crystalline morphology of the PP matrix in PP/PET/POE-g-MA blends from spherulite into shish-kebab. The authors found that the joint action of shish-kebab crystals and spherical core-shell structure enabled excellent mechanical performance with a balance of strength and toughness for samples containing 10 wt% PET and 4 wt% POE-g-MA, of which the yield strength and impact strengths were 50.87 MPa and 13.71 kJ/m², respectively. Chen et al.

[173] developed bio-based PLA/NR-PMMA/NR ternary TPVs with balanced stiffness and toughness and soft-hard core-shell rubber phase. With 20 wt% of the total fraction of modifier phases, the blend containing 10 wt% NR and 10 wt% NR-PMMA displayed a yield stress of 41.7 MPa (38% loss compared to neat PLA) and an impact strength of 91.3 kJ/m² (nearly 32 times greater than that of neat PLA). It is claimed that the flexibility of the soft NR core and outer hard NR-PMMA shell with excellent PLA/rubber interfacial adhesion are responsible for the super toughness of the PLA/NR-PMMA/NR ternary TPVs. Sui and Xie [174] utilized two multi-monomer melt-grafted compatibilizers, SEBS-g-(MA-co-St) and ABS-g-(MA-co-St) as compatibilizers for PA6/ABS (70/30) blends. A core-shell structure was formed in blend compatibilized with SEBS-g-(MA-co-St), where ABS phase was the core and SEBS was the shell. The size of dispersed domains was smaller in the ternary blends as compared with that in PA6/ABS (70/30) binary system. Among the ternary systems, the PP/ABS-g-(MA-co-St)/SEBS-g-(MA-co-St) (70/15/15) blend showed the finest dispersion of the modifier particles (which led to lead to superior tensile strength, elongation at break and impact resistance) while the PA6/ABS blend compatibilized with ABS-g-(MA-co-St) exhibited the largest particle size. A considerable amount of SEBS domains existed as discrete particles in the matrix of ternary blends [174]. Ishigami et al. [175] studied the effect of presence of extended SEBS-g-MA having 50 wt% paraffin oil of low-, medium-, and high-molecular weights on the morphology and properties of PA6/SEBS-g-MA/PS (70/15/15) blends. The blends showed a core-shell morphology with extended SEBS-g-MA as the shell and PS as the core forming phases. Oil extension significantly decreased T_g of soft middle block and hard end block of

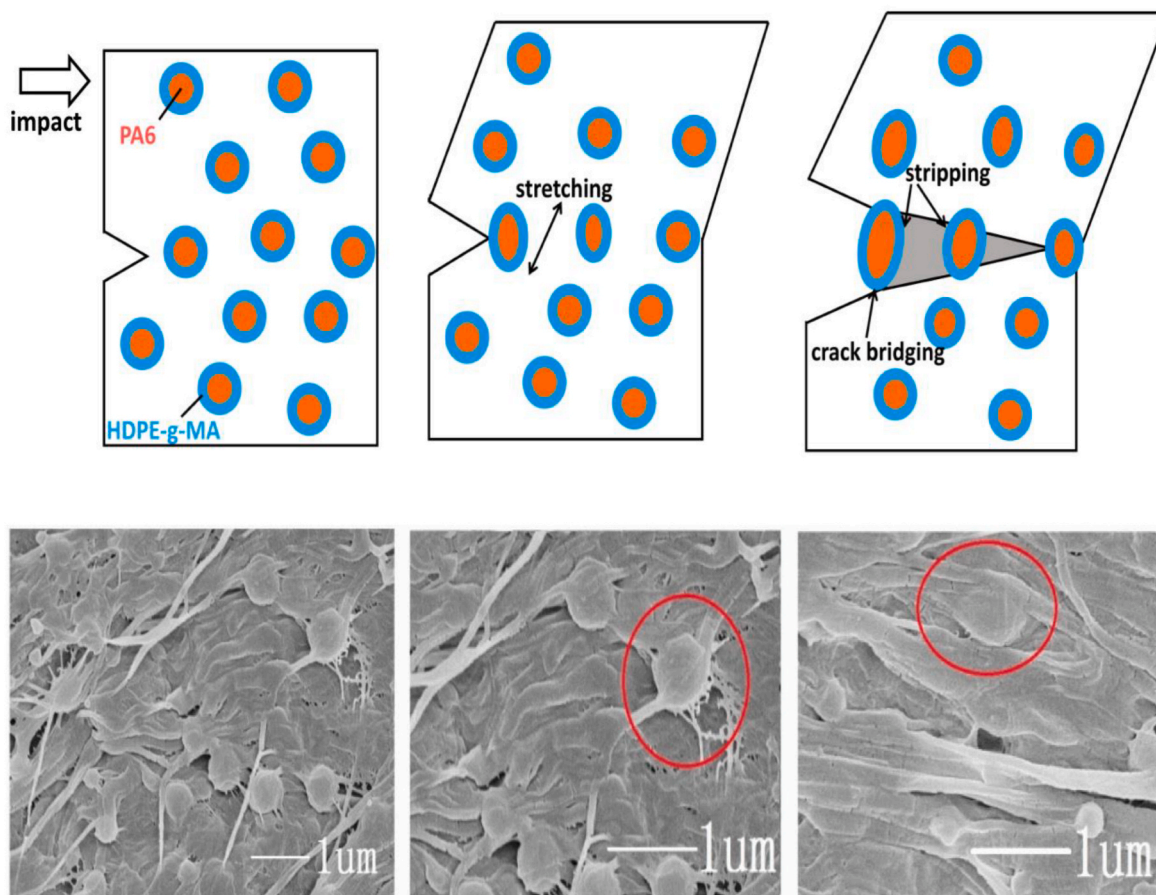


Fig. 15. (top) toughening mechanism of the core-shell structure under impact loading, showing undeformed particles, stretched particles, and the stripping of core-shell particles and the change of cracking propagation direction. (below) SEM micrographs of impact-fractured surface of HDPE/HDPE-g-MA/PA6 (80/5/15) blend showing plastically stretched core-shell domains. (reproduced from Zhu et al. [171], with kind permission of MDPI).

SEBS-g-MA, and the magnitude of this shift increased with the decreasing molecular weight of the oil [175]. The maximum NIIS of the ternary blends (60 kJ/m² with partial break of impact specimen) was significantly higher than that of PA6/SEBS-g-MA binary blends (25 kJ/m²), revealing the greatly beneficial effect of SEBS-g-MA in the form of a shell interlayer of composite dispersed droplets in ternary blends rather than a pure domain as in the case of binary blends. All the ternary blends exhibited the same value of impact fracture energy, regardless of the MW of paraffin oil in the extended SEBS-g-MA systems [175]. Hu et al. [176] prepared a series of sustainable polymer blends composed of PLA, P_{3,4}HB, and ECO elastomer. With PLA as the matrix, the morphology was dependent on the P_{3,4}HB:ECO weight ratio (fixed at 30 wt%), and there was a change in morphology from separately dispersed phases (for 10:20 and 15:15 wt ratio) to a core-shell type (for 20:10 ratio) with increasing P_{3,4}HB proportion in the modifier phases. For ternary blends, the tensile ductility increased while the NCIS significantly decreased with gradual increase in P_{3,4}HB:ECO weight ratio in the blend. The obtained results indicated that core-shell structures had limited toughening efficiency compared with the phase-separated structure of modifier components [176].

In order to closely determine the blend composition corresponding to the change in the dispersion state of modifier domains from discrete domains to aggregated structures, Mehrabi Mazidi et al. [177] studied the effect of EPDM-g-MA addition at 0 to 9 wt% on the morphology, mechanical properties and fracture characteristics of PP/PA6 (80/20) blends. A marked change in the dispersion state of core-shell domains from relatively large isolated particles to finely aggregated core-shell structures was identified at 7 wt% EPDM-g-MA, which was the threshold composition for the appearance of stress-whitening on the impact-fractured specimens, that is, a transition from brittle to semi-ductile fracture mode [177]. NIIS, quasi-static fracture energy, the size of crack tip plastic zone, and the crack tip opening displacement were all monotonically increased with EPDM-g-MA loading, at the cost of a steady decrease in blends' stiffness; however, the blend containing 9 wt% rubbery phase exhibited a good balance of stiffness-toughness. Yield stress and tensile strength increased at first with EPDM-g-MA content up to 4 wt% and then decreased with further increase in rubbery phase up to 9 wt%. The initial increase in strength parameters was due to the compatibilization effect (improving phase adhesion and preventing early debonding) of functionalized rubbery phase whereas the subsequent decline was mainly due to the toughening effect of the soft rubbery phase which outweighed its compatibilization effect [177]. Wang et al. [178] found that a core-shell structure of POE-g-MA/TPAS obtained during melt blending plays an important role in toughening of PP. At 30 wt% modifier polymers, very high values for the NIIS were achieved for ternary blends with up to 15 wt% TPAS, and further increase the latter component up to 30 wt% led to a substantial fall in impact toughness [178]. In other work, Mehrabi Mazidi and Razavi Aghjeh [179] closely examined the morphology development and micro-mechanical deformations operating in PP/PA6/EPDM-g-MA blends containing 30 wt% dispersed phase as a function of dispersed phase composition under both impact and quasi-static fracture mechanics tests. A gradual change in morphology from discrete core-shell particles to aggregates of core-shell domains, and eventually to an extended structure of core-shell particles in PP matrix was observed with gradual increase in proportion of EPDM-g-MA in the blend. This change in the dispersion state of modifier domains was accompanied by a steady improvement in the PA6/PP compatibility, interfacial strength and increased shell thickness with EPDM-g-MA loading [179]. The blend composition 70/10/20 showed the highest impact strength, higher than the impact resistance of PP/EPDM-g-MA (70/30) blend, reflecting the importance of morphology; however, the quasi-static works of fracture steadily increased with rubber content up to 30 wt% regardless of phase morphology. Debonding-cavitation around the dispersed modifier domains as well as inside the dispersed structures was the underlying fracture micromechanism responsible for micro-crack nucleation and

subsequent propagation at low and intermediate rubbery phase content. At high rubber content, no evidence of crack formation was detected and multiple void formation within and around the dispersed core-shell structured were the main source of energy dissipation (Fig. 16) [179].

Wei et al. [180,181] reported supertough PA6/rPVB/POE-g-MA blends prepared by a two-step processing method. The rPVB used was a plasticized grade having 28.5 wt% triglycol dioclate. The authors first reported the compatibilization effect of POE-g-MA in PA6/rPVB blend by studying the morphology and properties of ternary systems with different rPVB/POE-g-MA weight ratios at a fixed 30 wt% content. The blends having 10/20 and 20/10 wt ratios of modifier phases showed higher impact resistance than the PA6/POE-g-MA and PA6/rPVB (70/30) binary blends. The compatibilization effect of POE-g-MA was clarified according to the morphological and impact strength results [180]. In another work, Wei et al. [181] prepared rPVB/POE-g-MA masterbatch at first and then melt mixed the different amounts (5–35 wt%) of masterbatch with PA6. Although a multicore structure was claimed by the authors, the developed morphology was not dissimilar to an interpenetrated structure of rPVB/POE-g-MA phases dispersed in the PA6 matrix. A substantial increase in impact toughness (with a tough response) was observed at 25–35 wt% masterbatch, which was at a cost of a great fall in yield stress of the resulting blends. Under low masterbatch loading, cavitation was the main toughening mechanism. When the masterbatch content exceeded 20 wt%, large deformation of the dispersed phase and massive plastic flow of the matrix material during impact fracture were the main sources of energy absorption [181].

Chen et al. [182] reported a new core-shell dynamic vulcanization approach to prepare poly(vinylidene fluoride) (PVDF)-based thermoplastic vulcanizates (TPV) containing cross-linking-controlled silicone rubber (SR)/fluororubber (FKM) core-shell particles. Different curing agents were adopted to vulcanize FKM and SR components in the blend. DCP was very effective to cross-linking SR but had little effect on curing FKM while AF-BPP had an opposite effect [182]. The high pertinence effects of DCP and AF-BPP on cross-linking of respective SR and FKM provided the possibility to design and control the cross-linking status of the core-shell structures. The TEM images of biccrosslinked PVDF/FKM/SR (40/30/30) TPV provided the evidence for core-shell structure with SR and FKM represented as the core-forming and shell-forming polymers, respectively. The size of the core-shell SR/FKM particles was ~2 μm, and the thickness of the FKM shell was approximately 380–400 nm [182]. The formation of such core-shell sphere structures reduced the interfacial tension between PVDF and SR and produced a compatible blend with stabilized phase morphology through promotion of intimate interactions between the rubber particles and PVDF continuous phase. The core/shell biccross-linked TPV exhibited good mechanical properties in which its tear strength was as high as 58 kN m⁻¹ and tensile strength was 12.4 MPa. Lv et al. [183] prepared PP/EPDM/butadiene acrylonitrile rubber (NBR) ternary TPVs with good oil resistance using core-shell dynamic vulcanization. In these blends, the rubber phases exhibited a special core-shell structure, in which the cross-linked NBR-core was encapsulated by the EPDM-shell. The core-shell structure effectively improved the interfacial compatibility between PP and NBR phases. Prepared PP/EPDM/NBR ternary TPVs exhibited good oil resistance [183]. The PP/EPDM/NBR (40/30/30) ternary TPV showed enhanced tensile strength of 12.57 MPa, compared with 10.71 MPa of PP/EPDM (40/60) TPV and 11.11 MPa of PP/NBR (40/60) TPV, respectively [183]. Concerning the mechanical and oil resistance properties, the mass ratio of EPDM/NBR = 1:1 in the PP/EPDM/NBR ternary TPV showed the optimal comprehensive performances. Peng et al. [184] found that in PP/EPDM/NBR ternary TPVs prepared by dynamic vulcanization, at high content of NBR, EPDM could not encapsulate NBR completely, which led to the formation of imperfect core-shell structure. Therefore, the mechanical strength and processability of the TPVs decreased. The imperfect core-shell structure hindered the stress transmission between different phases and the elasticity recovery of the TPVs [184].

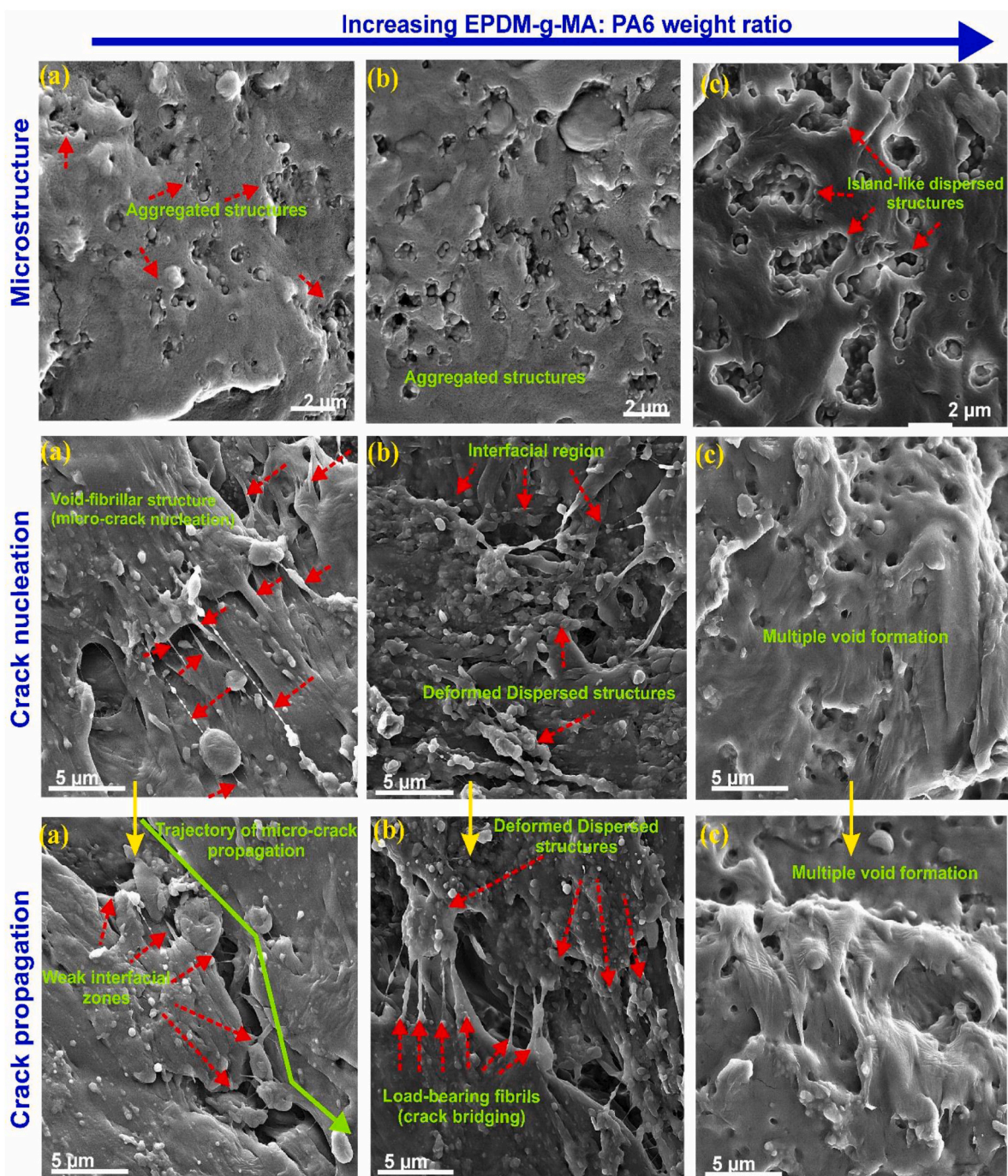


Fig. 16. morphology development and micromechanical deformations under impact test in PP/PA6/EPDM-g-MA (70/30-x/x) blends as a function of PA6:EPDM-g-MA proportions. The EPDM-g-MA was etched by cyclohexane for microstructural analysis. (reproduced from Mehrabi Mazidi and Razavi Aghjeh [179], with kind permission of Wiley-VCH GmbH).

Stiffness, strength, and toughness are the key parameters that determine whether a thermoplastic polymer material can be used as an engineering material. The core-shell composite droplets with a hard core and a soft shell are typical of two-phase modifiers. The dependence of mechanical properties of resulting blend on the structure of core-shell polymer domains is theoretically examined by a few researchers and the results are described in the following section.

9.3. Modeling of mechanical properties; stiffness and strength prediction

Materials combining stiffness with strength and toughness are very attractive. For engineering purposes, the modulus is among the most

important parameters, and several procedures for predicting the modulus of multicomponent systems have therefore emerged [185]. In multiphase polymeric systems when flexibilizing elastomers as well as reinforcing rigid phase are present in a matrix, the resulting modulus and strength depends decisively on morphology. Whether the elastomer component is present as a separate dispersed phase, as an elastomer shell around the rigid inclusions, or as elastomer subinclusions within rigid microphases will strongly influence the resulting stiffness and strength [185,93]. For designing advanced materials it is important to estimate the modulus for specified blend morphologies. Therefore, especially in the field of composite materials, various types of model calculations have developed. Such multiphase models have been proposed by

Takayanagi [186], Van der Poel [187], Hashin and Shtrikman [188], Christensen [189], Kerner [190] and many others. The popular Kerner model relies on a self-consistent approach and is of a more general form. A number of investigators [185,93,190] have shown that satisfactory predictions of the modulus in multiphase systems can be accomplished. The modulus of elasticity can be calculated according to the Kerner model, if the volume fraction, modulus, and Poisson's ratio of the constituent components are known. The Kerner model relies on the assumption of a perfect phase coupling, which means that deformation applied to the matrix is transferred completely across the phase boundary [190]. As for the polymer blends, this affords good adhesion between the matrix and the dispersed phase(s). In general, this is fulfilled in compatible blends or incompatible blends containing compatibilizers. The composite structure is modeled as a spherical dispersed phase particle surrounded by a concentric layer of the matrix resin. This particle is thought to be embedded in a continuous body having the (unknown) elastic properties of the composite. The unknown elastic properties are derived from the component properties by an averaging procedure that yields equation (7) for the shear modulus of the composite [185,190]:

$$\frac{G_c}{G_1} = \frac{\varphi_1 G_1 + (\alpha + \varphi_2) G_2}{(1 + \alpha \varphi_2) G_1 + \alpha \varphi_2 G_2} \quad (7)$$

where G_c , G_1 , and G_2 are the shear moduli of the composite, matrix and dispersed phase, respectively. The φ_1 and φ_2 are the volume fractions of the dispersed phase and matrix phase, respectively. The coupling parameter, α , is determined by the Poisson ratio μ of the matrix, as

denoted in equation (8).

$$\alpha = \frac{2(4 - 5\mu)}{(7 - 5\mu)} \quad (8)$$

The Young's modulus, E , is obtained from the shear modulus by equation (9):

$$E = 2G(1 + \mu) \quad (9)$$

The Kerner model is valid for inclusions of spherical geometry and random packing, and application to polymer blends therefore seems to be justified. Particle size, affecting the interface-to-volume ratio, and particle size distribution, affecting packing and agglomeration, are not taken into account. Rosch et al. [185] compared the modulus of elastomer-modified PP/PA (70/30) blends with different types of core-shell morphology, developed by using precompounding method and using different functionalized elastomers such as EPR-g-MA and SEBS-g-MA, to predictions derived from the Kerner model. The first morphology type was consisted of spherical PA6 particles with EPM-g-MA rubber subinclusions, prepared by precompounding the polyamide with the EPM-g-MA rubber. The other morphology types were comprised of core-shell particles containing PA6 cores encapsulated by EPM-g-MA or SEBS-g-MA rubber in the PP matrix, formed upon simultaneous mixing of these components. In core-shell blends, EPM-g-MA had a Young's modulus of only 4 MPa, therefore formed very soft interlayers whereas SEBS-g-MA with a rather high modulus of 100 MPa formed a stiffer rubbery interlayer around the rigid PA6 cores [185]. Then, the modulus of the total blend was calculated by using the modulus values of the isolated particles for the dispersed phase

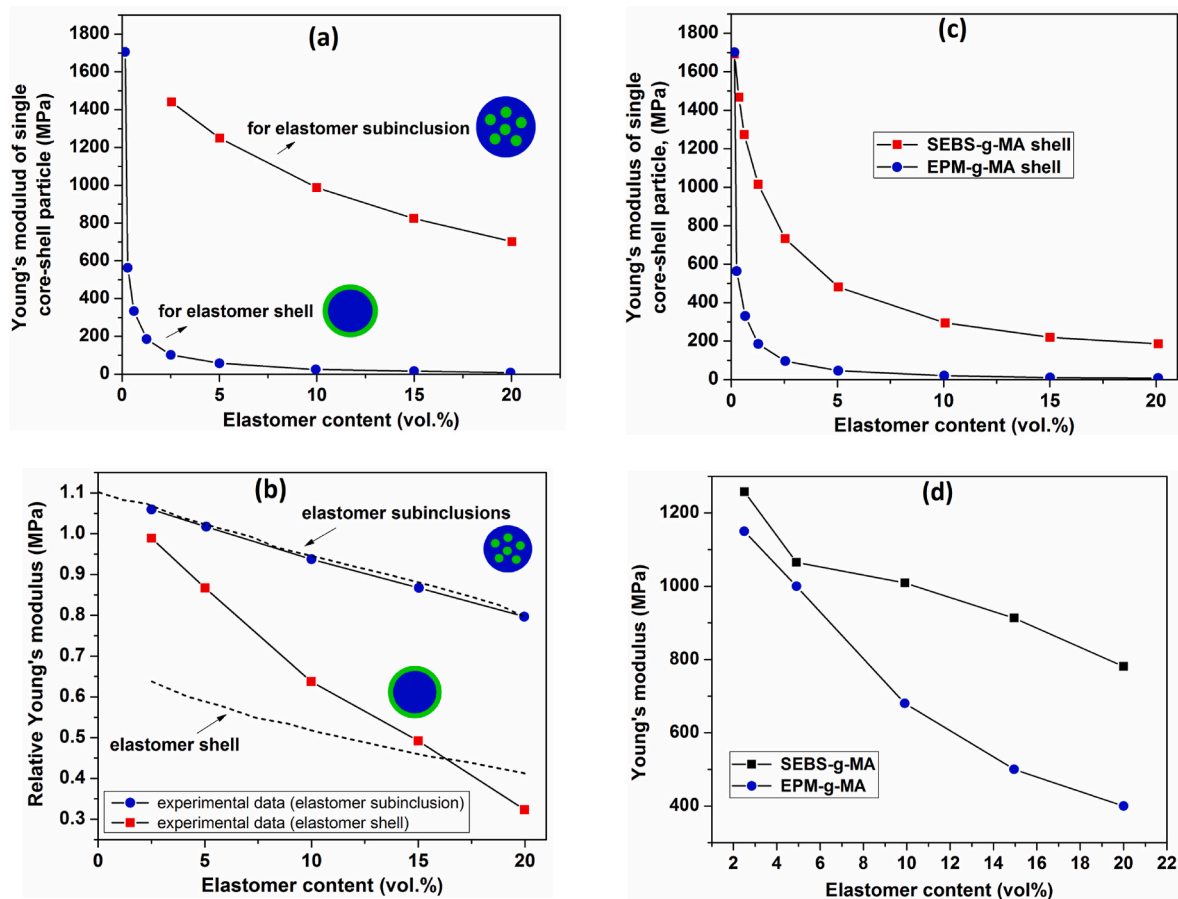


Fig. 17. (a) calculated moduli of isolated modifier particles for toughened PP/PA6 (70/30) blends in the case of elastomer subinclusions and elastomer shell. (b) comparison of calculated and experimental blend moduli as a function of elastomer content for elastomer subinclusions and elastomer shell. (c) calculated moduli of isolated core-shell particles in the case of EPM-g-MA and SEBS-g-MA elastomer shell. (d) calculated blend moduli as a function of elastomer content (redrawn after Rosch [185], with kind permission of John Wiley & Sons, Inc.).

(calculated using the Kernel model) and the stiffness of PP for the continuous phase. For the particles with EPM-g-MA subinclusions, PA6 was assumed to be the continuous phase and a Poisson's ratio of 0.39 was used. For the core-shell particles, the elastomer was assumed to be the continuous phase and a Poisson ratio of 0.49 for EPM was used. The calculated moduli for the isolated particles as a function of elastomer volume fraction showed that the presence of rubbery inclusions in the dispersed PA6 phase decreased stiffness of these particles only slowly, resembled the behavior of stiff PA6 particles (Fig. 17) [185]. By contrast, the particles with an EPM-rubber shell suffered from a dramatic drop in modulus. Even for small elastomer volume fractions, the modulus was decreased to the level of a pure elastomer (Fig. 17a for EPM-g-MA). Such core-shell particles should therefore lead to a strong flexibilization when incorporated into blends. In the case of the blend with elastomer modified PA-6 phases, experimental values agreed with the predicted ones. Experimental values of blends containing core-shell particles showed a steady decrease in the modulus, while the calculated values drop to a low level even for small elastomer volume fractions. At high elastomer volume fractions, experimental and calculated modulus values were at the same level, but for low elastomer volume fractions, they differed (Fig. 17b, for EPM-g-MA) [185]. For particles with stiffer SEBS-g-MA rubbery shell, the modulus of such particles decreased only slowly with increasing elastomer content (Fig. 17c, comparison of EPM-g-MA and SEBS-g-MA). Therefore, blends with stiff core-shell-type morphologies can be produced with PP/PA6 blends containing SEBS-g-MA. The moduli of blends containing SEBS-g-MA, are compared with calculated values using the Kerner equation according to the data shown in Fig. 17, Predicted and experimental values are in good agreement [185].

Only for low elastomer volume fractions do the predictions lead to higher moduli (Fig. 17d for SEBS-g-MA). Similar results were obtained by the Mehrabi Mazidi [93,94] considering the dependence of Young's modulus of PP/PA6/EPDM-g-MA (70/15/15) ternary blends on the phase morphology and, more precisely, on the distribution and location of PA6 and EPDM-g-MA modifier component in the PP matrix [93]. The authors studied the effect of mixing sequence of blend components on blend properties, which resulted in the developed different morphologies similar to those produced by Rosch et al. [185]. Different elastic moduli were obtained for ternary systems, depending on the location of rubbery phase in the blend systems, with highest elastic modulus for the blend in which the EPDM-g-MA was mainly located within the PA6 phase, and the lowest modulus for the blend in which the PA6 phase was completely engulfed by the EPDM-g-MA soft interlayer in the PP matrix [93,94]. Kolarik et al. [191] proposed a predictive scheme, based on a two-parameter equivalent box model (EBM) and the equations rendered by the percolation theory, for the simultaneous calculation of the modulus and yield (or tensile) strength of ternary polymer systems of various phase structures. The authors claimed that the predictive scheme will allow the experimentalists: (i) to anticipate selected mechanical properties of envisaged blends (for presumed phase structures); (ii) by comparing experimental and theoretical data, to assess to which percentage the potential of a material has been exploited; (iii) to analyze the phase structure of prepared ternary blends; and (iv) to evaluate interfacial adhesion or the extent of interfacial debonding [191]. An extended EBM suitable for modeling the PP/PE/EPR blends was obtained by adding the third element (corresponding to the EPR component) to both parallel and series branches of the EBM, and the related eq. assumed the following form for shear modulus:

$$G_P v_P = G_1 v_{1P} + G_2 v_{2P} + G_3 v_{3P} \quad (10a)$$

$$v_S/G_S = v_{1S}/G_1 + v_{2S}/G_2 + v_{3S}/G_3 \quad (10b)$$

where G and v are the shear modulus and volume fraction of different phases in the blend. In the case of PE/PP/EPR ternary blends with core-shell morphology, the yield stress fitted very well with the proposed

model whilst for modulus the experimental data were somewhat higher than the model ones, but the dependences were parallel. The authors concluded that the model with an EPR interlayer between PP and PE fits available experimental data quite well, which was in conformity with microscopic observations [192]. Saeb et al. [193,194] used a number of theoretical models to predict the modulus of HDPE/EVOH/PA6 blends of core-shell morphology as a function of EVOH-PA6 shell-core phase composition. All the models anticipated a decrease in elastic modulus with increasing EVOH/PA6 weight ratio in agreement with the experimental results. However, a negative deviation from the models was detected, and the Kolarik [191] and Barensten [195] models were closer to the experimental values. Li et al. [196] developed a model, similar to Ji's model [197] for calculating the tensile modulus of polymer nano-composites, from one phase modifier to two phases modifier to obtain the high impact thermal plastic polymer composites with less rigidity loss by optimizing the structure and the properties of the core and shell phases. The following Equations were obtained for modulus of composite material and modulus of core-shell particles.

$$\frac{E_c}{E_m} = \left(1 - \beta + \frac{\beta - \lambda}{(1 - \beta) + \beta \frac{E_s}{E_m}} + \frac{\lambda}{(1 - \beta) + (\beta - \lambda) \frac{E_s}{E_m} + \lambda \frac{E_d}{E_m}} \right)^{-1} \quad (11)$$

$$\frac{E_{cs}}{E_m} = \left(\frac{1 - \sqrt{\varphi_d}}{\frac{E_s}{E_m}} + \frac{\sqrt{\varphi_d}}{(1 - \sqrt{\varphi_d}) \frac{E_s}{E_m} + \sqrt{\varphi_d} \frac{E_d}{E_m}} \right)^{-1} \quad (12)$$

where E_c , E_m , E_s , E_d , and E_{cs} are the moduli of composite, matrix, shell phase, core phase, and core-shell particles, respectively. The φ_d is the volume fraction of the core in the core-shell particles, and λ and β are parameters relating to the mixing state and the composition of the composite [196]. By considering that the ratio of core-shell particles to matrix phase modulus (E_{cs}/E_m) equal to 1/10 is the most advantageous for the composite stiffness [198–201], the results of modeling studies of Li et al. [196] led to the following conclusions: (1) In order to obtain the high impact polymer composites with low rigidity loss, the modulus of the core should be as higher and the modulus of shell should be as lower as they can; (2) Comparing to one phase impact modifier, core-shell rubber particles toughened polymer composites can have less rigidity loss. The lowest modulus loss for the high impact PP can decrease from 26.1% for one phase modifier, to 13.5% for the core-shell modifier with PE core, and to 5.4% for the core-shell modifier with PP core; (3) The impurity, i.e. the rubber shell contains homo PP or PE and the core contains EPR, leads to the increase of the rigidity loss for the high impact PP alloys in reactor [196].

9.4. Micromechanical deformation processes (toughening mechanisms) during (in-situ) uniaxial tensile tests

Close examination of material's mechanical behavior under uniaxial tensile tests can provide useful information on the nucleation and propagation of various nano- and micro-deformations occurring in blends systems, and the role of dispersed modifier components on the activation of these processes can be studied. Obviously, in-situ tensile tests are greatly advantageous since they allow the monitoring of sequence of deformation processes from initiation to propagation, and final fracture of the material. Thus, to produce toughened polymer materials without significantly impairing other desirable mechanical properties, it is extremely helpful to understand in detail the micro-mechanical deformation processes which account for synergisms of high toughness and stiffness. Rosch et al. [202] used PA6, PA12, PA12 plasticized with N-butyl-phenylsulfonamide, and flexible PA36,6 as blend components in PP-based blends containing 30 vol % of these polyamides. Due to the surface tension gradient, the more flexible PA36,6

encapsulated the dispersed PA6 during melt processing and a core-shell morphology was observed for PP/PA6/PA36,6 blend. When the yield stresses of PA and PP were matched, large elongations at break of the resulting blends was achieved. Compared to PP/PA6 compatibilized with PP-g-MA, the in-situ formation of PA6/PA36,6 core-shell micro-particles gave much better performance, especially in terms of higher NCIS and elongation at break [202]. Upon straining, the more flexible shell underwent plastic deformation until voids were formed and the shell was ruptured. These energy-absorbing processes were accompanied by extensive yielding of the PP matrix. As a result of simultaneous plastic deformations and shell cavitation, multiphase PP exhibited improved toughness [202]. In order to characterize micromechanical deformation processes in PP/PA6/SEBS-g-MA blends, Rosch et al. [137] and Kim et al. [203,204] carried out in-situ tensile experiments in an HVEM at room temperature. In PP/PA6 (70/30) blend toughened by 5 wt% SEBS-g-MA with a percolated morphology of core-shell particles, fibrillized cavitation was observed at the interface of PA6 inclusion and surrounding SEBS-g-MA layer [137], reflecting excellent interfacial adhesion. As a result of percolation, this fibrillized cavitation, combined with shear yielding, involved a much larger sample volume and dissipated impact energy effectively. Percolated structures were functioning similar to larger rubber particles embedded in the PP matrix. The nucleation and development of fibrillized cavitation process during the in-situ uniaxial test in PP/PA6/SEBS-g-MA (70-x/30/x) ternary blends of core-shell morphology having different dispersed structures (discrete, intermediate and percolation structures) was further closely examined and proposed by Kim et al. [148,149,203,204]. According to the microscopic observations (Fig. 18a), the process of fibrillation at the interface between matrix and dispersed particles was described as follows [148,149,203,204]: During the in-situ uniaxial tensile test, at first, the SEBS-g-MA shell is slightly stretched in the tensile direction. Once the strain of the shell has reached a certain critical value, a microvoid is formed at the interface between the PA inclusion and the SEBS-g-MA phase in the polar region of the modifier particle, and simultaneously homogeneous shear yielding of the matrix between the particles is activated.

With increasing strain of the rubbery shell, successive formation of microvoids is occurred in the longitudinal direction of PA inclusion toward the equator. Until no further successive microvoids form in the stretched rubbery shell, the microvoids already created elongate in the direction of applied stress and intense shear yielding easily develops in the matrix around the particles [203,204]. This deformation process was defined as a *fibrillized cavitation process*. This fibrillized cavitation begins primarily at larger particles and jumps to smaller particles in the neighborhood with increase of strain. As soon as a particle cavitates, a shear yielding propagates in the matrix around this particle until it reaches another particle, which cavitates in turn. The number of cavitated particles must increase steadily with strain, the damaged particles being located along inclined lines. The prerequisite for this kind of fibrillized cavitation is a strong interfacial adhesion between the PA inclusion and the surrounding matrix (Fig. 18a) [203,204].

Fibrillized cavitation, which predominantly formed between the PA inclusions inside percolation structures, was clearly recognized for blends of different SEBS-g-MA contents, i.e. different dispersion states (Fig. 18b and c). The dispersed clusters are strongly elongated in the tensile direction and the fibrils at the interface remain without breaking down. Simultaneously, microvoids form by the fibrillized cavitation process, which occurs predominantly inside clusters [203,204]. As a result of tilting of clusters, successive microvoid formation and a continuous plastic growth of microvoids themselves, a more intense shear yielding of the matrix occurs in the whole specimen, which effectively dissipates the applied energy. This micromechanical deformation process has been defined as multiple cavitation with fibrillization inside the cluster. From the findings obtained during the in-situ electron microscopic investigation, a model illustrating a three-stage mechanism was proposed [148,149,203,204]: stage I, stress

concentration; stage II, void and shear band formation; stage III, induced shear yielding (Fig. 18b and c). Due to the differences of the Poisson ratio and the bulk modulus between the matrix and the dispersed modifier particles, the maximum stress concentration occurs at the equator of modifier particle (Fig. 18). This stress concentration gives rise to a higher hydrostatic stress inside the particle. This triaxial stress causes a slight volume dilatation in the interior of rubber particles (Fig. 18). Once the triaxial stress has reached its maximum, one microvoid appears in the plastically stretched rubbery shell at the pole of modifier particle causing partially release of triaxial stress (Fig. 18b and c, stage 2). With increasing strain, microvoid formation propagates from the pole to the equator of the modifier particle. With continuous growth of voids, shear band formation takes place in the matrix. Through the continuous plastic growth of voids and the propagation of new voids in the modifier particle, the triaxial stress will be further released, thereby considerably accelerating the plastic deformation of the ligaments of matrix material [148,148,203,204]. In stage III, when the polymer specimen is further strained, the fibrils break down at the interface and the plastic void growth may be facilitated: As a result, the shear yielding will be significantly enhanced in the matrix.

According to the Kim et al. [203,204] the successive deformation processes can be divided into two regions: (1) the elastic region, and (2) the plastic region (Fig. 19). The stress concentration around particles, development of triaxial stress state followed by small volume dilatation in the interior of rubber particles, where some applied energy (E_D) is dissipated, all take place within the elastic region, because on removal of the external load the specimen fully recovers. Until the maximum triaxial stress is reached, the microvoid formation occurs in the specimen, which is caused by either cavitation or debonding processes depending on the types of modifier particles. Through the initiation of microvoids, the extra additional applied energy (E_V) in the specimen is dissipated. Once the microvoids are formed in the matrix, the hydrostatic stress caused by stress concentration is released, with the stress state in the ligaments of matrix material between the voids being converted from a triaxial to more biaxial or uniaxial tensile stress state [203, 204]. This stress state is significant for the initiation of shear bands. The microvoids gradually grow in the applied stress direction with increasing strain in the specimen. Through the continuous plastic growth of voids, the triaxial stress will be further released, by which the plastic deformation of the ligaments of matrix material is considerably accelerated. For these processes the applied energy through the growth of voids (E_{GV}) and the plastic deformation of matrix material (E_M) is dissipated. Cavitation or debonding process itself contributes to a small part of energy dissipation, but it plays an important role for the activation of further plastic deformation of matrix material [203,204].

The formation of void-fibrillar structures around and/or inside the core-shell dispersed structures under uniaxial tensile fracture tests has also been reported by Mehrabi Mazidi and Razavi Aghjeh [179] for PP/PA6/EPDM-g-MA ternary blends of different PA6:EPDM-g-MA compositions. The detailed fractography studies revealed that the dispersed agglomerated structures act as crack nucleation sites and preferred crack propagation trajectories under both high speed impact and quasi-static fracture tests at low EPDM-g-MA content. The resistance to crack initiation and subsequent crack propagation was increased as the EPDM-g-MA content was increased in the blends. Multiple void formation, plastic growth of microvoids, development of void-fibrillar structure and shear yielding, and plastic deformation were found as the main sources of energy absorption and/or dissipation during the fracture tests (Fig. 20) [179].

The stability of void-fibrillar structure developed during mechanical loading to sustain greater stress and/or strains (without early breakdown and void coalescence) is claimed essential for stable shear yielding of the surrounding matrix and prevention of premature failure of the material as the load-bearing capacity of void-fibrillar structures postpone the microcrack nucleation and subsequent propagation within the material [179]. This stability is controlled by the level of interfacial

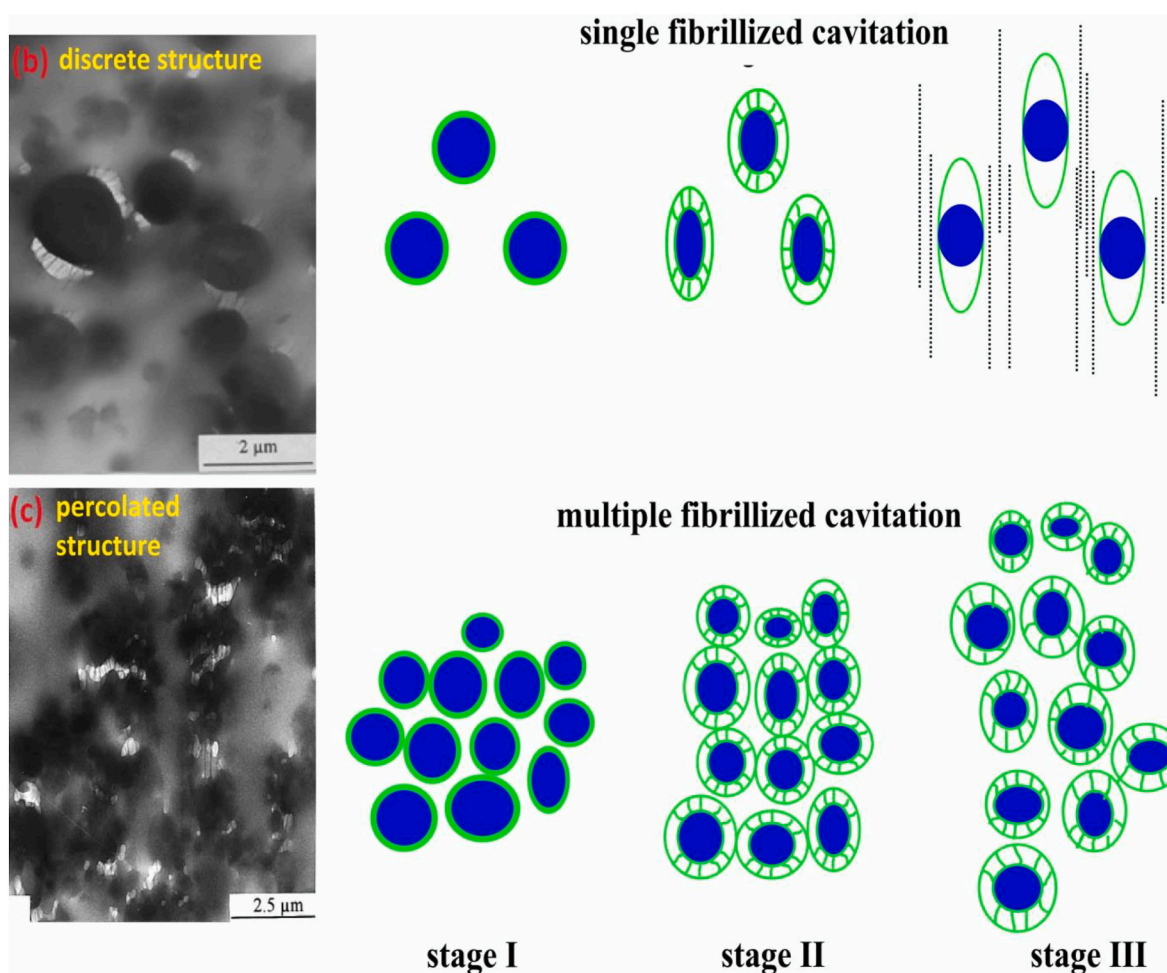
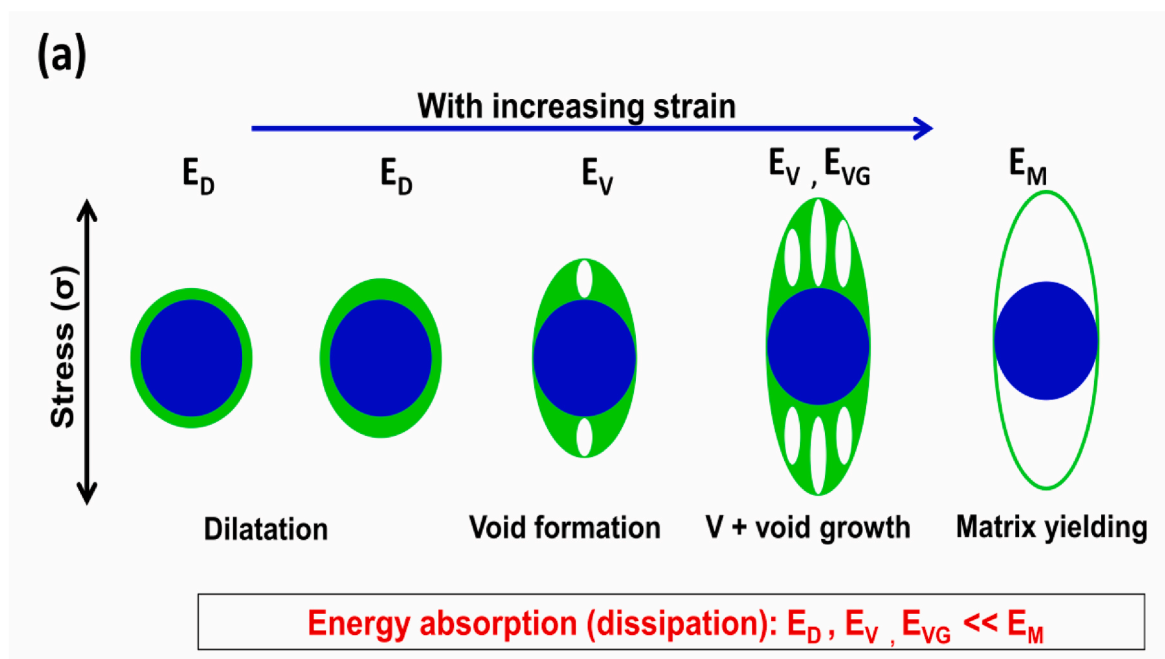


Fig. 18. (a) Schematic model of the micromechanical deformation process and associated energies in single core-shell particles (fibrillized cavitation): stress concentration, dilatation (E_D), void formation (E_V), and plastic void growth (E_{VG}). (redrawn after Kim et al. [148,149], with kind permission of Wiley-VCH Verlag GmbH). (b, c) TEM images from in-situ deformed PP/PA6/SEBS-g-MA (70-x/30/x) blends of various dispersion states of core-shell domains as well as the schematic representation of different stages of deformation processes during the uniaxial test for each phase morphology. (b) 2.5 vol% with discrete core-shells, and (c) 20 vol% with percolation of core-shells. (reproduced from Kim et al. [148,149,203,204], with kind permission of, John Wiley & Sons, Ltd.).

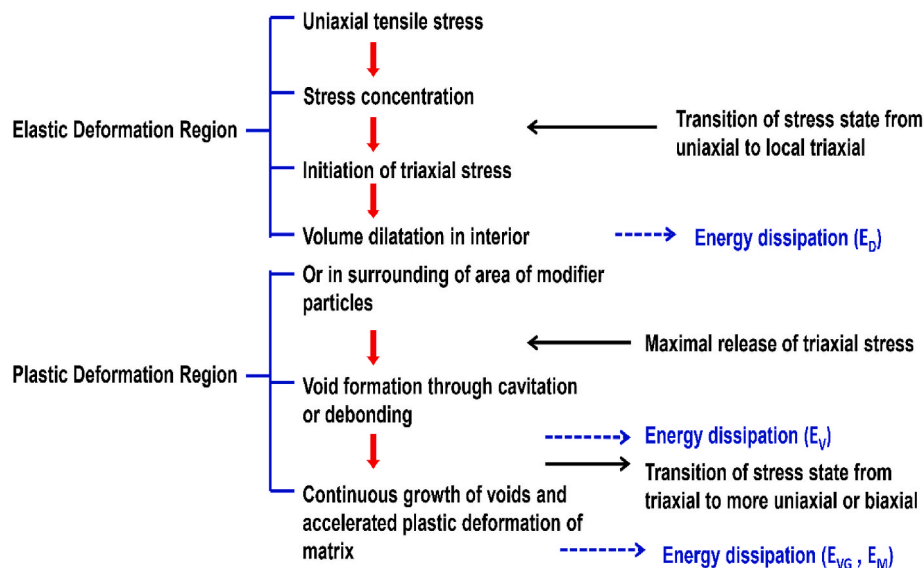


Fig. 19. Schematic illustration of energy dissipation and stress state during uniaxial tensile test. (redrawn after Kim and Michler [203,204], with kind permission of Elsevier Science Ltd).

adhesion and the thickness of rubbery phase located around PA6 core nodules within dispersed structures as well as at the interfacial region connecting the core-shell structures to the surrounding PP matrix (interfacial strength), which in turn, is governed by the EPDM-g-MA content for the blends prepared [179].

Considering the various micromechanical deformations operating in toughened blends of core-shell morphology, it is useful to get more insight into such microscopic phenomena in terms of their qualitative and quantitative contribution to the energy absorption capacity of the multiphase system. Dilatometry analysis can provide useful information on the proportion of shear yielding and dilatational micro/nano-deformations in these blends. This issue is examined in the following section.

9.5. Micromechanical deformations and volume strain

Tensile dilatometry involves measurement of volume strain during the slow uniaxial deformation of a polymer sample and has proven useful to elucidate the various processes that occur during tensile testing of single-phase and multiphase systems [79,205–212]. It is possible to estimate the contribution of shear yielding versus dilatational processes (crazing, cavitation, voiding, etc.) to the post-yield deformation of the material. Deformation by shear yielding occurs essentially without change of volume, and the total volume strain beyond the yield point is roughly that associated with the deformation in the elastic zone (i.e. Poisson dilation). Deformation by dilatational processes such as crazing, voiding and cavitation occurs with a significant increase of volume strain [79,205–212]. Tensile dilatometry cannot distinguish between these different processes, so it is useful to complement such measurements with electron microscopy techniques. Crazing is a very important form of damage in blends whose matrix is brittle. Decohesion of the particles from the matrix is another important damage mechanism in blends with ductile matrix and poorly adherent particles. Generally speaking, increasing the adhesion and/or thickness of the elastomer interphase around the particles reduces decohesion and favors cavitation [207–212]. The test procedure and the apparatus used for measuring the tensile volume strain are described in the relevant literature and are not elucidated here. The Hencky definition for strains (also called ‘true’ or ‘natural’ or ‘logarithmic’) was used by G’Sell et al. [213, 214] for determining of the volume strain, which led to the following equation:

$$\varepsilon_v = \varepsilon_1 + \varepsilon_2 + \varepsilon_3 = \ln\left(\frac{L_1}{L_{10}}\right) + \ln\left(\frac{L_2}{L_{20}}\right) + \ln\left(\frac{L_3}{L_{30}}\right) = \ln(V/V_0) \quad (13)$$

where axis x_3 is the tensile direction, x_1 the direction across width and x_2 across thickness. The V_0 and V are the initial and current volume of the representative volume element (RVE) under investigation in the tensile sample. Volume strain can be usefully decomposed in three contributions [213,214]:

$$\varepsilon_v = \varepsilon_v^{el} + \varepsilon_v^{pl} + \varepsilon_v^{ca} \quad (14)$$

The first term represents the elastic component that is related to Poisson’s effect by the equation $\varepsilon_v^{el} = (1 - 2\nu_{el})\varepsilon_3^{el}$, where ε_3^{el} is the elastic component of axial true strain. The second term, ε_v^{pl} , corresponding to plastic shear, is usually considered to be zero in metals, but it is shown that it can be slightly negative in some polymers [215], due to the compaction of macromolecular chains subjected to strain-induced orientation. The last term, ε_v^{ca} ; measures the contribution of cavitation and/or crazing to the macroscopic volume change of the tensile specimen [216]. Gonzalez-Montiel et al. [217] used tensile dilatometry approach to study the toughening micromechanisms in PA6/PP blends toughened by EPR-g-MA or SEBS-g-MA. Both the type of rubber modifier and the PA6:PP weight ratio in the blend affected the toughening mechanism. PA6/PP/EPR-g-MA blend showed both volume dilation and shear yielding during deformation. Dilatational processes were more prevalent at the early stages of the deformation for blends with PA6 as the matrix phase, whereas in blends where the PP formed a co-continuous or continuous phase the dilatational mechanisms became more prominent in the later stages of the deformation. The dilation resulted from cavitation of the rubber phase (in the PA6 matrix and interfacial region) as identified by electron microscopy. PA6/PP blends modified with SEBS-g-MA showed negligible change in volume during slow tensile deformation with the exception of the 66/33 blend composition, where volume dilation was detected. The structure of the rubber modifier and its particle size were factors that contribute to the differences observed in the extent of cavitation of PA6/PP blends modified with SEBS-g-MA or EPR-g-MA [217]. Bai et al. [218] investigated the plastic damage behavior of PP-based PP/PA6/POE-g-MA blends under cyclic tension by SEM analysis. The true stress-strain, volume variation and energy dissipation were measured via a video-controlled tensile testing system. Based on the obtained results, these researchers concluded that the mechanical behavior depends

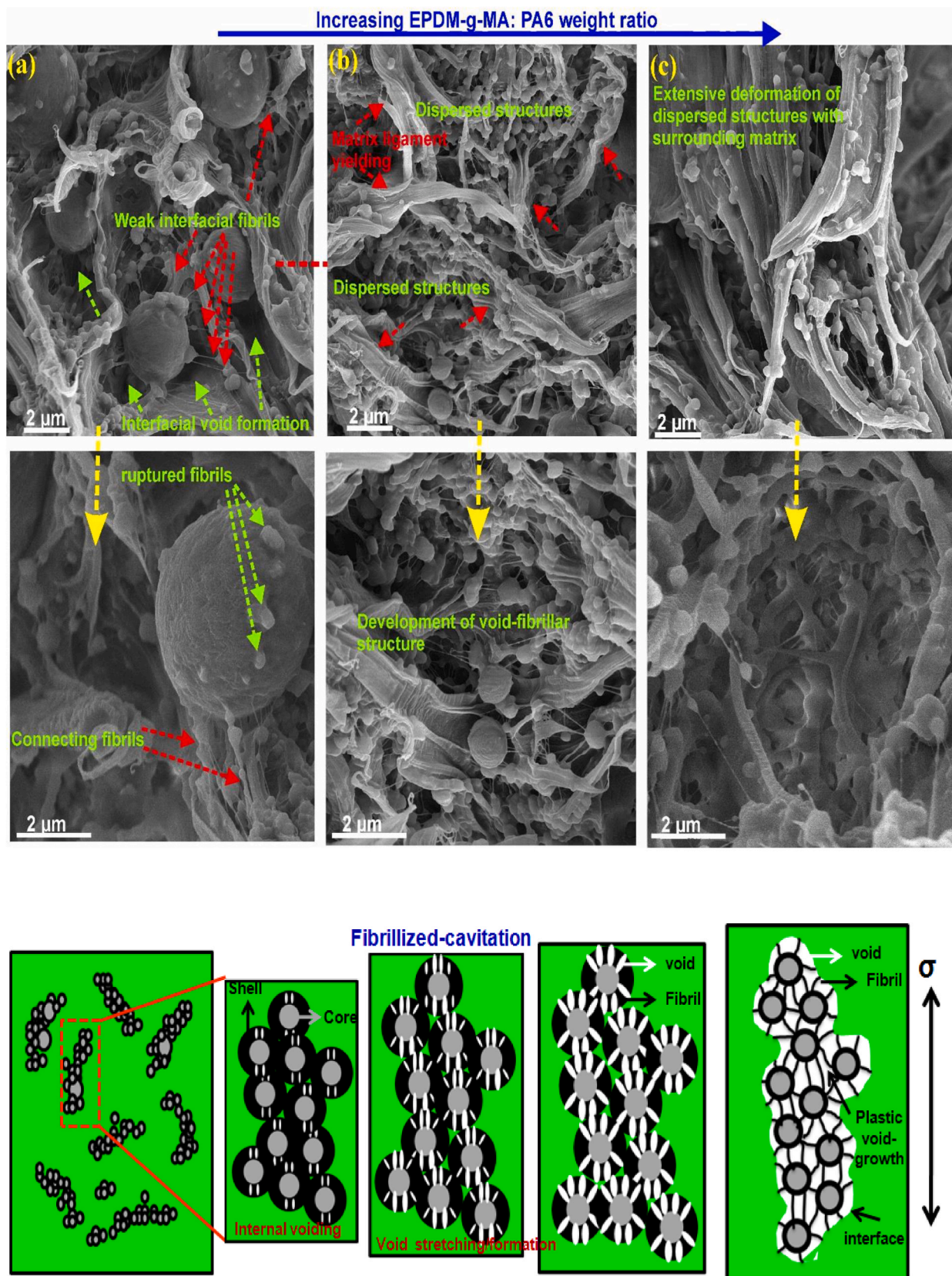


Fig. 20. (top) SEM micrographs showing the micromechanical deformations in PP/PA6/EPDM-g-MA (70/30-x/x) ternary blends containing 10, 15, and 20 wt% EPDM-g-MA fractured under quasi-static uniaxial tensile test. (below) Schematic representation of the sequence of micromechanical deformations around and/or within the core-shell structures accompanying the quasi-static fracture process. (reproduced from Mehrabi Mazidi and Razavi Aghjeh [179], with kind permission of Wiley-VCH GmbH).

strongly on the proportion of the blend's constituents. On the whole, with the increase of PA6 and POE content, (1) The yield stress and volume strain decreased, while energy dissipation increased, (2) The strain softening disappeared and strain hardening became important. According to detailed examination of the cryo-fractured surfaces under SEM, the volume dilatation was produced by the interfacial debonding at two poles of the particles (Fig. 21) [218]. The interfacial cracks transformed progressively into microcavities with the increasing applied strain. However, large volume strain corresponded to low energy dissipation. This result proved the basic viewpoint for the toughening mechanisms of polymer blends, i.e. the energy dissipation is caused mainly by the matrix shearing deformation, instead of cavitation, which results in volume change [218].

G'Sell et al. [220] studied the volume dilatation during plastic deformation under uniaxial tension of PP/PA6/POE-g-MA blend using a video-controlled tensile testing method which allowed recording simultaneously axial strain, axial stress and volume strain while axial strain-rate was regulated at a constant value even after necking has begun. The mechanisms described above contributed to the overall dilatation of the material under tension, and it was not easy to assign to each process its relative importance in the recorded damage rate, Δ . The decrease of the damage rate (volume strain) at high alloying (both PA6 and POE-g-MA) content in the PP/PA6/POE-g-MA blends was explained based on the evolution of the microstructure itself. According to Bai and G'sell [218,220], the POE-g-MA elastomer tends to form more and more isolated nodules at high alloying content with respect to the proportion in the PP/PA6 interphase. As such, the contribution of these rubber-like nodules increases correlatively. It is probable that the two types of particles induced different mechanisms (Fig. 22). In the case of decohesion of the matrix from a hard nodule and/or cavitation in the rubbery interphase (Fig. 22a), large voids develop by stretching the matrix in the vicinity of the particle poles, while the matrix is unable to contract near the equator because of the rigidity of the particle. That induces locally a large axial strain, but very small transverse strains. It results that volume strain is very large $\Delta \approx 1$ [218,220]. By contrast, if cavitation occurs in rubber-like particles (Fig. 22b), it appears schematically that the material is free to contract transversally. It results that volume strain is small $\Delta \ll 1$. Consequently, the lower damage rate of blends with high alloying content with respect to neat PP was attributed to the enhancement of microscopic shear banding from the voids (decohesion and/or cavitation) formed early after the yield point (Fig. 22c) [218, 220].

Considering the mechanisms of volume dilatation during plastic deformation under uniaxial tension of PP/PA6/POE-g-MA blends of different alloying content (amount of PA6 and POE-g-MA), Bai et al. [219] found debonding and cavitation as the two factors that contribute to the volume increase of the blends studied. Interfacial debonding is preferentially observed at the poles of PA6 particles when the POE interphase was thin, that is in blends with low alloying content. The interfacial debondings were transformed into voids, and later into longitudinal cracks as plastic strain was increased. The cavitation occurred both at POE interphase around PA6 particles and in isolated POE particles. As the alloying content is increased, it was observed that: (i) interfacial debonding of PA6 particle decreased, (ii) POE cavitation increased, (iii) elongation of dispersed POE particles increased and, (iv) plasticity of the PP matrix was enhanced [219]. These evolutions explained the decline of volume strain along with a considerable increase of impact strength as the alloying content was increased. The dissipation of impact energy in the blends is probably due to following factors: (i) the isolated elastomer particles play a small but significant role in either arresting the cracks or at least reducing their propagation rate, (ii) the high adhesion of the interfacial layer avoids early decohesion at the POE interphase between the PP matrix and the PA6 particles, and is later capable of cavitation, (iii) the ellipsoidal geometry of the particles improves somehow the impact resistance thanks to its favorable orientation perpendicular to the crack propagation direction

[219].

As discussed above, the use of functionalized impact modifiers is essential for morphology control and producing improvements in the mechanical properties of blends under investigation in this paper. However, a research survey indicates that there is an optimum degree of rubber functionality which gives rise to the best dispersion state of modifier polymer components with core-shell structures which brings about superior mechanical properties for resulting polymer alloy, as clarified in the following section.

9.6. Effect of rubber phase functionality

Although functionalized elastomers as shell-forming components effectively promote compatibilization through improving dispersion and enhancing phase adhesion between the matrix and core-forming polymer in reactive ternary blends, there are numerous reports in the literature indicating that the use of functionalized elastomer in combination with its non-functionalized counterpart can even produce blends of superior mechanical performance, especially impact toughness, compared with the blend containing only the functionalized elastomer. Thus, Horiuchi et al. [22,23] studied the morphology and mechanical properties of PA6/PC blends containing SEBS, SEBS-g-MA or a combination thereof. The in-situ chemical reaction between the maleated SEBS and PA6 during melt mixing induced the encapsulation of SEBS-g-MA on the PC domains in PA6 rich blends, which improved the adhesion between PA6 and PC and thus the mechanical properties were enhanced. The use of both SEBS-g-MA and non-functionalized SEBS as compatibilizers provided significant change in the phase morphology, followed by a further remarkable improvement of mechanical properties of PA6/PC blends (Fig. 23). The encapsulation of SEBS around the PC domains became gradually incomplete by the use of both SEBS-g-MA and non-functionalized SEBS in the PA6 rich blends and at the same time the dispersed SEBS domains in the PA6 matrix enlarge with increasing the non-functionalized SEBS:SEBS-g-MA weight ratio, but the PC domains showed no drastic change in size [23]. The replacement of only 1 phr of SEBS-g-MA with unfunctionalized SEBS led to a remarkable improvement of impact strength from 130 to 600 J/m, indicating that SEBS-g-MA alone forms domains that are too small for effective toughening (Fig. 23) [23]. With an increase of the fraction of unfunctionalized SEBS, the domain size can go beyond the critical lower limit size and maximum impact strength can be achieved. As with the impact strength, the fracture strain also showed the maximum value when a certain combination of SEBS-g-MA and SEBS was used [23]. In the PA6/PC blends having a certain ratios of both SEBS-g-MA and unfunctionalized SEBS, the void formation at the PA6/PC interface promoted the shear yielding of the matrix and leads to a significant increase of the elongation at break and the impact strength [221].

The imperfection of the encapsulation by SEBS on the PC domains caused local debonding at the PA6/PC interface, but the debonding could not spread on the PA6/PC interface rapidly by the deformation of SEBS rubber located at the interface. Thus the voids located at the PA6/PC interface were in appropriate size, which promoted the local shear yielding of the matrix. According to these results, the authors [221] suggested that the level of phase adhesion and toughness of the interface are important in achieving high mechanical properties in incompatible polymer blends. The fracture mode progressed from debonding to partial drawing and fibril fracture by the use of a proper combination of SEBS-g-MA and SEBS. In the blends compatibilized with SEBS-g-MA alone, the dissipation of strain energy was insufficient and hence debonding occurred. On the other hand, in the blends compatibilized with SEBS-g-MA/SEBS combination, the SEBS phase encapsulating the PC domains were thick enough to deform significantly, to dissipate the energy effectively, and the PC domains were also fibrillated (Fig. 23) [221]. Wong et al. [222,223] studied the effect of rubber functionality on the microstructure and fracture toughness of PA6,6/PP blends modified by 20 wt% SEBS-g-MA of different MA contents. The authors

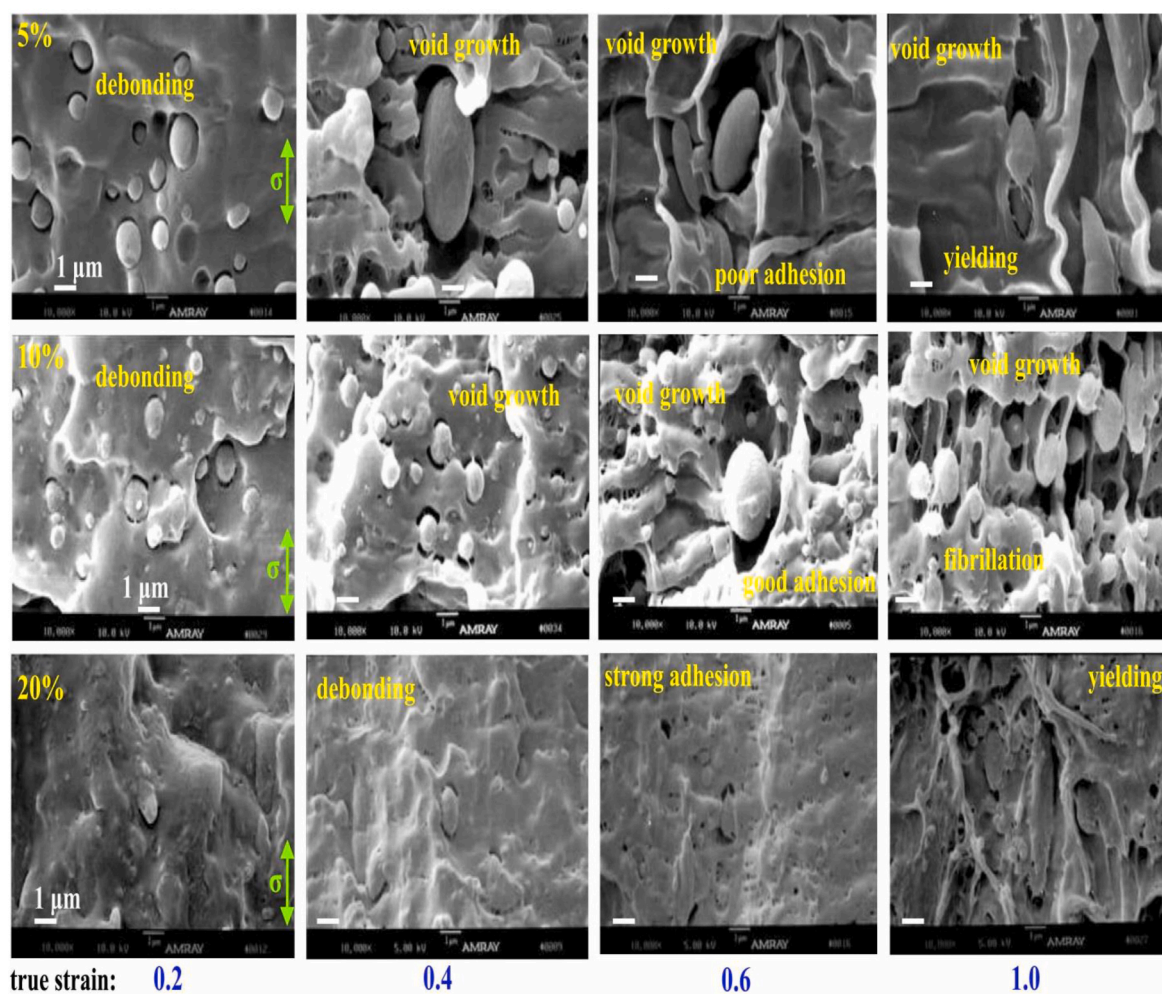
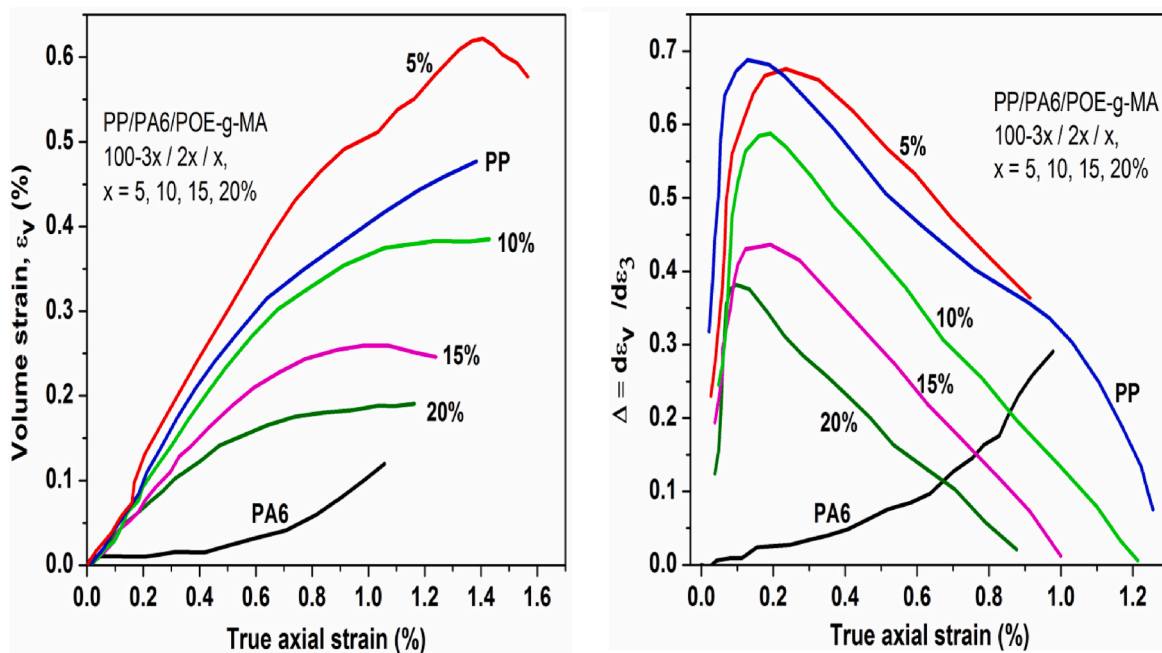


Fig. 21. (top) Volume strain vs. true axial strain, and evolution of damage rate vs. true axial strain for PP/PA6/POE-g-MA (100-3x/2x/x) blends of different compositions (x = 5, 10, 20 wt%) (redrawn after G'sell et al. [211], with kind permission of Elsevier Ltd). (below) SEM micrographs of Cryo-fractured surfaces of blends containing 5, 10, and 20 wt% POE-g-MA at different levels (0.2–1.0) of applied true strain (the deformation direction is vertical). (reproduced from Bai and Wang [218,219], with kind permission of Elsevier Ltd).

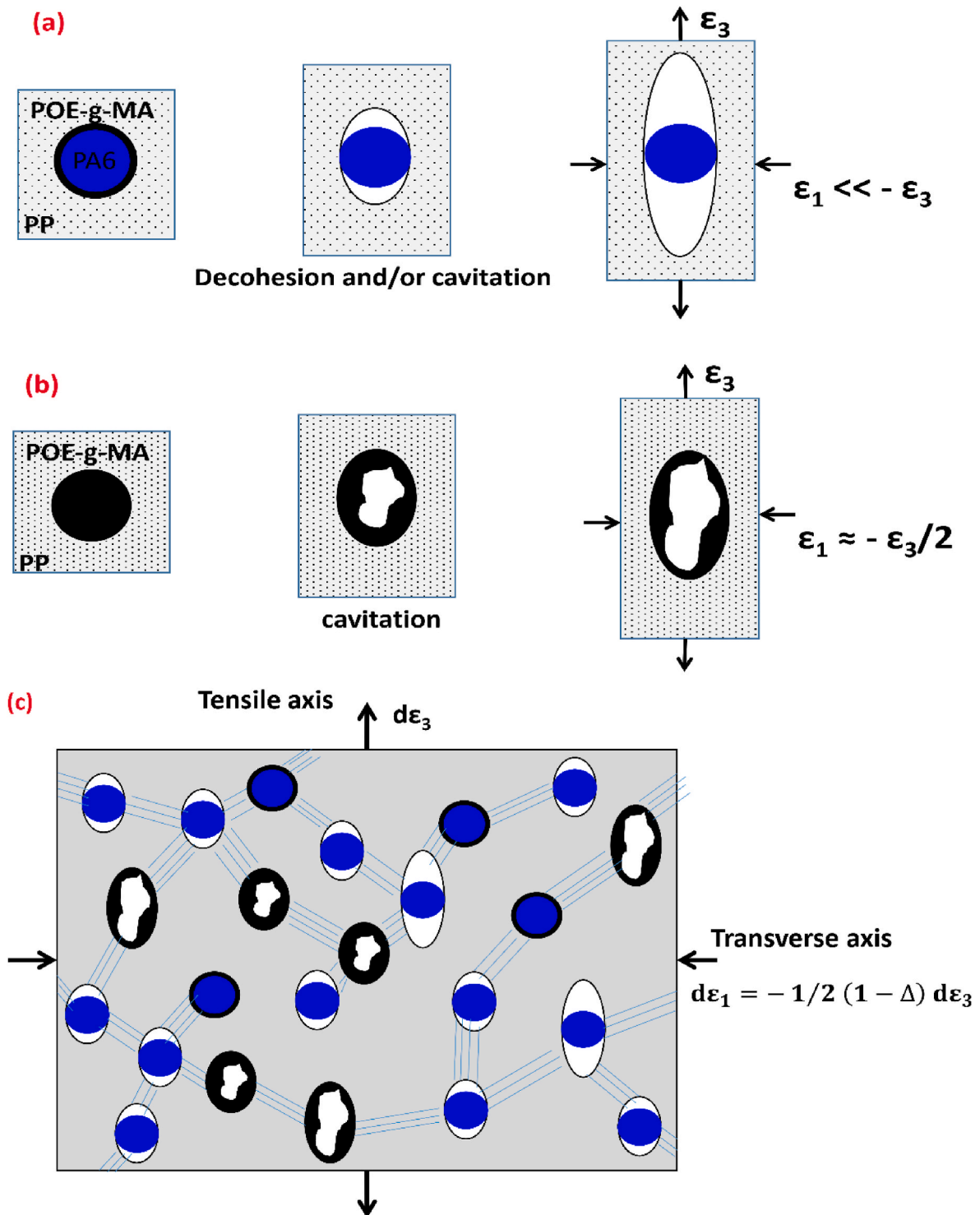


Fig. 22. Schematic model of contraction mechanisms under tension for PP/PA6/POE-g-MA blend. (a) by decohesion and/or cavitation of POE interphase at PA6 nodule; (b) by cavitation of isolated POE particle. (c) Schematic model of preferential activation of plastic shear between damaged particles. ϵ_1 , ϵ_2 , and Δ stand for transverse strain, axial strain, and damage rate, respectively. (redrawn after G'sell et al. [220,219], with kind permission of Elsevier Ltd).

prepared physical mixtures of non-maleated SEBS and maleated SEBS (having 1.84 wt% MA) at different levels at first to produce SEBS systems with various MA functionalities and then used them in the PA66/PP blends. For PA66/PP (75/25) blends, the SEBS inclusions in the nylon-rich matrices appeared to disperse in the nylon matrix and at the nylon-PP interface for blends with 0.74% or less MA content (Fig. 24). However, these SEBS inclusions formed aggregates in the nylon phase for blends at higher MA levels (Fig. 24). An optimized

morphology for maximum fracture-mechanical properties was found to exist in the 0.74%-maleated blend (Fig. 24) [222]. Tensile strength and stiffness increased with MA-grafted SEBS content in the 75/25 nylon 6, 6/PP blends but an opposite trend occurred in the 50/50 nylon 6,6/PP blends. Phase inversion occurred in the 50/50 system where PP became the continuous phase.

Migration of the functionalized styrenic block copolymers from the PP phase or nylon-PP interface to the nylon phase occurred in both

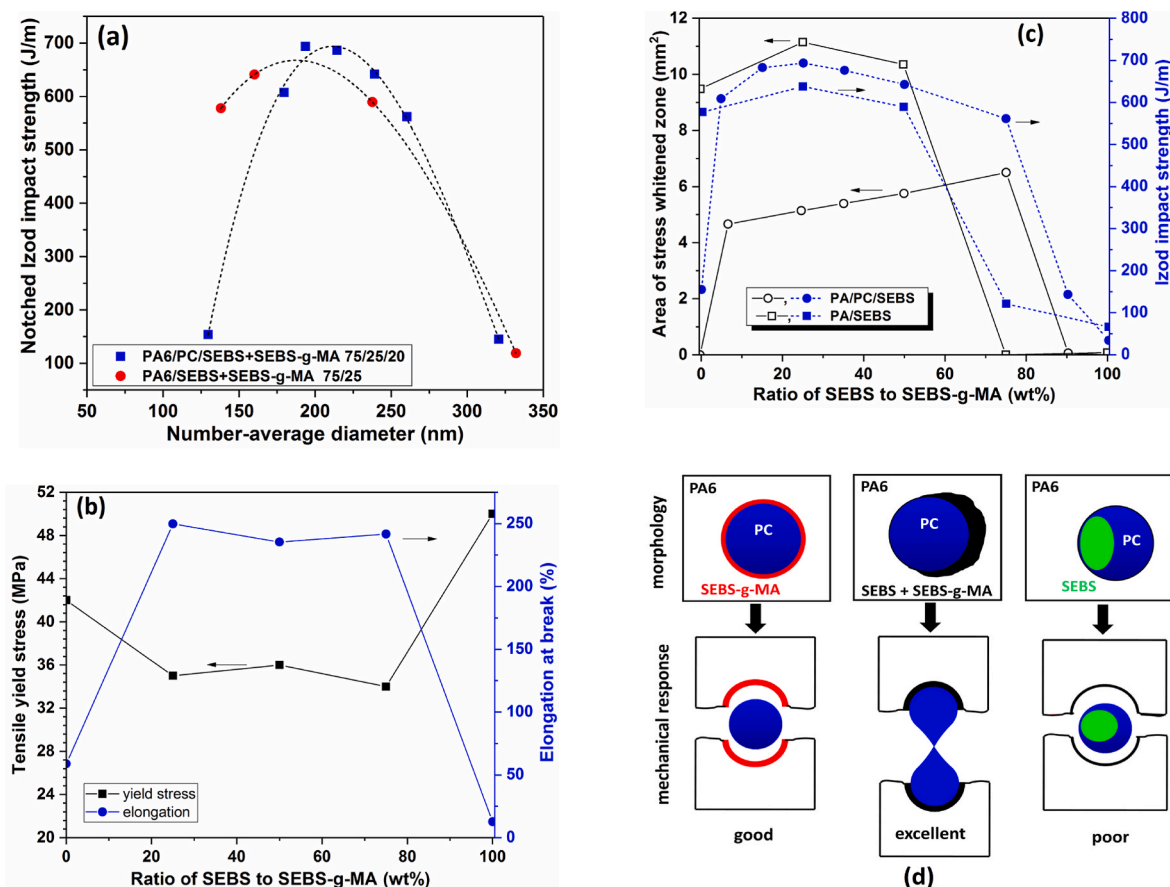


Fig. 23. Mechanical properties and macroscopic mechanical response of PA6/PC/(SEBS-g-MA + SEBS) (75/25/20) blends as a function of the ratio of SEBS to SEBS-g-MA. (a) Notched izod impact strength as a function of dispersed SEBS domain size. (b) Tensile yield stress and elongation at break. (c) Area of stress-whitened zone and the Izod impact strength. (d) Schematic illustration of morphology and corresponding fracture mode as a function of compatibilizer system used. (redrawn after Horiuchi et al. [22–24], with kind permission of Elsevier Science Ltd).

systems. An intrinsic strengthening behavior by the rigid polystyrene blocks of the functionalized SEBS copolymers was claimed to be the cause for stiffening in the nylon-rich blends [222]. It was concluded that nylon inclusions in SEBS-modified PP matrices did not provide any reinforcement effect because of the poor interfacial adhesion [222]. The fracture toughness of the blends was dramatically altered by the grafted MA level and intimately related to the phase morphology and microstructures. It was suggested that the tensile strength and ductility are two important factors that affect the fracture toughness of the nylon 6, 6/PP blends. While tensile ductility controlled J_C of the 75/25 nylon 6, 6/PP blends, tensile strength appeared to control J_C of the 50/50 blends (Fig. 24) [214]. Wong et al. [223] used DN-4PB tests to study the sequence of events and toughening mechanisms of these blends as a function of MA functionality of SEBS phase. It was found that under triaxial constraint interfacial cavitation followed by multiple crazing and subsequently massive shear yielding of the matrix contributed to an enormous toughening effect in core-shell microstructures observed in 0.92%-maleated blend [223]. The crazes were formed by micro-necking and cavitation of the SEBS sub-inclusions in the nylon phase (Fig. 24). These crazes had numerous microvoids and a fibrillar microstructure. Their prevalent presence also explained the large stress-whitened zone surrounding the crack tip. The crack tip triaxial stresses promoted the dilatational deformation (cavitation followed by multiple crazing). This was followed by the plane strain relief by the dilatational deformation, with the result of significantly enhanced distortional plasticity in the region adjacent to the crack tip (Fig. 24) [223]. Wilkinson et al. [224] studied the effect of reactivity of SEBS on the morphology and mechanical properties of PP/PA6/(SEBS + SEBS-g-MA) (70/15/15) blends.

The progressive replacement of SEBS with reactive SEBS-g-MA increased the degree of interfacial reaction between the SEBS and PA6 phases, reduced interfacial tension and provided a driving force for encapsulation of the PA6 by the SEBS. Consequently, the dispersed-phase morphology was transformed from two separate phases to acorn-type (partial wetting) composite particles, then to individual core-shell particles (complete wetting) and finally to agglomerates of the core-shell particles (Fig. 25) [224].

The resultant blends exhibited significant morphology-induced variations in both thermal and mechanical properties [224]. Regarding mechanical behavior, the blends generally exhibited inferior low-strain tensile properties (modulus and yield stress) compared to the matrix PP, but superior ultimate tensile properties (stress and strain at break) and impact strength upon progressive replacement of SEBS with SEBS-g-MA (Fig. 25). The transformation in dispersed-phase morphology driven by the reaction between the SEBS and PA6 phase produced a range of PP ternary blends with much superior ductility and impact-strength, compared to the base PP, but at the cost of significant reductions in modulus and yield stress [224].

Moini-Jazani et al. [225] studied the effect of SEBS:SEBS-g-MA weight ratio on the morphology and mechanical properties of PP/PC/(SEBS + SEBS-g-MA) (70/15/15) blends. In blend containing only nonreactive SEBS, PC particles were encapsulated by the SEBS phase to form core-shell composite particles. When SEBS-g-MAH is incorporated into the blend, the type of morphology and the size of dispersed phases changed from core-shell composite particles to a mixed of core-shell composite particles, individual particles and rod-like composite particles [225]. No significant change was observed in

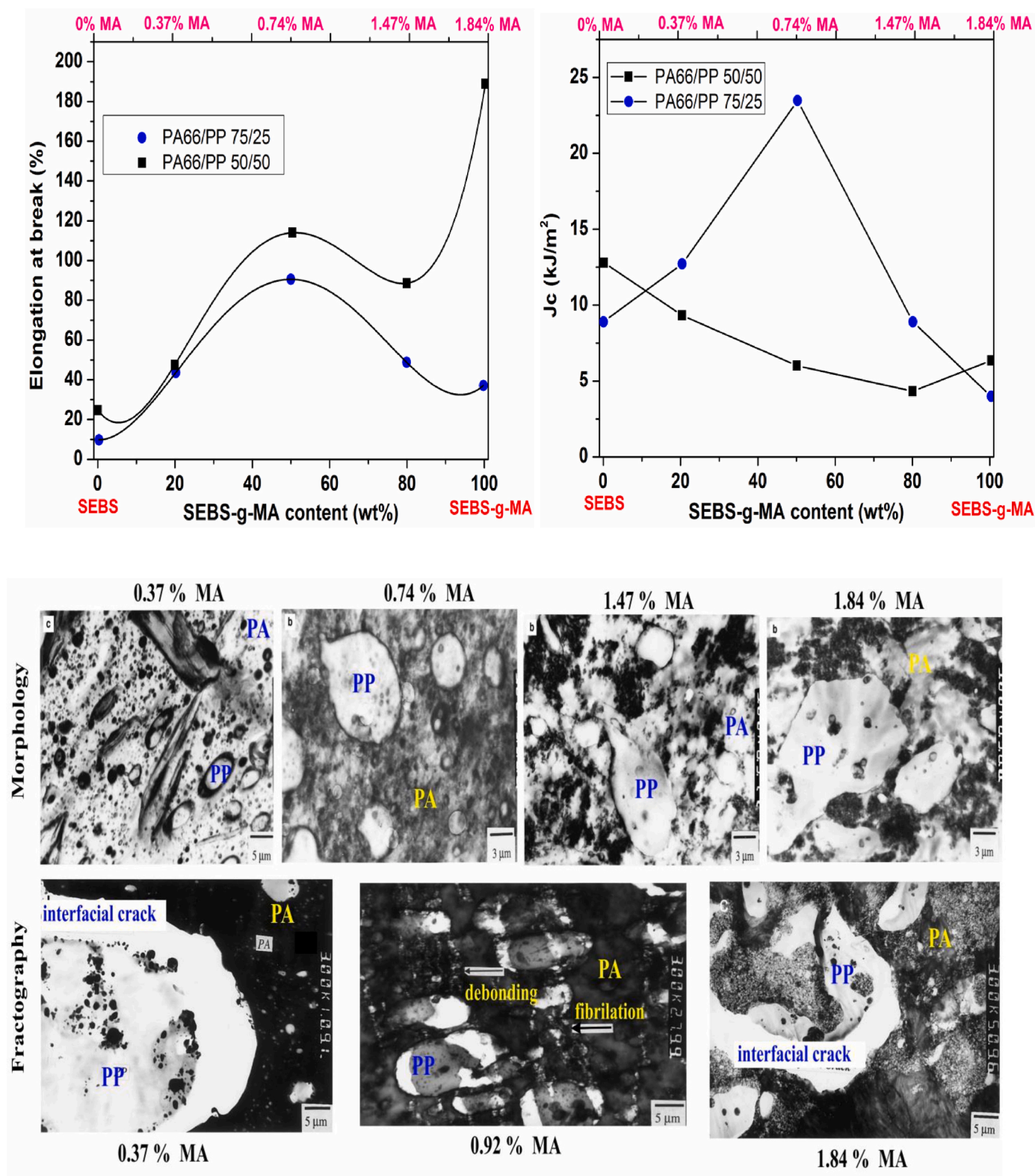


Fig. 24. Effect of rubber functionality on the elongation at break, J-integral fracture initiation toughness, phase morphology and micro-deformations of nylon 6,6/PP blends modified with 20 wt% SEBS-g-MA of various MA contents (0–1.84%). TEM photomicrographs are related to the modified nylon-66/PP 75/25 blends. (reproduced from Wong and Mai [222,223], with kind permission of Elsevier Science Ltd).

mechanical properties of the blends with various SEBS:SEBS-g-MA proportions; however, these blends exhibited significantly improved impact resistance, lower yield stress, and comparable elastic modulus compared with pure PP resin [225]. Mehrabi Mazidi et al. [226] studied

the effect of EPDM:EPDM-g-MA weight ratio on the morphology, mechanical properties, and work of fracture parameters of PP/PA6/(EPDM + EPDM-g-MA) (70/15/15) ternary blends. The phase morphology of the dispersed domains changed gradually from a coarse and separately

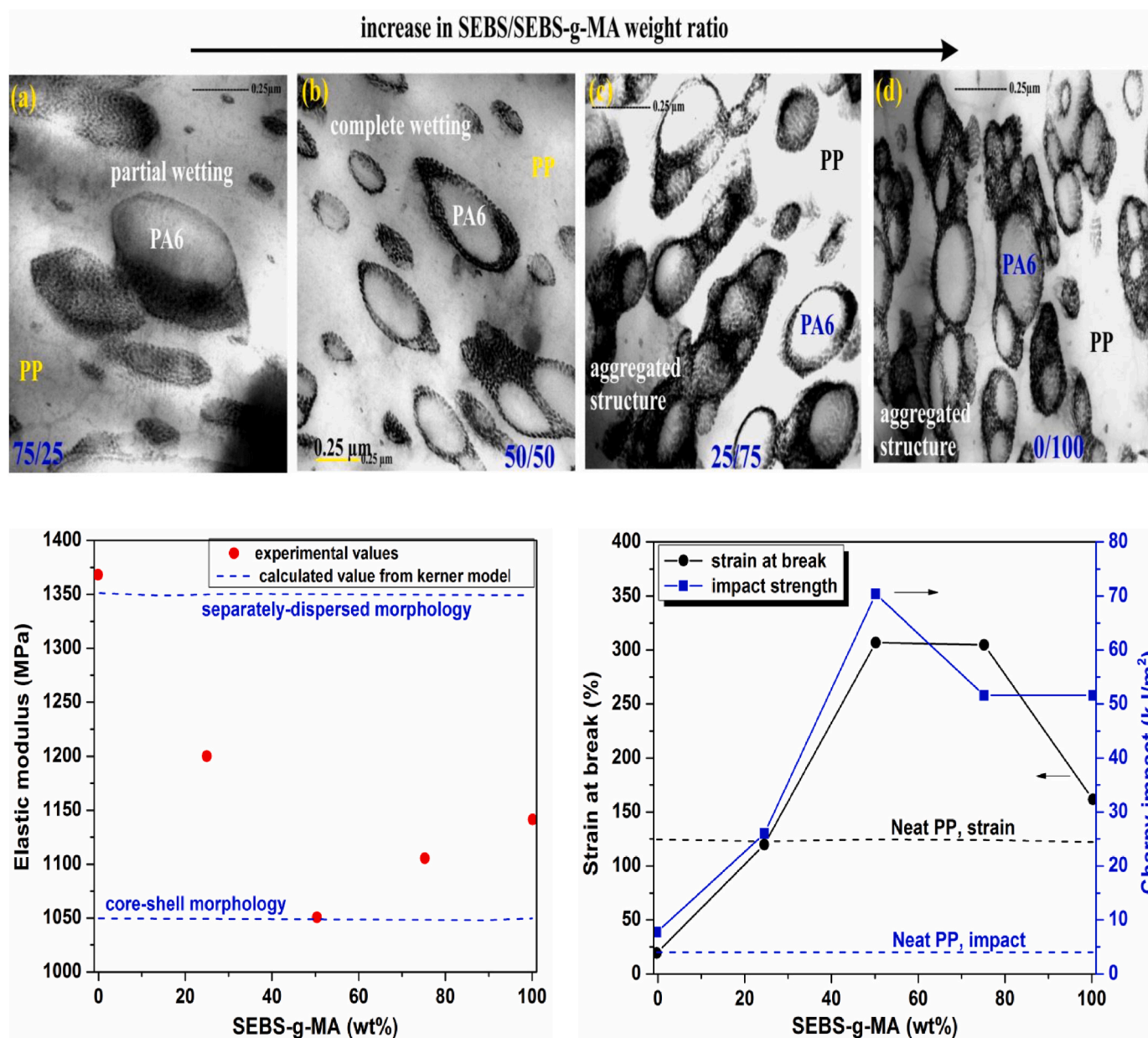


Fig. 25. (top) TEM images of PP/PA6/(SEBS + SEBS-g-MA) 70/15/15 blends containing various proportions of SEBS:SEBS-g-MA (reproduced from Wilkinson et al. [224], with kind permission of Elsevier Ltd). (below) trend of blend stiffness, tensile ductility and impact toughness as a function of SEBS-g-MA weight fraction. Comparison of calculated Young's modulus, E; (dashed lines) for PP/PA6/SEBS ternary blends with either (i) two dispersed phases (PA6 and SEBS) or (ii) a composite dispersed phase (core-shell particles of PA6 encapsulated with SEBS), and experimental tensile modulus. (redrawn after Wilkinson et al. [224], with kind permission of Elsevier Ltd).

dispersed PA6 and EPDM particles for blend with EPDM phase only to finer, aggregated PA6-EPDM core-shell structures with progressive replacement of EPDM with EPDM-g-MA in the blends, so that the blend containing EPDM-g-MA as the sole rubbery phase showed clusters of core-shell domains in the PP matrix (Fig. 26) [226]. The yield stress, tensile strength, and NIIS were steadily increased, whereas the elastic modulus, strain at break, quasi-static works of fracture (w_e and βw_p) and their tearing components were monotonically decreased with EPDM-g-MA:EPDM weight ratio. Thus, Mehrabi Mazidi et al. [226] claimed that the high speed impact tests conducted on relatively thick specimens mainly in the plane strain condition are far more sensitive to phase morphology, dispersion state and interfacial adhesion between the components than the low-speed quasi-static fracture mechanics tests conducted on the relatively thin sheets mainly in the plane stress state. The extent of stress-drop after yielding, i.e. strain softening during the

tensile tests gradually intensified with progressive replacement of EPDM with EPDM-g-MA component, suggesting more localization of deformation processes in the blends, which eventually led to less stable neck propagation zone and reduced ductility [226]. Although the change in morphology and dispersion state of PP/PA6 blends as a function of EPDM:EPDM-g-MA ratio was similar to what observed by Wilkinson et al. [224] for the same blend but modified by different SEBS:SEBS-g-MA ratios, the trend of the change in the mechanical properties was not the same for both rubbery systems.

The toughening of PK/PC (80/20) blends using a mixture of PA6/(SEBS + SEBS-g-MA) at 5 wt%/10 wt% was examined by Jeon et al. [227]. The morphology of the blend was changed with SEBS:SEBS-g-MA weight ratio. An encapsulated morphology in which PC was covered by SEBS and PA6 was observed for PK/PC/SEBS-g-MA/PA6 blend, but for blends containing a mixture of SEBS and SEBS-g-MA an incomplete

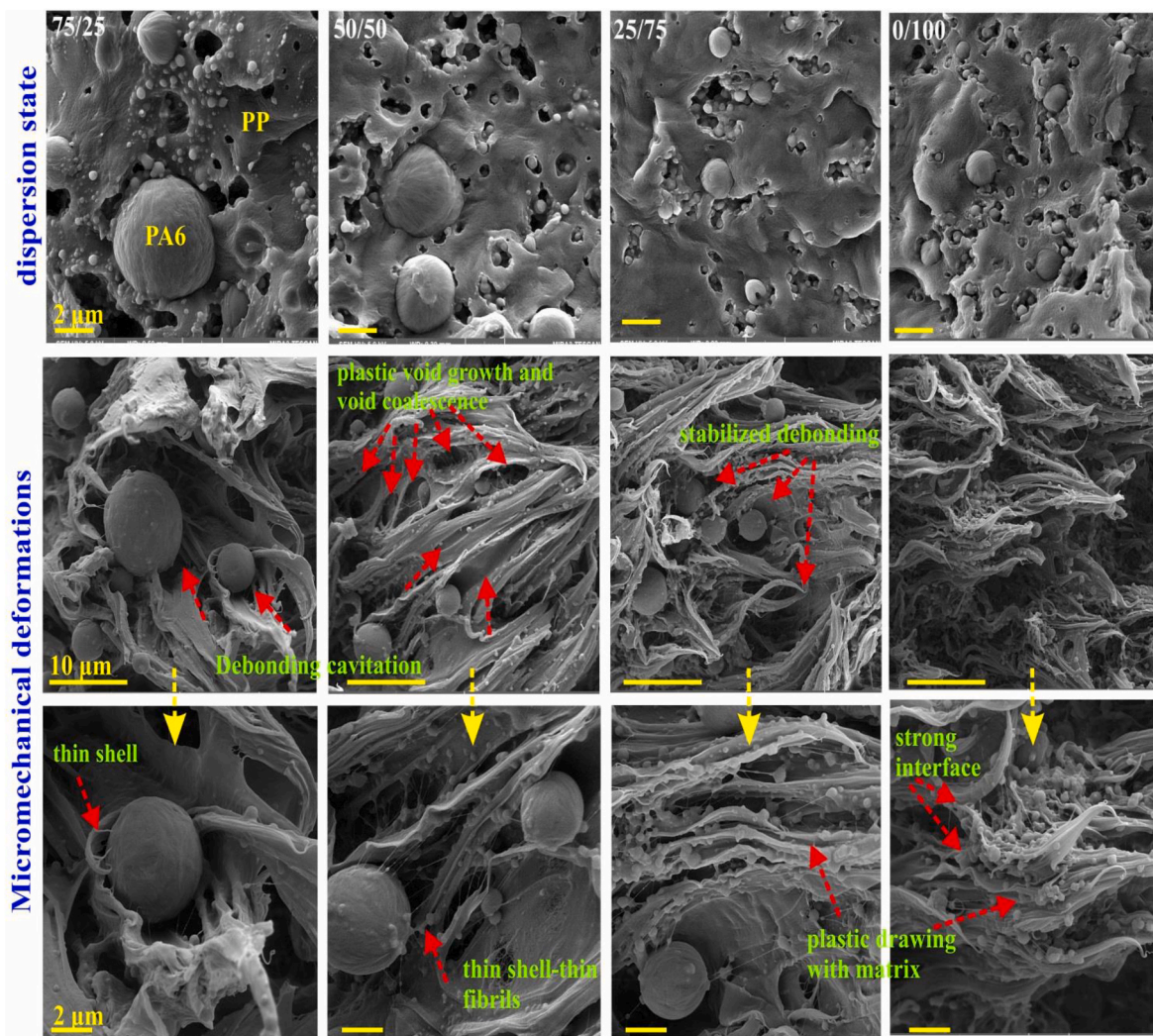


Fig. 26. SEM micrographs showing the change in the structure and dispersion state of modifier domains (first row) in PP/PA6/(EPDM + EPDM-g-MA) (70/15/15) blends as a function of EPDM:EPDM-g-MA ratio followed by the corresponding micro-deformations during quasi-static fracture test (second and third row). The EPDM and EPDM-g-MA are etched by cyclohexane for morphology analysis (first row). (reproduced from Mehrabi Mazidi et al. [226], with kind permission of Elsevier Ltd).

encapsulation was obtained. For blend containing only SEBS, the rubbery phase was separately dispersed in the PK matrix. This change in morphology was reflected in the mechanical properties of the blends. The presence of PA6 was beneficial to the tensile ductility and impact strength, and the modifier composition PA6/SEBS-g-MA/SEBS 5/7/3 had the best toughening effect in the PK/PC systems. Zare et al. [228] studied the impact of SBS:SEBS-g-MA weight ratio on the microstructure and ultimate performance of PP/PBT/(SBS + SEBS-g-MA) 70/15/15 blend. A gradual change in the structure of modifier domains from isolated phases to stack formation and then to encapsulation morphology was observed as the SEBS-g-MA proportion was steadily increased, which resulted in an improved blend homogeneity and finer dispersion of PBT domains with SEBS-g-MA concentration [228]. No change in the dispersion state of modifier domains (into aggregated or clustered structures) was detected with increase in SEBS-g-MA proportion and the blends revealed discrete core-shell particles. Young's modulus declined whereas yield stress, tensile strength, tensile ductility, and NIIS steadily enhanced upon progressive replacement of SBS with SEBS-g-MA in the blend, due to improved blend compatibility and interfacial adhesion. Increased resistance against particle debonding along with development of microvoids induced by rubber phase was responsible for enhanced impact fracture energy [228].

The literature findings reported above clearly reveal that in reactive ternary blends of core-shell morphology, the degree of core-polymer encapsulation, the shell thickness, the extent of interfacial strength (phase adhesion), and eventually the morphology and dispersion state of modifier polymers can be altered by using a combination of functionalized and non-functionalized rubbery phase as compared with using the functionalized elastomer alone. There are a number of evidence that the former elastomer combination can bring about substantial improvement in mechanical properties and impact resistance as a result of a change in the nano- and micro-deformations accompanying the mechanical tests compared with the latter blend system.

9.7. Effect of processing conditions (mixing order and feeding sequence)

In reactively compatibilized toughened ternary blends the morphology and performance of resulting blend can be highly influenced by a change in the sequence of mixing of blend components. Ohlsson et al. [229] studied the effect of mixing procedure on the morphology and mechanical properties of PP/PA6/SEBS-g-MA (47.5/47.5/5) blends. The blends were obtained using three mixing procedures, representing different ways of introducing the compatibilizer, (A) one-step mixing of the three components, (B) mixing a preblend

of SEBS-g-MA and PP with PA6, and (C) mixing a preblend of SEBS-MA and about one-third of the total amount of PA6 with PP and the rest of the PA6. In all blends the continuous phase was identified as PP and dispersed phase as PA6. Blends A and B had rather similar morphologies, differing mainly with respect to the size of the PA6 domains ($0.36\ \mu\text{m}$ in A and $0.85\ \mu\text{m}$ in B) [229]. The morphology of the blend C was considerably different from that of the other blends. In this case, the continuous phase contained dispersed phase domains of two different sized populations. Blend A showed the highest NCIS; the blend B exhibited the highest tensile ductility while the lowest values of Impact strength and elongation at break were obtained for blend C, due to the fact that a considerable fraction of the compatibilizer ended up in small, well dispersed phase domains with a high weight ratio of compatibilizer to PA6 [229]. Shokoohi et al. [230,231] employed Taguchi experimental design methodology to study the effect of barrel temperature ($220\ ^\circ\text{C}$, $230\ ^\circ\text{C}$, $240\ ^\circ\text{C}$), screw speed (90 rpm, 120 rpm, 150 rpm) and blending sequence on the morphology and mechanical properties of PP/PA6/(EPDM + EPDM-g-MA) (70/15/7.5 + 7.5) blends. The optimum processing conditions for the ternary blends to achieve balanced tensile and impact properties, were $220\ ^\circ\text{C}$, 150 rpm and blending sequence in which a master batch of (EPDM + EPDM-g-MA + PA6) was prepared at first followed by its blending with PP in the second stage [230,231]. Li et al. [232] investigated the dependence of phase morphology, interfacial interactions and properties of PA6/EPDM-g-MA/HDPE (70/15/15) blends on processing method. In one-step processing method, the EPDM-g-MA and HDPE were directly melt blended with PA6 matrix, whereas in two-step method EPDM-g-MA and HDPE were firstly melt blended in the twin-screw extruder, and then

the master-batch was blended with pure PA6. Compared with blend prepared by one-step method, more EPDM-g-MA component distributed on PA6/HDPE interface in blend produced by two-step method, which resulted in better interface adhesion between dispersed particles and PA6 matrix in the latter ternary system (Fig. 27) [232]. The NIIS of ternary blend prepared by one-step method was about one-third of that for the blend prepared by two-step method. The NIIS of ternary blends prepared by two-step processing method was remarkably higher than that of PA6/EPDM-g-MA (70/30) binary blend, although the rubber content of ternary system (15 wt%) was one-half of that of binary system. Accordingly, the authors concluded that the formation of core-shell structure in PA6/EPDM-g-MA/HDPE ternary blends can effectively improve toughness, and the perfection degree of core-shell structure, which is dependent on interfacial shell thickness, is also an important factor influencing toughness of blends [232].

In another report Yin et al. [233] further examined the fracture toughness and toughening mechanisms of these blends with focus on the shell thickness as the controlling factor of mechanical properties; hypothesizing that due to better distribution of EPDM-g-MA at the interface between PA6/HDPE in ternary blend, the blend prepared by two-step mixing method is more helpful to form core-shell structures with thicker EPDM-g-MA shell (Fig. 25). This was supported by the fact that large interfacial voids (as overlarge defects between core/shell particles and PA6 matrix) was observed for blend prepared by one-step mixing having thin EPDM-g-MA shell; while intensive plastic deformation without interfacial debonding and overlarge voids was observed for two-step mixed blend of core/shell structure and thicker EPDM-g-MA shell under impact loading (Fig. 27) [233]. Thus, the thicker

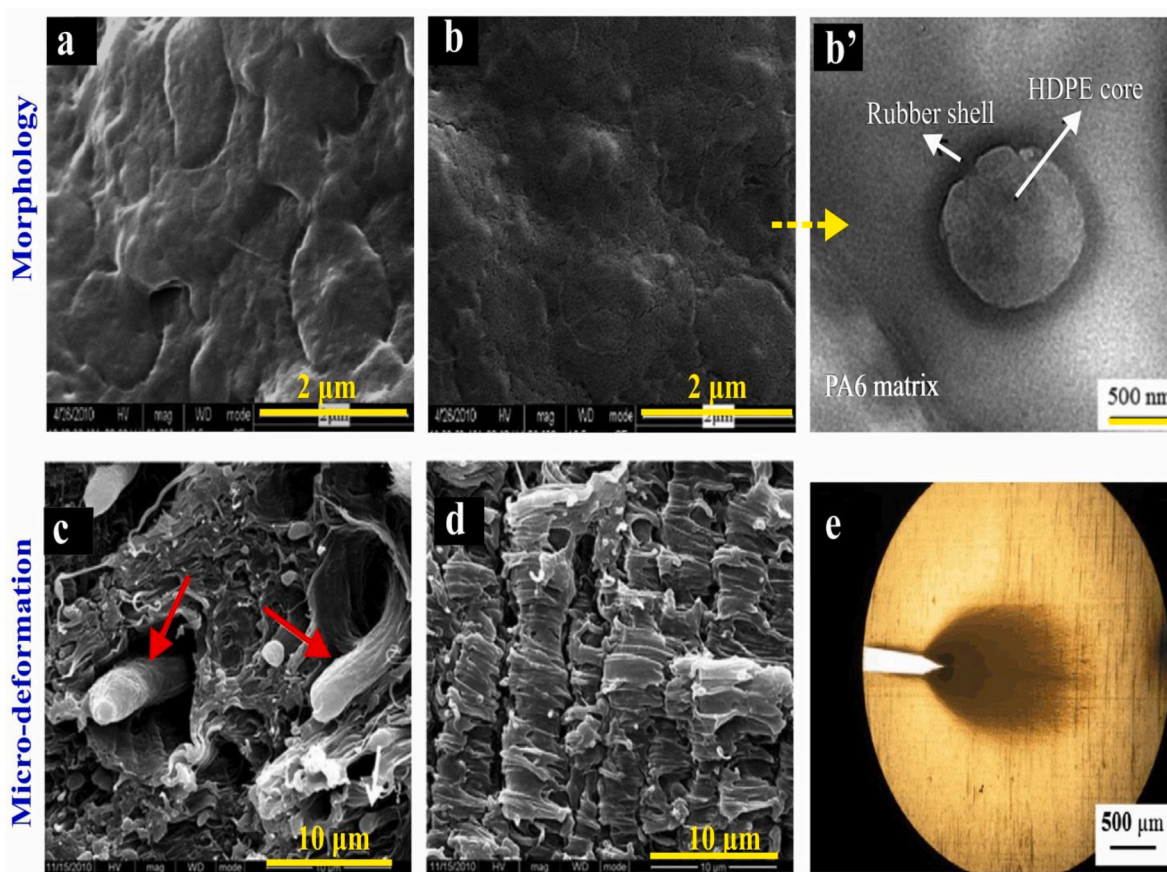


Fig. 27. Phase morphology and micro-deformations of PA6/EPDM-g-MA/HDPE (70/15/15) blend prepared by different mixing orders. (a, c) one-step mixing; (b, b', d, e) two-step mixing (PA6 blended with already prepared HDPE/EPDM-g-MA masterbatch). The micrographs (c) and (d) are related to the impact fractured samples, and optical image (e) is a crack-tip damage zone obtained under quasi-static fracture test. (reproduced from Li et al. [232] and Yin et al. [233], with kind permission of Elsevier Ltd).

EPDM-g-MA shell can prevent debonding at the interface region, ensure satisfactory stress transfer between the dispersed particles and the polymer matrix. The ternary blend prepared by two-step mixing method exhibited higher w_e value than the PP/EPDM-g-MA (70/30) binary blend under quasi-static fracture tests. However, the w_e value for ternary blend prepared by one-step mixing method sample was not reported by the authors [233]. Mehrabi Mazidi et al. [94,234] prepared PP/EPDM-g-MA/PA6 (70/15/15) ternary blends of core-shell morphology (core: PA6, shell: EPDM-g-MA) with greatly improved impact strength via different processing procedures. For blend A, the EPDM-g-MA and PA6 was directly melt blended with PP; for blend B, the EPDM-g-MA and PA6 were firstly melt mixed, and then the resulted blend master-batch was blended with PP; and for blend C, the EPDM-g-MA and PP were firstly melt mixed, and then the resulted blend master-batch was blended with PA6. The typical morphologies observed were similar to those reported by Ohlsson et al. [229]. For blend A the morphology was composed of agglomerated core-shell particles (sea-island type morphology) in the matrix. The phase morphology of the ternary blend B was composed of the mainly individual core-shell type dispersed particles containing big PA6 particles, together with small aggregates of these particles. In contrast with blend A and blend B, a homogeneous and much more uniform distribution of agglomerated core-shell particles were developed throughout the matrix material in the blend C, resembled to an "interconnected" structure of core-shell clusters with the PA6 particles inside the interconnected structures of far

more uniform size distribution than those in the ternary blends A and B (Fig. 28, a-d) [94].

The stress-strain response of these blends was strongly dependent on the mixing procedure employed, as a consequence of different morphologies developed in ternary blends (Fig. 28) [94]. The blend B showed the highest values of elastic modulus, yield stress and tensile strength whilst the lowest values of these parameters were obtained for blend C. The presence of rubbery phase in the interfacial region (as compatibilizer) and/or PP matrix (as toughener) is severely restricted upon two-step mixing for blend B preparation. The result was the formation of larger PA6 droplets in the blend B with the stress-strain behavior of ternary system close to that of PP/PA6 binary blend, that is, lowest tensile ductility and impact strength among the ternary blends (Fig. 28). For blend C a fine and uniform distribution of EPDM-g-MA particles throughout the PP matrix was developed during the first step of blend preparation which effectively improve the dispersion of PA6 phase domains within the matrix added in the second stage of blending. Consequently, a much more efficient performance of the rubbery phase as a compatibilizing agent (interfacial modifier) is achieved in the blend C as compared with other ternary blends. For this reason, this system represented the smallest Young's modulus among the ternary systems as the stiff PA6 particles were encapsulated by soft rubbery phase [94]. The higher interfacial adhesion between the components together with finer and percolated structure of core-shell particles in the ternary blend C not only increased the yield stress and ultimate strength of the material but

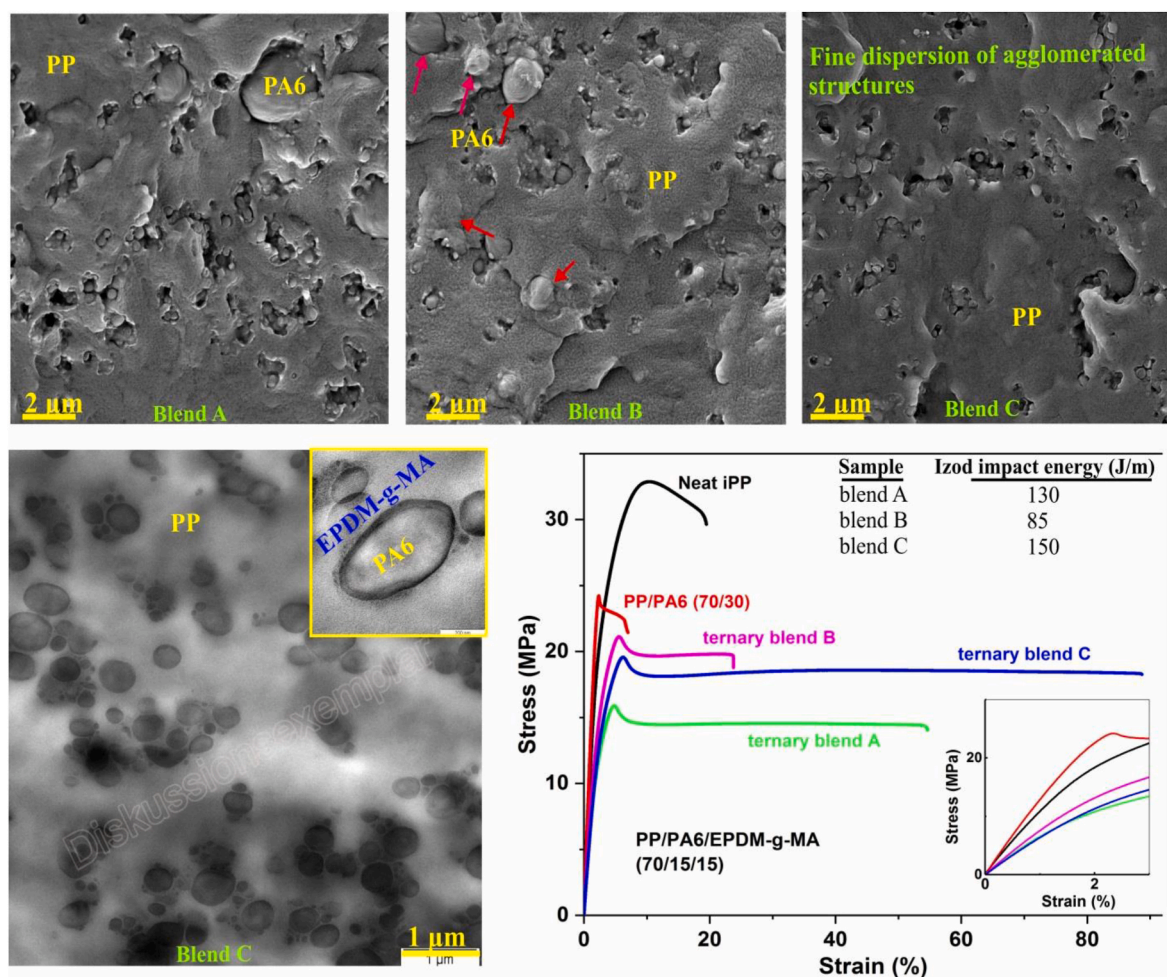


Fig. 28. phase morphology and mechanical response of PP/PA6/EPDM-g-MA (70/15/15) blend prepared by different mixing sequences. Blend A (simultaneous mixing of all components); Blend B (mixing PP with a separately prepared PA6/EPDM-g-MA masterbatch); and Blend C (mixing PA6 with a separately prepared PP/EPDM-g-MA masterbatch). The EPDM-g-MA was etched by cyclohexane for morphology analysis. (reproduced from Mehrabi Mazidi et al. [94,234], with kind permission of Royal Society of Chemistry and Elsevier Ltd.).

also would participate larger volume of material in the energy absorption processes, which in turn improved the tensile ductility and impact resistance of the blend. The NIIS dependence on the mixing order was exactly the same as what observed for tensile ductility. The lowest impact toughness was obtained for blend B, whereas the highest value was found for blend C, indicating that the development of a percolated structure of core-shell particles is more effective than the discrete clusters of core-shell particles in energy dissipation under the impact loading [94]. Under impact tests, shear yielding of the matrix material and micro-void formation within or around the dispersed agglomerates were detected for blend A; more significant interfacial voiding/debonding

and much less matrix shear yielding was observed for blend B. The relatively poor interfacial adhesion between the modifier particles and the matrix promoted crack formation during the impact loading, which results in very limited improvement in the toughness of blend B (Fig. 29). For blend C massive shear yielding and plastic deformation of the matrix was occurred, and the interfacial adhesion of dispersed structures with the matrix was strong enough to inhibit crack formation. In fact, the finer and more homogeneous dispersion of core-shell particles in the form of interconnected phase morphology was much more efficient in activation of extensive shear yielding of the matrix material in comparison with other dispersed phase structures. Percolated

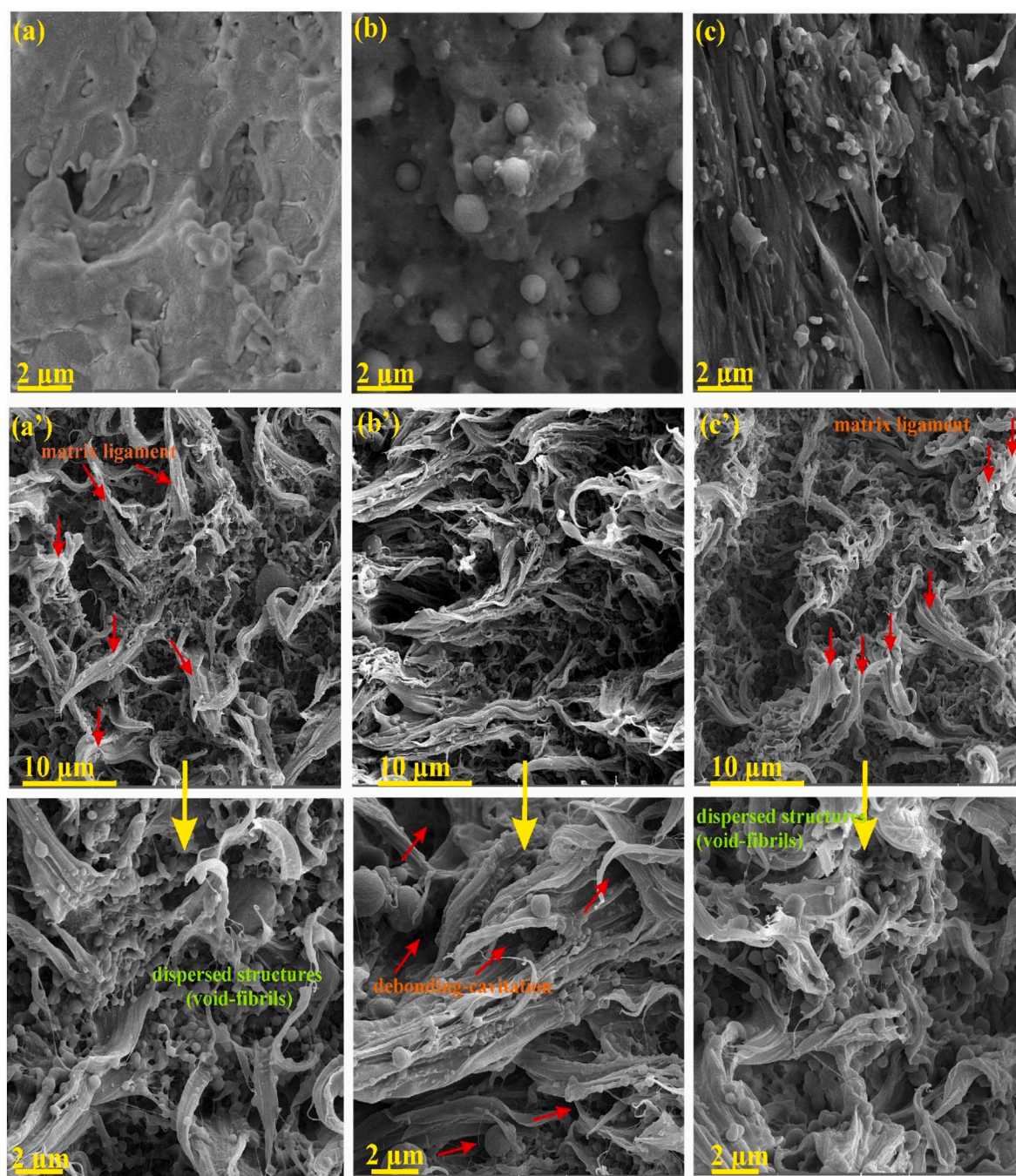


Fig. 29. Micrographs showing micro-deformations accompanying the fracture process under Izod impact (a-c) and quasi-static fracture mechanics (a'-c') tests for PP/PA6/EPDM-g-MA (70/15/15) blends prepared by different mixing sequences. (a, a') simultaneous mixing of all components, (b, b') mixing PP with a separately prepared PA6/EPDM-g-MA masterbatch, and (c, c') mixing PA6 with a separately prepared PP/EPDM-g-MA masterbatch. (reproduced from Mehrabi Mazidi et al. [94,234], with kind permission of Royal Society of Chemistry and Elsevier Ltd.).

morphology can enable the deformation bands to grow and thus consumes more energy before fracture [134–137,148,149,203,204,94]. Improved fracture energy may also be due to crack deflection around the dispersed structures. The discrete clusters and extended structures, in blends A and C respectively, could increase the impact toughness via preventing the crack propagation through the material. Moreover, it should be noted that overlapping of stress fields around the dispersed structures along with the crack deflection effects become progressively more pronounced as the dispersion state of modifier particles transforms into larger agglomerates and finally to percolated structures. The more continuous stress fields throughout the matrix material with higher intensity as a result of overlapping of stress fields, not only facilitates and, thereby, intensifies the shear yielding and plastic deformation of matrix material but also participates the much larger volume of the material in different energy absorption/dissipation processes [134–137,148,149,203,204,94]. The results of work of fracture parameters obtained from quasi-static fracture tests showed the same trend as what observed during impact tests: blend C > blend A > blend B, and the percolated morphology exhibited highest resistance to crack initiation (w_c) and subsequent crack propagation (βw_p) [234].

A network-like void-fibril morphology was generated in the blends during the quasi-static fracture test [234], and the voids were developed both inside the agglomerated/percolated structures and also at the interface between the dispersed structures and the surrounding matrix (Fig. 29). Strong adhesion between the matrix and dispersed structures led to destruction of agglomerated structures, followed by the elongation of the interconnecting fibrils together and the plastic growth of the microvoids either within the agglomerated structures or at the interface of agglomerates with the matrix (Fig. 29) [234]. This type of void-fibril formation has been attributed to the multiple cavitation/debonding of rubbery phase either as a shell around the PA6 particles inside the agglomerates or as an interfacial layer between the dispersed clusters and the matrix [134–137,148,149,203,204,234]. This fibrillized multiple cavitation phenomenon is an energy-absorbing viscoelastic process, which relieves the concentrated triaxial stress fields on the dispersed clusters to biaxial stress state on the surrounding matrix, promoting the shear yielding and plastic flow of the matrix [134–137,148,149,203,204,234]. Zare et al. [235] found that among the processing parameters such as mixing sequence, temperature profile, and mixing intensity (screw speed), the mixing order of blend components was the most important processing parameter that strongly affected the morphology and properties of PP/PBT/(SBS + SEBS-g-MA) 70/15/7.5 + 7.5 blends. A combination of core-shell and separately dispersed morphologies were identified in these blends. In their work, Zare et al. [235] found that the mixing order where the PBT, SEBS-g-MAH, and SBS components were melt blended at first and this pre-blend was then melt mixed with PP component in the second stage showed the highest impact strength. Highly toughened PP-based blends exhibiting nine-fold increase in notched impact strength with little loss in stiffness (<15%) compared to neat PP resin were successfully developed. Numerous void-formations in the matrix and around the dispersed PBT domains were found as the energy absorbing mechanism during impact loading [235].

In reactively toughened blends of core-shell morphology, the physical characteristics of the rigid core-forming polymer can also greatly affect the deformation behavior and energy dissipation capability of the resulting alloy under mechanical loads, as described in the following section.

9.8. Effect of stiffness of core forming polymer

The literature about the role of core-polymer physical properties on the performance of reactive blends of encapsulated morphology is very limited. Shi et al. [236] studied the morphology, mechanical properties and fracture behavior of PA6 toughened by Low molecular weight PB-g-MA containing different core-forming polymers, LDPE and PP. PB-g-MAH was first melt blended with PP with DCP as initiator and to

form PP-g-PB-g-MAH graft copolymer, and then the mixture of pre-modified PP was further blended with PA6. In the case of core-shell PA6 blends containing 5 wt% PB-g-MAH, the NIIS in PP-g-PB/PA6 blend was lower than that of LDPE-g-PB/PA6 blend, whereas the tensile yield strength and elastic modulus of the blends with PP core were much higher than those with LDPE core. The size of stress whitened plastic deformation zone around the impact-fractured samples was larger for sample with LDPE core than the sample with PP core. The results demonstrated that although the decrease of tensile modulus cannot be avoided with increasing impact strength, increasing the elastic modulus and yield strength of the core material in the rigid core-soft rubber shell toughener is an effective way to obtain a good balance of elastic modulus, tensile yield strength and impact strength [236]. Quite different impact-fractured surface patterns were detected depending on the core-forming polymer in the blends [236]. In LDPE-g-PB/PA6 blend, a large matrix void with many elongated fibrils derived not only from the rubber shell, but also included some LDPE and PA6 material drawn from the core and the matrix. Such fibrils were absent in the PP-g-PB/PA6 blends. Unlike the elongation and fibrillation of the LDPE core during impact testing, PP core could not be severely deformed [236]. In the zone near the notch tip the broken of rubber fibrils structures will result in discontinuous stress transfer in PP-g-PB/PA6 blend and relatively lower impact strength than that in LDPE-g-PB/PA6 blend (Fig. 30). In the fast crack propagation region on the fracture surface, no fibrillation was found in both core/shell toughened blends with LDPE core and PP core (Fig. 30), probably due to the very fast strain rate imposed on the materials. Contrary to the impact test, the PP core could be deformed and elongated during the slow strain rate tensile test. In this case, large fibril structures formed around the elongated PP phase can be stabilized in the whole tensile process [236]. According to the experimental results, a possible deformation mechanism of core-shell particles with different core material under different strain rates was illustrated (Fig. 30).

Although the toughness of PP-g-PB/PA6 blend was lower than that of LDPE-g-PB/PA6, their DBTT were very similar (around -10 °C). Utilizing the Corte and Leibler's model [237], these authors showed that the cavitation ability of the rubber particles in both blends is similar, suggesting that although the final impact strengths are different, the fibrillation ability of the rubber shell of the core-shell toughener with LDPE core and PP core are nearly the same, resulting in very similar brittle-ductile transition temperature of both blends [236].

As mentioned before, the morphology of polymer alloys is strongly influenced by the melt rheology of constituting polymers. Consequently, the macroscopic mechanical properties would also profoundly change with an alteration in phase morphology. The influence of rheological behavior of various constituting polymers in reactive alloys of core-shell morphologies are discussed in the following sections (sections 9.9, 9.10, and 9.13).

9.9. Effect of viscosity (molecular weight) of core forming polymer

Molecular weight of blend's components is the other influential factor which determines the morphology and properties of the blends. This section reviews the variation of microstructure and subsequent properties with the viscosity of matrix and core-forming polymers in toughened ternary blends. Gonzalez-Montiel et al. [138,139] studied the effects of PA6 and PP molecular weights on the morphology and mechanical properties of PA6/PP 66/33 blends toughened by 20 wt% EPR-g-MA. The modulus of these blends decreased with increasing nylon-6 molecular weight and with decreasing PP molecular weight (increasing melt flow rate) (Fig. 31). Use of PPs with low melt flow rates (high MWs) produced blends with lower DBTTs. As the MFR of the PP increased, the DBTT of the blend increased and the room temperature impact strength decreased (Fig. 31). In addition, the absolute level of toughness above this transition temperature, e.g. room temperature, decreased as the PP molecular weight decreased. Similar, but less

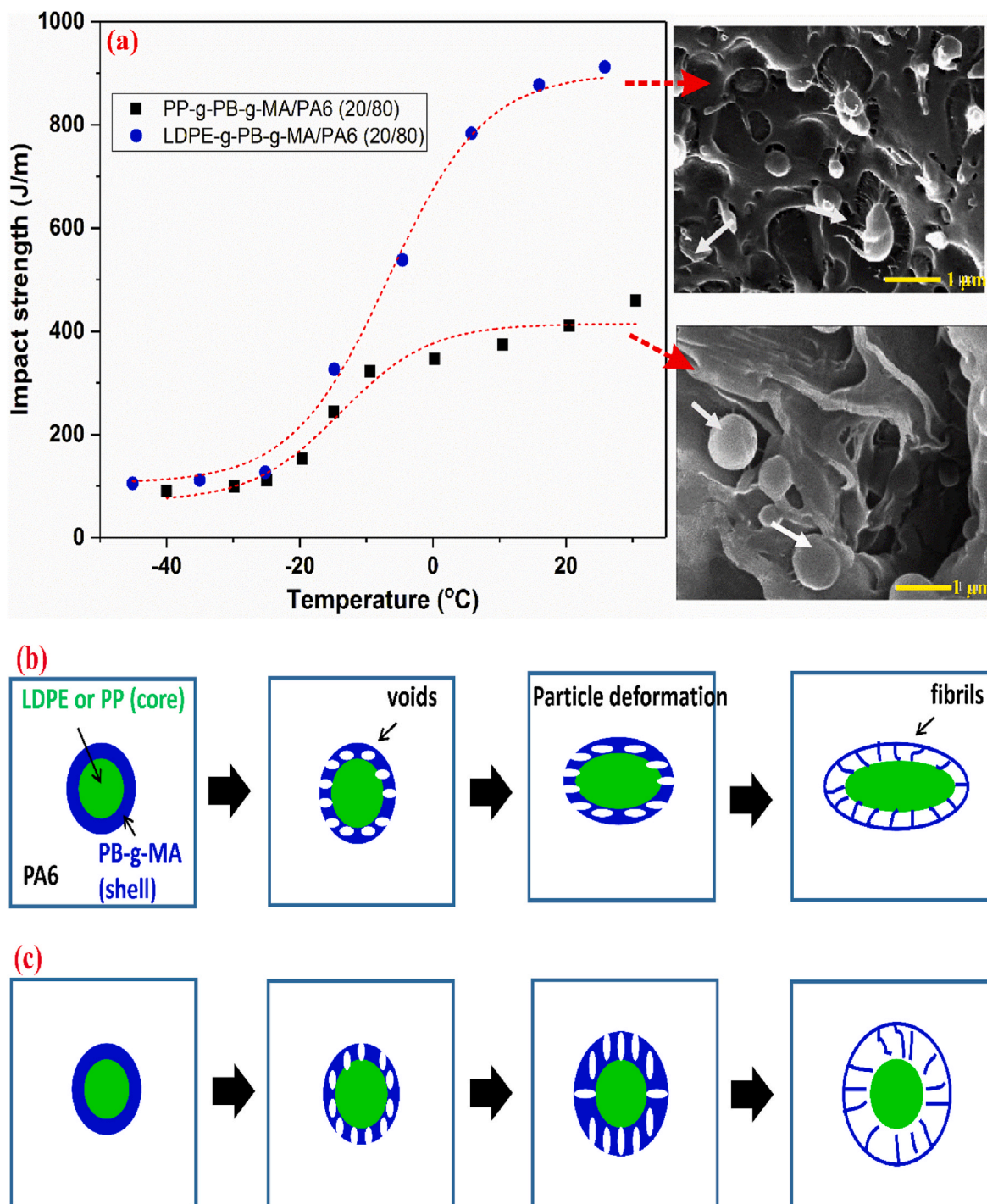


Fig. 30. (a) impact energy vs. temperature along with micrographs of impact-fractured samples of PA6/PB-g-MA blend containing different (PP and LDPE) core-forming phases. (b,c) Schematic representation of deformation micro-mechanism of core-shell domains (for various cores of different stiffness: (b) LDPE and PP core under tensile test or LDPE core under impact test; and (c) PP core under impact test. (reproduced from Shi et al. [236], with kind permission of Royal Society of Chemistry).

significant, trends were observed for blends modified with SEBS-g-MA. These results were in part a consequence of the change in blend morphology that occurred as the molecular weights of PP and nylon-6 were varied. The highest molecular weight PP generated a morphology where nylon-6 was the continuous phase, the medium molecular weight PP led to a co-continuous morphology and the lowest molecular weight PP gave rise to a PP continuous phase. It is reported for nylon-6/PP blends that the crystallization kinetics and the final degree of crystallinity of each component can be affected by the formation of

graft copolymers [238,239]. It was claimed that a decreased degree of crystallinity of either the PP or the nylon-6 phase could also be a contributing factor to the decrease in modulus observed for these blends. The lowest DBTT corresponded to the blend where the nylon-6 was the matrix phase [138,139].

Shen et al. [240], examined the morphology and mechanical properties of PA6/EPDM-g-MA/HDPE blends containing HDPE cores of different viscosities. A single core structure was observed for blends containing low-viscosity HDPE (L-HDPE), while a multi-core structure

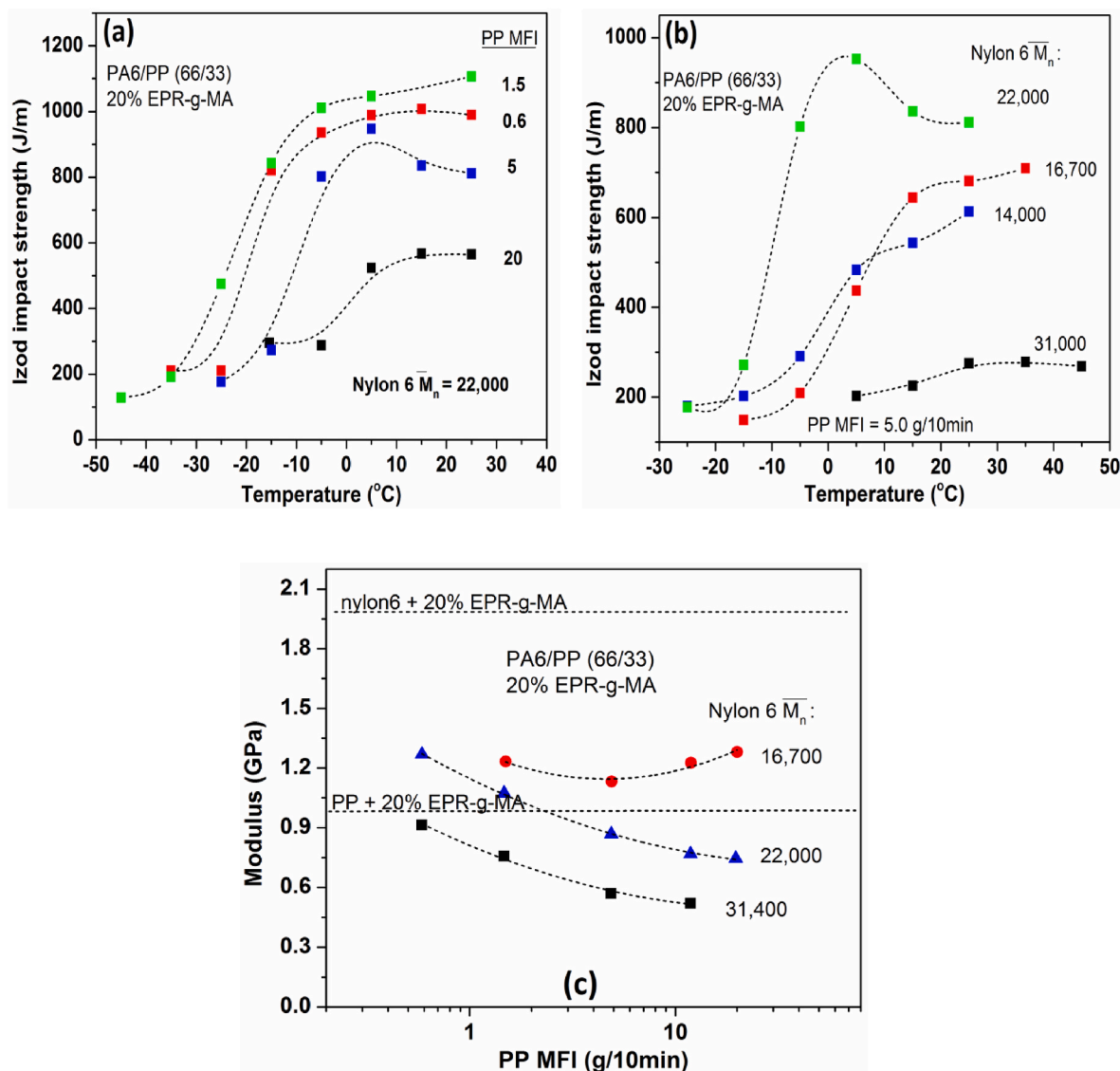


Fig. 31. Effect of polypropylene molecular weight (expressed as MFR) and nylon-6 molecular weight on the mechanical properties of nylon-6/PP (66/33) blends modified with 20% EPR-g-MA rubber. (a, b) Izod impact strength vs. temperature response, and (c) Young's modulus values. The horizontal lines indicate the modulus for the binary blends nylon-6/EPR-g-MA and polypropylene/EPR-g-MA blends. (redrawn after Gonzalez Montiel et al. [138,139], with kind permission of Elsevier Science Ltd).

was obtained for blends with high-viscosity HDPE (H-HDPE) [240]. At a fixed HDPE content, the d_n of the dispersed droplets containing H-HDPE was lower than that of droplets with L-HDPE phase. The increase in the HDPE content in the blends up to 15 wt% (the EPDM/HDPE total dispersed phase was fixed at 30 wt%) caused an increase in tensile strength, flexural modulus and impact strength of the resulting blend with a decrease in the elongation at break for blend composed of L-HDPE phase. With the exception of flexural modulus, the tensile strength, strain at break and impact strength of the blends containing H-HDPE core were significantly higher than those for blends with L-HDPE core [240]. The blends with PA6/EPDM-g-MA/HDPE (70/15/15) composition showed much higher impact strength values at much lower rubber content compared with the PA6/EPDM-g-MA (70/30) binary blend. Massive matrix shear deformation was found as the prevalent energy absorbing mechanism in ternary blends. Moreover, the extent of plastic drawing was more severe for ternary blend containing H-HDPE compared with the blend with L-HDPE, indicating higher capability for energy dissipation and, consequently, much higher resistance against crack propagation during the impact test in the former blend system

[240]. Dou et al. [241] prepared PA6/HDPE-g-MA/EPDM ternary blends containing EPDM component of low and high viscosities. The dispersed domains in low-viscosity EPDM blends displayed a single core-shell structure while a multi-core structure with HDPE-g-MA particles existed in blends with high-viscosity EPDM (Fig. 32). During annealing, the lower viscosity EPDM blends displayed a core-shell size coarsening phenomenon without the core-shell morphological type changing. However, for higher viscosity EPDM blends, the initial multi-core structure evolved into a complete EPDM single-core structure after annealing (Fig. 32) [241].

The increase of annealing time reduced the toughness of the both ternary blends markedly, and a ductile-brittle transition behavior was noticed. The impact strength of the high-viscosity EPDM system was higher than that of the low-viscosity EPDM system during the whole annealing process [241]. The microstructural changes happened during the annealing process were responsible for the change in impact toughness. Shear yielding and plastic deformation was the main source of impact energy dissipation for un-annealed blends containing both low- and high-viscosity EPDMs with more intense deformation for blend

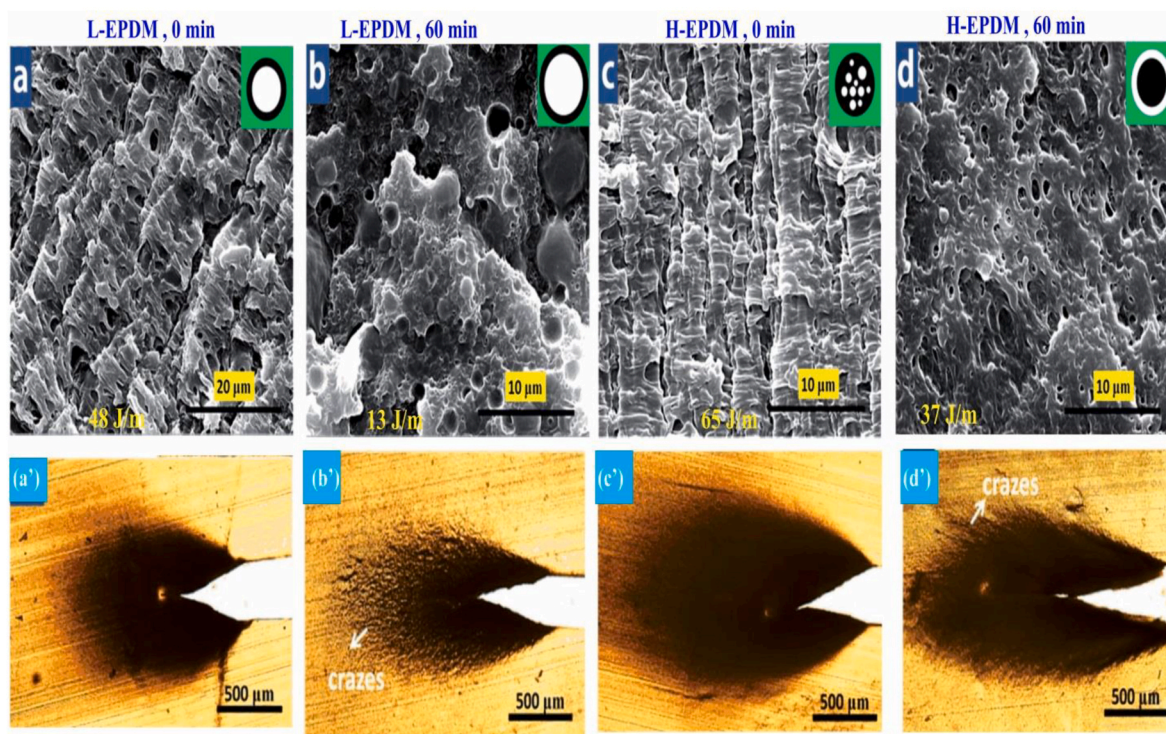
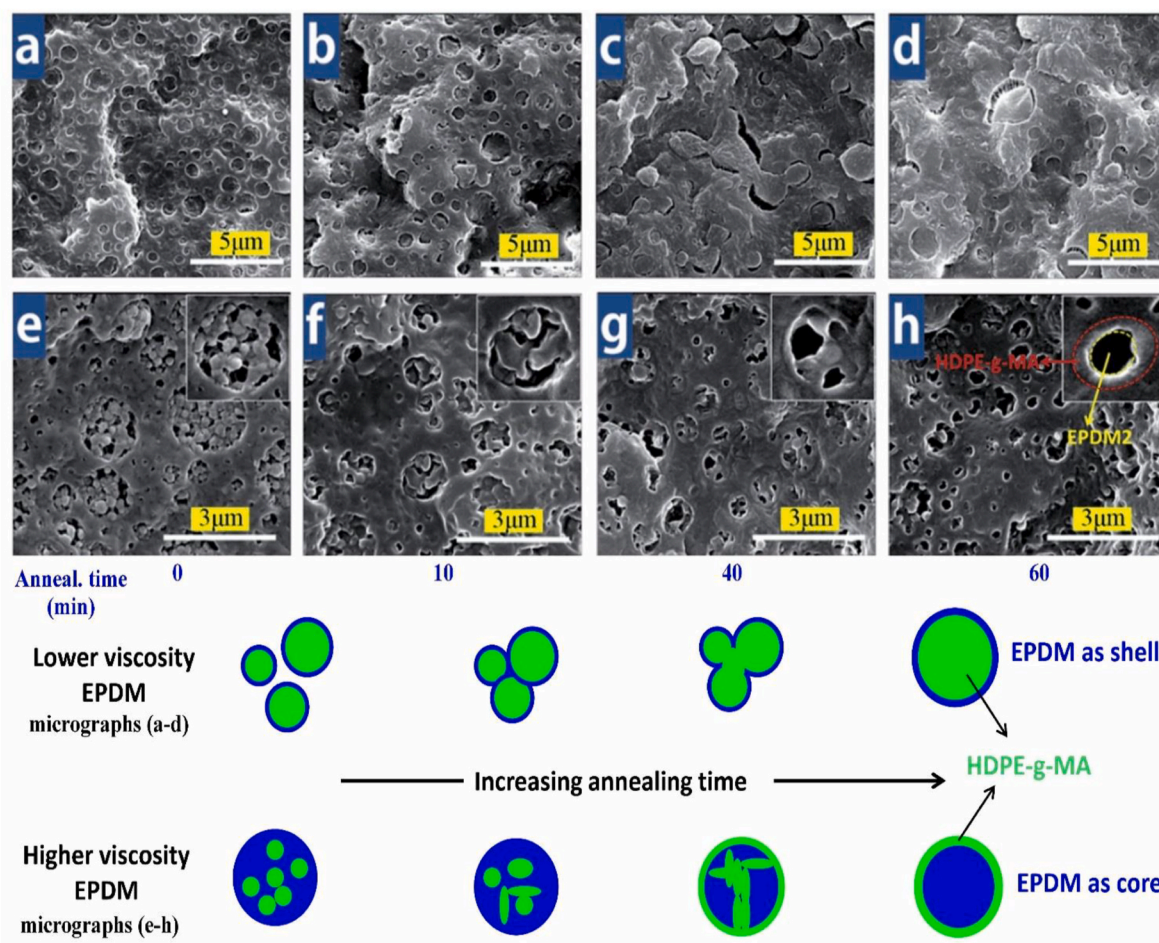


Fig. 32. Effect of EPDM viscosity and time of annealing at 250 °C on the microstructure and impact toughness of PA6/HDPE-g-MA/EPDM blends. (top) Morphology development along with a sketch of core-shell morphology evolution, EPDM was etched by xylene. (below) impact-fracture behavior and images of crack tip damage zone under impact test. (reproduced from Dou et al. [241], with kind permission of Royal Society of Chemistry).

with the latter rubbery phase. After annealing, the intensity of shear deformations was significantly reduced for both blend systems, particularly for blend having low-viscosity EPDM. Debonding of coarsened dispersed domains was observed for blend having low-viscosity EPDM, whilst a multiple void formation together with limited local plastic deformation was detected for blend having high-viscosity EPDM [241].

Moini Jazani et al. [54] examined the structure-property correlations in PP/PC/SEBS + SEBS-g-MAH blends containing three grades of PC of different melt viscosities. Changes in blend morphology from PC/SEBS core-shell particles partially surrounded by SEBS-g-MAH to inverse SEBS/PC core-shell particles in PP matrix were observed upon varying the viscosity ratio of PC to SEBS. It was found that the viscosity ratio completely controls the size of the core-shell droplets. Ternary blends with PC cores showed the highest Young's modulus values and the lowest impact strength [54]. Shang et al. [242] investigated the effects of viscosity and content of PP on the phase morphology and mechanical properties of PBT/POE-g-GMA/PP blends containing 30 wt% total modifier polymers. POE-g-GMA and PP showed significant synergistic toughening effect, and PBT/POE-g-GMA/PP (70/15/15) ternary blends displayed higher impact resistance and quasi-static work of fracture parameters (w_e and βw_p) than the PBT/POE-g-GMA (70/30) binary blend, regardless of viscosity of PP phase. The ternary blend having PP of higher viscosity showed superior NIIS and work of fractures than blends having PP of lower melt viscosity [242]. The ternary blends also possessed much better resistance to quasi-static crack propagation than PBT/POE-g-GMA binary blends. The decrease of inter-particle distance and the fibrillation of core-shell particles activated intense matrix shear yielding, which was the reason for the high crack resistance of ternary blends [242].

9.10. Effect of viscosity (molecular weight) of shell forming polymer

Besides the viscosity of matrix and core-forming polymers, the structure and properties of toughened reactive blends of encapsulated morphology is influenced by the molecular weight of shell polymer as well. Nonetheless, the open literature on this subject is scarce. Zhou et al. [243] studied the effect of EPDM-g-MA molecular weight on the morphology and properties of PA6/EPDM-g-MA/HDPE ternary blends. Three different EPDM-g-MAs of various weight-average molecular weights (100,000; 135,000 and 200,000 g/mol) were used. A core-shell morphology, with EPDM-g-MAH as shell and HDPE as core, was observed for blends containing EPDM-g-MA of lower molecular weights, whilst a separated dispersion of EPDM-g-MAH and HDPE phases was identified for blend containing EPDM-g-MA of highest molecular weight

(Fig. 33) [243]. Blends with core-shell morphology exhibited a remarkable rise in the elongation at break. With more perfect core-shell composite droplets and co-crystal formation, the impact strength of the ternary blends greatly increased, almost 10 times higher than that of pure PA6 [243].

9.11. Effect of degree of rubber functionality

In reactively compatibilized toughened ternary blends of encapsulate morphology, the presence of polar reactive moieties on the compatibilizing agent is vital for control and stabilization of morphology as well as promotion of phase adhesion across the interface between the polar and non-polar components of the blend. Effective compatibilization can be achieved at very small amounts of suitable functional groups grafted on the compatibilizing ingredient. Variation in the extent of functionalization of compatibilizer polymer beyond the optimum level can produce significant impacts on the morphology and respected properties of ultimate blend. For example, Dou et al. [244] studied the effect of amount of MA-functionality (0.28–1.12%) of EPDM-g-MA rubbery phase on the phase morphology and mechanical properties of PA6/EPDM-g-MA/HDPE (70/15/15) blends. Core-shell phase morphologies of different shell thicknesses were developed by varying the amount of grafted MA on the rubbery phase. The change in the reactivity of rubbery phase by changing its level of functionality with MA also affected the size of dispersed domains as well as the interfacial strength between the HDPE phase and surrounding PA6 matrix [244]. The MA grafting degree of EPDM-g-MA had no significant influence on the type of morphology of ternary blends. However, the size of composite droplets and the core gradually increased with grafting degree of EPDM-g-MA. The ternary blend containing the rubbery phase of the lowest functionality degree exhibited the smallest size of core-shell composite droplets. With increasing MA grafting degree of EPDM-g-MA, the tensile yield strength of ternary blends increased, and elongation at break of ternary blends decreased to some extent, but always far higher than pure PA6 sample [244]. The notched impact strength of ternary blends displayed an apparent maximum at low MA grafting degree of EPDM-g-MA, which was almost 2–3 times greater than that of other ternary blends with higher MAH grafting degree of EPDM-g-MAH and 9–10 times higher than that of pure PA6. The significantly higher impact toughness at lower MA functionality was attributed to the smaller size of core-shell composite droplets and the larger thickness of EPDM-g-MA shell in the corresponding blend system [244]. For the blends with higher MA grafting degree of EPDM-g-MA, limited matrix shear yielding took place with vast debonding of dispersed particles and over-large

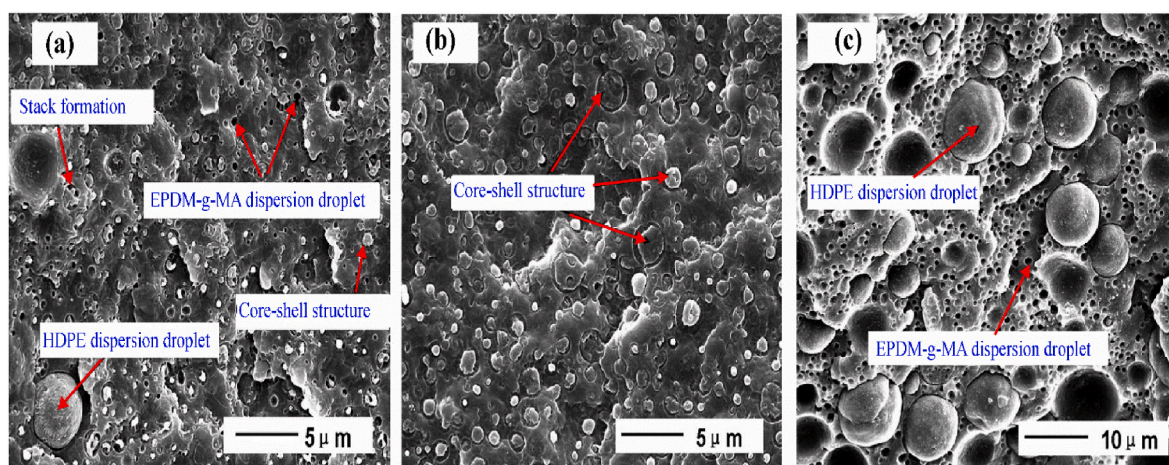


Fig. 33. Morphology development in PA6/EPDM-g-MA/HDPE ternary blends containing three EPDM-g-MA of different molecular weights. (a) 100,000 g/mol; (b) 135,000 g/mol; and (c) 200,000 g/mol. EPDM-g-MA is etched by xylene in the micrographs. (reproduced from Zhou et al. [243], with kind permission of John Wiley & Sons, Inc.).

interfacial cavitations (Fig. 34). However, extensive shear yielding, plastic deformation and a large amount of fibrillar structure were seen throughout the entire region in the blends with low MA grafting degree of EPDM-g-MA (Fig. 34). No cavitation and debonding of spherical dispersed particles could be detected [244].

Accordingly, the authors declared that the thicker EPDM-g-MA shell can prevent debonding from occurring, ensure stress transfer between dispersed particles and polymer matrix. Thus, the fibrillation progress of core-shell dispersed particles without overlarge defect can absorb plenty of fracture energy and improve greatly the notched Izod impact strength of resulting blends [244]. While for the blends with higher MA grafting degree of EPDM-g-MA, and thinner EPDM-g-MA shell, the interfacial adhesion of PA6/EPDM-g-MA is relatively poor, and debonding occurs during impact loading which results in inefficient stress transfer from the matrix onto the dispersed domains, leading to limited improvement in impact toughness of resultant blend [244]. Wang et al. [178] studied the effects of POE and POE-g-MA on the morphology and properties of PP/TPAS blends. While toughened PP/POE and PP/POE-g-MA exhibited comparable uniaxial tensile behavior and NIIS values, the ternary blends displayed large difference in mechanical properties depending on the type of toughener used. For PP/TPAS/toughener (70/15/15) blends, the blend containing POE-g-MA represented smaller modulus with much higher tensile strength, elongation at break, work to fracture, and NIIS [178]. For blend having POE modifier, the TPAS easily pulled out from the matrix, led to poor tensile ductility and impact strength, whereas for blend loaded with POE-g-MA a uniform dispersion and improved interfacial adhesion was detected which resulted in greatly enhanced ductility and impact resistance [178].

9.12. Effect of weight fraction of core- and shell-forming polymer

Gonzalez-Montiel et al. [139] claimed that in PA6/EPR-g-MA/PP blends significant impact strength is achieved, even at 10% rubber levels, when there is 10–30% PP in the blend, and 15% EPR-g-MA rubber is sufficient to achieve toughness over a wide range of compositions at room temperature. In addition, the amount of rubber strongly influenced the low temperature behavior of the blends. Blends containing 10% EPR-g-MA were within the ductile-brittle region at room temperature. The DBTT of these blends was dramatically shifted to lower temperatures as more EPR-g-MA was added to PA6/PP 80/20 blend (Fig. 35). The size of the polypropylene domains decreased as the amount of EPR-g-MA in the blend increased, indicating their role as compatibilizers in addition to being impact modifiers [139].

Wu et al. [245] studied the effects of PP and SEBS-g-MA loadings (5–15 wt%) on the morphology and mechanical properties of PA6/SEBS-g-MA/PP ternary blends. Ternary blends with various amounts of PP showed core-shell morphology with PP as core and SEBS-g-MA as shell. As the loading of SEBS-g-MA increased to 15 parts, the size of core-shell particles gradually decreased (owing to the compatibilization effect) and some multilayer core-shell particles were formed [245]. The NIIS gradually increased with SEBS-g-MA loading at a fixed PP content. The same trend was observed when PP content was increased at a fixed rubbery phase. The highest impact strength value was observed for ternary blend with SEBS-g-MA:PP ratio of 15:15. Cavitation inside the SEBS-g-MA shell and matrix shear yielding were the micromechanisms of deformation in the blends. The blend with special multilayer structure, showed intense shear yielding. For the multilayer particles, the cavitation occurred both at the internal and the external of the core-shell particles [245]. The elastic modulus and tensile

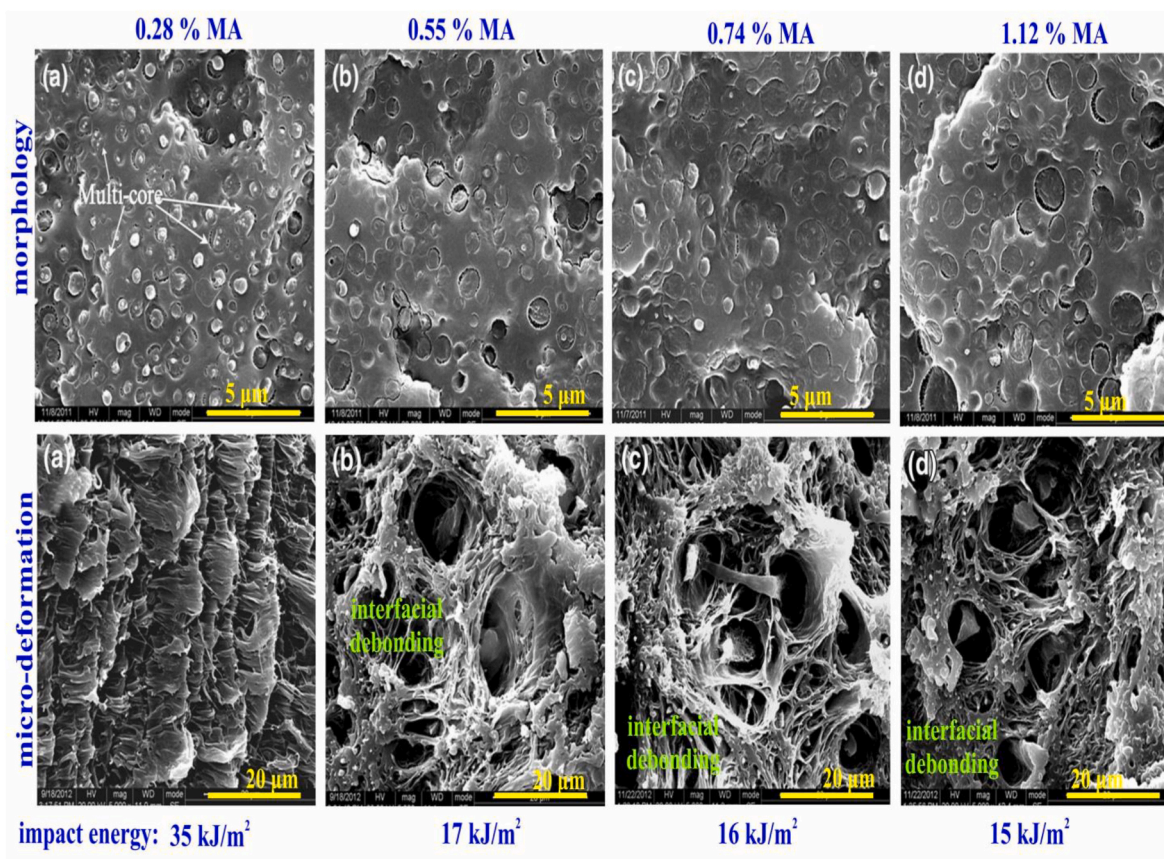


Fig. 34. Morphology development, micro-mechanisms of deformations under impact test, and impact fracture energy values for PA6/EPDM-g-MA/HDPE blends as a function of level of maleic anhydride (MA) functionality (0.28–1.12%) of EPDM-g-MA component. EPDM-g-MA is extracted using xylene for morphology analysis. (reproduced from Dou et al. [244], with kind permission of Springer-Verlag Berlin Heidelberg).

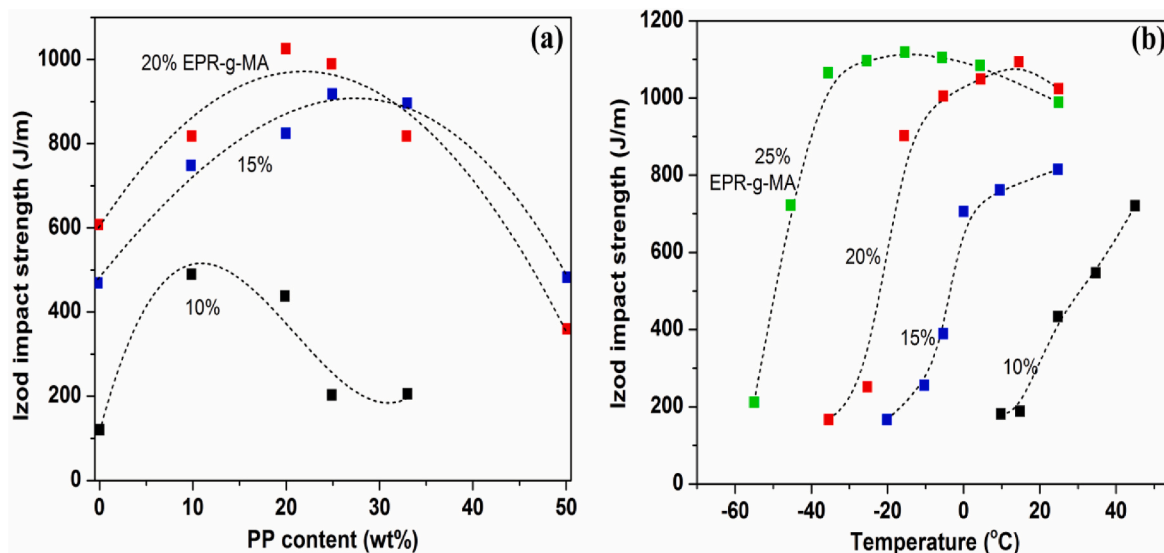


Fig. 35. Izod impact strength of nylon-6/PP blends modified with different amounts of EPR-g-MA. (a) Effect of PP weight fraction, and (b) Effect of temperature at a nylon-6/PP (80/20) composition. The rubber content is based on the total mass of the ternary blend. (redrawn after Gonzalez Montiel et al. [138,139], with kind permission of Elsevier Science Ltd).

strength gradually decreased with SEBS-g-MA content. Similar trend was observed for elastic modulus of ternary blends with PP content at a fixed concentration of rubbery phase [245].

9.13. Effect of major phase molecular weight

Little research has been conducted on the dependence of morphology and properties of reactive ternary blends of encapsulated morphology on molecular weight of major (matrix) phase in the blend. Gonzalez Montiel et al. [139] found that for PA6/PP 66/33 blends containing 20 wt% EPR-g-MA the toughness is strongly affected by the PA6 molecular weight. The blend with the highest molecular weight nylon-6 was brittle and did not show ductile behavior even well above room temperature. The blend based on a medium molecular weight nylon-6 had a low DBTT and showed excellent toughness at room temperature (Fig. 31). Use of nylon-6 materials with lower molecular weights gave higher DBTTs and lower room temperature toughness. Changing the molecular weight of the nylon-6 component led to large changes in blend morphology; the low toughness of the blend based on the highest molecular weight nylon-6 corresponded to a morphology where PP formed the continuous matrix phase. The blend with the lowest DBTT had a co-continuous morphology. The blends based on low molecular weight nylon-6 had large, poorly dispersed domains of nylon-6 and PP, which seemed to be the reason for the lower toughness observed for these blends. A similar trend was observed for blends with an 80/20 nylon-6/PP ratio, but in this case the nylon-6 molecular weight at which co-continuity or phase inversion occurred was higher [139].

9.14. Effect of mixing time

The development of core-shell structures over time during reactive melt processing has attracted little attention. Dou et al. [246] found that the size of core-shell dispersed domains in PA6/EPDM-g-MA/HDPE (75/15/15) ternary blends was changing with mixing time from 2 to 15 min. The dispersed phase changed from long threads to uniform dispersed droplets and then to a few large particles with broader size distribution. The increase in the size of dispersed particles with mixing time was ascribed to the aggregation (coalescence) effect of dispersed domains at long mixing times [246]. For these blends, the NIIS was strongly dependent on the mixing time; the impact strength increased with mixing time up to 8 min and then decreased with further increase in

mixing time to 15 min, with the highest impact strength was obtained at a mixing time of 8 min. Nonetheless, the impact strength of blend with 15 min mixing time was still significantly higher than that of neat PA6 resin. The fall in impact strength at higher mixing times was attributed to the bigger core-shell particles with thin rubber shell formed at longer mixing times [246].

10. Concluding remarks and outlook

Modification of polymers by blending with other polymers is well-known as an effective and economically justified method of enhancing their performance. In incompatible blends of polar and apolar polymers, both compatibilization and rubber toughening are essential to achieve acceptable mechanical performance for structural applications. Thus, a functionalized rubbery phase is commonly used in these blends to address these issues. The thermodynamics and kinetic aspects of blend's components during reactive melt processing give rise to an encapsulated (core-shell) morphology for the resulting (ternary) reactive blends, where the rubbery phase functions as an interfacial layer surrounding the other minor component of the blend. In blends with encapsulated morphology, the dispersion state of composite modifier domains can vary from discrete droplets to clusters of droplets, percolation of core-shell droplets, or an interpenetrated structure of core- and shell-forming polymers dispersed in the matrix of parent polymer depending on the blend composition and mixing protocols. The dispersion state of core-shell domains profoundly influences the macroscopic mechanical properties of resulting blend system. Besides blend composition, the morphology is strongly influenced by molecular, architectural, and rheological properties of blend components, especially those for core- and shell-forming polymers. Moreover, in reactive blends of core-shell morphology the microstructure is greatly affected by the sequence of mixing of blend components. As an interfacial layer between the matrix and core-forming polymer, the mechanical properties and fracture toughness of resulting blend are directly connected with the degree of core-encapsulation, level of interfacial interactions and shell thickness as well as the physical properties of rubbery interphase such as Young's modulus, strength, glass transition temperature.

Compared with conventional rubber-toughened binary blends containing homogeneous rubbery domains dispersed in the matrix of parent polymer, toughened reactive ternary blends having composite core-shell droplets offer significant advantages in terms of cost, stiffness-toughness

balance, and processability, all of which are of paramount industrial importance. Understanding of micromechanics of toughening and the underlying microstructural deformations accompanying the mechanical stresses in these blends can pave the way for developing new multi-component polymeric systems with yet enhanced properties. The results show that the dispersed composite particles (structures) are the stress concentrating sites in the matrix under mechanical stresses. The response of dispersed structures to mechanical stresses is dependent on the deformation rate, interfacial adhesion (shell thickness), dispersion state of core-shell particles as well as the physical properties of core- and shell-forming polymers. Dilatational stress fields around the modifier structures give rise to void formation within the rubbery shell and/or at its interface with the surrounding matrix. A fibrillized cavitation process usually develops inside the rubbery shell of core-shell particles. In the case of poor interfacial adhesion (thin shell of rubbery phase) debonding-cavitation and internal cavitation followed by plastic void growth can lead to nucleation of microcracks which serve as the trajectory of crack propagation through the material. However, when there is a suitable interfacial adhesion, void formation and subsequent plastic growth of nano/micro-voids activate the matrix shear yielding and plastic deformation. Void-fibrillation process stabilizes the generated cavities, prevent them from early-stage coalescence, and permit stable plastic growth of nano/micro-voids during deformation, which in turn greatly improve the matrix capability for massive shear yielding. Consequently, the fracture energy is highly increased.

Many studies indicate that blends containing percolated structure of core-shell particles give better toughness than the blends having the clusters of core-shell particles, and the latter one produce higher impact toughness than the blends having discrete core-shell particles. The extent of void formation (or fibrillized cavitation process) of rubbery phase around and/or within the dispersed agglomerated structures is much greater for blends with percolated morphology than the other blend systems, which assist in far greater amounts of energy absorption and dissipation during the fracture tests.

Finally, it is well-established that the toughened immiscible blends of core-shell morphology can exhibit improved stiffness-toughness balance over the traditional rubber-toughened binary blends. Nonetheless, the amount of stiffness in the current core-shell systems, especially those with highly-tough or super-tough impact behavior, needs to be further enhanced to further narrow their gap with the stiffness of many engineering thermoplastic resins. Thus, further work on the design (formulation) of current toughened blends or developing new strategies (through physical blending, high performance reactor alloying) for producing toughened immiscible blends of excellent stiffness-toughness balance can be the next stage in this field.

The other subject that needs further investigation is the study on the mechanical response of such core-shell alloys under conditions other than frequently examined room temperature. For instance, low temperature toughness of these systems and its correlation with various microstructural parameters discussed above deserves extensive examination.

Declaration of competing interest

The authors report there are no competing interests to declare.

Data availability

Data will be made available on request.

References

- [1] D.R. Paul, *Polymer Blend*, 2, Academic press, 1978.
- [2] D.R. Paul, C.B. Bucknall, in: *Formulation. Polymer Blends 1*, Wiley-Interscience, 1999.
- [3] L.A. Utracki, *Commercial Polymer Blends*, springer science, 1998.
- [4] L.A. Utracki, *Polymer Blends Handbook*, springer science, 2003.
- [5] L.A. Utracki, *Polymer Alloys and Blends*, Hanser Pub. Inc., 1990.
- [6] L.A. Utracki, C. Wilkie, *Polymer Blends Handbook*, springer, 2014.
- [7] *Polymer blends and alloys market size*. www.industryresearchco.com, 2020.
- [8] J.S. Higgins, M.L. Tambasco, E.G. Jane, *Polymer blends; stretching what we can learn through the combination of experiment and theory*, *Prog. Polym. Sci.* 30 (2005) 832–843.
- [9] C.B. Bucknall, The effective use of rubbers as toughening agents for plastics, *J. Elastomers Plast.* 14 (1982) 204–221.
- [10] C.B. Bucknall, *Toughened Plastics*, Applied Science Publishers, London, 1977.
- [11] R.A. Pearson, *Toughening of Plastics: Advances in Modeling and Experiments*, 1, 2000, pp. 1–12, ch.
- [12] A.A. Collyer (Ed.), *Rubber Toughened Engineering Plastics*, springer Netherlands, 1994.
- [13] *Toughened plastics I: science and engineering*, in: C.K. Riew, A.J. Kinloch (Eds.), *ACS Advances in Chemistry* (No. 233 1 (1993)).
- [14] C.K. Riew, A.J. Kinloch (Eds.), *Toughened Plastics II. Novel Approaches in Science and Engineering*. Editor(s): *Advances in Chemistry*, 252, 1996.
- [15] C.K. Riew (Ed.), *Rubber-Toughened Plastics*, *Advances in Chemistry Series 222*, American chemical society, 1989.
- [16] H.H. Kausch, *Intrinsic Molecular Mobility and Toughness of Polymers*, springer, 2005.
- [17] R. Bagheri, B.T. Marouf, R.A. Pearson, Rubber-toughened epoxies: a critical review, *Polym. Rev.* 49 (3) (2009) 201–225.
- [18] D. Ratna, A.K. Banthia, Rubber toughened epoxy, *Macromol. Res.* 12 (2004) 11–21.
- [19] S.Y. Hobbs, M.E. Dekkers, V.H. Watkins, Effect of interfacial forces on polymer blend morphologies, *Polymer* 29 (1988) 1598–1602.
- [20] H. Ohishi, Phase morphology and compatibilization mechanism in ternary polymer blend systems of polyethylene terephthalate, polyolefin rubber, and ionomer, *J. Appl. Polym. Sci.* 93 (2004) 1567–1576.
- [21] G. Nakamura, T. Inoue, Morphology development in ternary polymer blends and the neumann's triangle, *Koubunshi Ronbunshu* 47 (1990) 409.
- [22] S. Horiuchi, N. Mahcariyakul, K. Yase, T. Kitano, H.K. Choi, Y.M. Yee, Compatibilizing effect of a maleic anhydride functionalized SEBS triblock elastomer through a reaction induced phase formation in the blends of polyamide 6 and polycarbonate: 1. Morphology and interfacial situation, *Polymer* 37 (1996) 3065.
- [23] S. Horiuchi, N. Mahcariyakul, K. Yase, T. Kitano, H.K. Choi, Y.M. Yee, Compatibilizing effect of maleic anhydride functionalized SEBS triblock elastomer through a reaction induced phase formation in the blends of polyamide 6 and polycarbonate: 2. Mechanical properties, *Polymer* 38 (1997) 59.
- [24] S. Horiuchi, N. Mahcariyakul, K. Yase, T. Kitano, Morphology development through an interfacial reaction in ternary immiscible polymer blends, *Macromolecules* 30 (1997) 3664–3670.
- [25] S. Shokoohi, A. Arefazar, A review on ternary immiscible polymer blends: morphology and effective parameters, *Polym. Adv. Technol.* 20 (2009) 433–447.
- [26] H.F. Guo, S. Packirisamy, N.V. Gvozdic, D.J. Meier, Prediction and manipulation of the phase morphologies of multiphase polymer blends: 1. Ternary systems, *Polymer* 38 (1997) 785–794.
- [27] H.F. Guo, N.V. Gvozdic, D.J. Meier, Prediction and manipulation of the phase morphologies of multiphase polymer blends: II, Quaternary systems, *Polymer* 38 (1997) 4915–4923.
- [28] N. Nemirovski, A. Siegmann, M. Narkis, Morphology of ternary immiscible polymer blends, *J. Macromol. Sci., Part B: Phys.* 34 (1995) 459–475.
- [29] A.K. Gupta, K.R. Srinivasan, Melt rheology and morphology of PP/SEBS/PC ternary blend, *J. Appl. Polym. Sci.* 47 (1993) 167–184.
- [30] M. Hemmati, H. Nazokdast, H.S. Panahi, Study on morphology of ternary polymer blends. I. Effects of melt viscosity and interfacial interaction, *J. Appl. Polym. Sci.* 82 (2001) 1129–1137.
- [31] J. Reignier, B.D. Favis, M.C. Heuzey, Factors influencing encapsulation behavior in composite droplet-type polymer blends, *Polymer* 44 (2003) 49–59.
- [32] H.J. Van Oene, Modes of dispersion of viscoelastic fluids in flow, *Colloid Interface Sci.* 40 (1972) 448–467.
- [33] R. Berahman, M.K.R. Aghjeh, M.M. Mazidi, et al., Evolution of shell formation process in PP/PMMA/PS ternary blends: correlation between the melt rheology and phase morphology, *J. Polym. Res.* 23 (2016) 227.
- [34] M. Khoshnood, A. Babaei, Elasticity or viscosity, which one is more influential on the internal structure of a core-shell morphology in ternary blends? *J. Polym. Res.* 25 (2018) 11.
- [35] S. Ravati, B.D. Favis, Morphological states for a ternary polymer blend demonstrating complete wetting, *Polymer* 51 20 (2010) 4547–4561.
- [36] I. Luzinov, C. Pagnouille, R. Jerome, Ternary polymer blend with core-shell dispersed phases: effect of the core forming polymer on phase morphology and mechanical properties, *Polymer* 41 (2000) 7099–7109.
- [37] I. Luzinov, K. Xi, C. Pagnouille, G. Huynh-Ba, R. Jerome, Composition effect on the core-shell morphology and mechanical properties of ternary polystyrene/styrene-butadiene rubber/poly-ethylene blends, *Polymer* 40 (1999) 2511–2520.
- [38] S. Wu, Calculation of interfacial tension in polymer systems, *J. Polym. Sci. Part C* 34 (1971) 19–30.
- [39] S. Wu, *Polymer Interface and Adhesion*, Marcel Dekker, New York, 1982 (Chapter 3).
- [40] N.G. Gaylord, Compatibilizing agents: structure and function in polyblends, *J. Macromol. Sci. Part A: Chem.* 26 (8) (1989) 1211–1229.
- [41] D. Feldman, Polyblend compatibilization, *J. Macromol. Sci., Pure Appl. Chem.* 42 (2005) 587–605.

- [42] C. Koning, M. Van Duin, C. Pagnouille, R. Jerome, Strategies for compatibilization of polymer blends, *Prog. Polym. Sci.* 23 (1998) 707–757.
- [43] S. Aparna, D. Purnima, R.B. Adusumalli, Review on various compatibilizers and its effect on mechanical properties of compatibilized nylon blends, *Polym. Plast. Technol. Eng.* 56 6 (2017) 617–634.
- [44] L.A. Utracki, Compatibilization of polymer blends, *Can. J. Chem. Eng.* 80 (2002) 1008–1016.
- [45] M. Xanthos, Interfacial agents for multiphase polymer systems: recent advances, *Polym. Eng. Sci.* 28 (27) (1988) 1392–1400.
- [46] M. Xanthos, S.S. Dagli, Compatibilization of polymer blends by reactive processing, *Polym. Eng. Sci.* 31 (13) (1991) 929–935.
- [47] J. Maris, S. Bourdon, J.M. Brossard, L. Cauret, L. Fontaine, V. Montembault, Mechanical recycling: compatibilization of mixed thermoplastic wastes, *Polym. Degrad. Stabil.* 147 (2018) 245–266.
- [48] A.R. Ajitha, S. Thomas, *Compatibilization of Polymer Blends: Micro and Nano Scale Phase Morphologies, Interphase Characterization and Properties*, Elsevier, 2020, <https://doi.org/10.1016/C2017-0-03891-0>.
- [49] M. Nechifor, F. Tanasă, C.A. Teacă, M. Zănoagă, Compatibilization strategies toward new polymer materials from re-/up-cycled plastics, *Int. J. Polym. Anal. Char.* 23 (2018) 740–757.
- [50] F. Ide, T. Kodama, A. Hasegawa, Reaction of isotactic polypropylene with maleic anhydride, and its ion cross-linking reaction, *Kobunshi Kagaku* 25 (1968) 107–115.
- [51] F. Ide, T. Kodama, A. Hasegawa, Examination of blending method of polypropylene and nylon using polymer reaction, *Kobunshi Kagaku* 29 (1972) 259–264.
- [52] F. Ide, A. Hasegawa, Studies on polymer blend of nylon 6 and polypropylene or nylon 6 and polystyrene using the reaction of polymer, *J. Polym. Sci.* 18 (1974) 963–974.
- [53] M.R. Saeb, H.A. Khonakdar, M. Razban, S.H. Jafari, H. Garmabi, U. Wagenknecht, Morphology prediction in HDPE/PA-6/EVOH ternary blends: defining the role of elasticity ratio, *Macromol. Chem. Phys.* (2012), <https://doi.org/10.1002/macp.201200158>.
- [54] O. Moini Jazani, V. Goodarzi, F. Hemmati, M.R. Saeb, Structure–property relationships in ternary polymer blends with core–shell inclusions: revisiting the critical role of the viscosity ratio, *J. Polym. Res.* 23 (2016) 231.
- [55] G.H. Michler, F.J. Baltá-Calleja, in: *Mechanical Properties of Polymers Based on Nanostructure and Morphology*, Taylor & Francis Group, LLC, 2005.
- [56] G.H. Michler, F.J. Baltá-Calleja, *Nano- and Micromechanics of Polymers*, Carl Hanser Verlag, Munich, 2012.
- [57] A.J. Kinloch, R.J. Young, *Fracture Behavior of Polymers*, Chapman & Hall, 1995.
- [58] C.B. Bucknall, Applications of microscopy to the deformation and fracture of rubber-toughened polymers, *J. Microsc. (Oxf.)* 201 (2001) 221–229.
- [59] G.H. Michler, H.H. Kausch-Blecken von Schmelting, The physics and micro-mechanics of nano-voids and nano-particles in polymer combinations, *Polymer* 54 (2013) 3131–3144.
- [60] G.H. Michler, Determination of the morphology and mechanical microprocesses in polymer combinations by electron microscopy, *Polymer* 27 (1986) 323–328.
- [61] A.S. Argon, R.E. Cohen, Toughenability of polymers, *Polymer* 44 (2003) 6013–6032.
- [62] Mechanical properties of polymer blends, in: L.A. Utracki, C.A. Wilkie (Eds.), *Polymer Blends Handbook*, Springer Science, Business Media Dordrecht, 2014.
- [63] R.J. Gaymans, K. Dijkstra, Comments on ‘Percolation model for brittle-tough transition in nylon/rubber blends, *Polymer* 31 (1990) 971.
- [64] A.J. Oshinski, H. Kesskula, D.R. Paul, Rubber toughening of polyamides with functionalized block copolymers: 1. Nylon-6, *Polymer* 33 (1992) 268–283.
- [65] A.J. Oshinski, H. Kesskula, D.R. Paul, The role of matrix molecular weight in rubber toughened nylon 6 blends: 3. Ductile-brittle transition temperature, *Polymer* 37 (1996) 4919–4928.
- [66] R. Buchdahl, E. Nielsen, Transitions in high polymeric materials, *J. Appl. Phys.* 21 (1950) 482–487.
- [67] E.H. Merz, G.C. Claver, M. Baer, Studies on heterogeneous polymeric systems, *J. Polym. Sci.* 22 (1956) 325–341.
- [68] J.N. Sultan, F.J. McGarry, Effect of rubber particle size on deformation mechanisms in glassy epoxy, *Polym. Eng. Sci.* 13 (1973) 29–34.
- [69] C.B. Bucknall, Deformation mechanisms in rubber-toughened polymers, in: D. R. Paul, C.B. Bucknall (Eds.), *Performance, Polymer Blends, 2*, Wiley-Interscience, New York, 2000, pp. 83–117.
- [70] C.B. Bucknall, New criterion for craze initiation, *Polymer* 48 (2007) 1030–1041.
- [71] C.B. Bucknall, Quantitative approaches to particle cavitation, shear yielding, and crazing in rubber-toughened polymers, *J. Polym. Sci., Part B: Polym. Phys.* 45 (2007) 1399–1409.
- [72] C.B. Bucknall, D.R. Paul, Notched impact behavior of polymer blends: Part 1: new model for particle size dependence, *Polymer* 50 (2009) 5539–5548.
- [73] C.B. Bucknall, D.R. Paul, Notched impact behaviour of polymer blends: Part 2: dependence of critical particle size on rubber particle volume fraction, *Polymer* 54 (2013) 320–329.
- [74] S. Newman, in: D.R. Paul, S. Newman (Eds.), *Polymer Blends, 2*, Academic, New York, 1978, pp. 63–89.
- [75] C.B. Bucknall, Fracture and failure of multiphase polymers and polymer composites, *Adv. Polym. Sci.* 27 (1978) 121–148.
- [76] E.B. Caldona, A.C. De Leon, B.B. Pajarito, R.C. Advincula, A review on rubber-enhanced polymeric materials, *Polym. Rev.* 57 (2017) 311–338.
- [77] J. Wang, X. Zhang, L. Jiang, J. Qiao, Advances in toughened polymer materials by structured rubber particles, *Prog. Polym. Sci.* 98 (2019), 101160.
- [78] J.A. Schmitt, Mechanism of reinforcement in rubber-modified polystyrene systems studied by use of a miniature dart drop test, *J. Appl. Polym. Sci.* 12 (1968) 533–546.
- [79] H. Kesskula, Rubber modified styrene polymers, *Appl. Polym. Symp.* 15 (1970) 51–78.
- [80] H. Kesskula, D.R. Paul, Toughening agents for engineering polymers, in: A. A. Collyer (Ed.), *Rubber Toughened Engineering Plastic S*, Chapman and Hall, London, 1994, pp. 136–164.
- [81] A.A. Collyer (Ed.), *Rubber Toughened Engineering Plastics*, Chapman and Hall, London, 1994.
- [82] F. Haaf, H. Breuer, J. Stabenow, Stress whitening and yielding mechanism of rubber-modified PVC, *J. Macromol. Sci. Phys.* 14 (1977) 387–417.
- [83] C.B. Donald, E.J. Kramer, Plastic deformation mechanisms in poly(acrylonitrile-butadiene styrene) [ABS], *J. Mater. Sci.* 17 (1982) 1765–1772.
- [84] C.B. Bucknall, D. Clayton, W.E. Keast, Rubber-toughening of plastics, *J. Mater. Sci.* 7 (1972) 1443–1453.
- [85] R.N. Haward, C.B. Bucknall, The provision of toughness in one and two phase polymers, *Pure Appl. Chem.* 46 (1976) 227–238.
- [86] C.S. Henkee, E.J. Kramer, Crazing and shear deformation in crosslinked polystyrene, *J. Polym. Sci. B* 22 (1984) 721–737.
- [87] S. Wu, Control of intrinsic brittleness and toughness of polymers and blends by chemical structure: a review, *Polym. Int.* 29 (1992) 229–247.
- [88] A.S. Argon, *The Physics of Deformation and Fracture of Polymers*, Cambridge University Press, Cambridge, 2013.
- [89] A.M. Donald, Failure mechanisms in polymeric materials, in: A.A. Collyer (Ed.), *Rubber Toughened Engineering Plastics*, Chapman and Hall, London, 1994, pp. 1–28.
- [90] C.B. Bucknall, P.S. Heather, A. Lazzeri, Rubber toughening of plastics, Part 12 Deformation mechanisms in toughened nylon 6,6, *J. Mater. Sci.* 24 (1989) 2255–2261.
- [91] L.L. Ban, M.J. Doyle, M.M. Disko, G.R. Smith, Morphology of ethylene-co-propylene rubber-modified nylon 66 blends, *Polym. Commun.* 29 (1988) 163–165.
- [92] P.Y.B. Jar, R. Lee, T. Shinmura, K. Konishi, Rubber particle cavitation on toughness enhancement of SMI-modified poly(acrylonitrile-butadiene-styrene), *J. Polym. Sci., Part B: Polym. Phys.* 37 (1999) 1739–1748.
- [93] M. Mehrabi Mazidi, Microstructure, Deformation Micro-mechanisms and Fracture Behavior of Polypropylene (PP)-based Blend Systems, Ph.D. Thesis, Sahand University of Technology, Iran, 2016.
- [94] M. Mehrabi Mazidi, M.K. Razavi Aghjeh, H.A. Khonakdar, U. Reuter, Structure–property relationships in super-toughened polypropylene-based ternary blends of core–shell morphology, *RSC Adv.* 6 (2016) 1508.
- [95] C.B. Bucknall, V.L.P. Soares, H.H. Yang, X.C. Zhang, Rubber toughening of plastics: rubber particle cavitation and its consequences, *Macromol. Symp.* 101 (1996) 265–271.
- [96] A.N. Gent, Cavitation in rubber: a cautionary tale, *Rubber Chem. Technol.* 63 (1990) 49–53.
- [97] E.J. Kramer, Microscopic and molecular fundamentals of crazing, in: H.H. Kausch (Ed.), *Crazing in Polymers, Advances in Polymer Science*, 52/53, Springer, Berlin, 1983, pp. 1–56.
- [98] S. Wu, Chain structure and entanglement, *J. Polym. Sci. B Polym. Phys. Ed.* 27 (1989) 723–741.
- [99] H. Liang, W. Jiang, J. Zhang, B. Jiang, Toughening mechanism of polymer blends: influence of voiding ability of dispersed-phase particles, *J. Appl. Polym. Sci.* 59 (1996) 505–509.
- [100] A. Lazzeri, C.B. Bucknall, Dilatational bands in rubber-toughened polymers, *J. Mater. Sci.* 28 (1993) 6799–6808.
- [101] C.B. Bucknall, A. Karpodinis, X.C. Zhang, A model for particle cavitation in rubber-toughened plastics, *J. Mater. Sci.* 29 (1994) 3377–3383.
- [102] H.J. Sue, Craze-like damage in a core-shell rubber-modified epoxy system, *J. Mater. Sci.* 27 (1992) 3098–3107.
- [103] C. Fond, A. Lobbrecht, R. Schirrer, Polymers toughened with rubber microspheres: an analytical solution for stresses and strains in the rubber particles at equilibrium and rupture, *Int. J. Fract.* 77 (1996) 141–159.
- [104] A. Dasari, Q.X. Zhang, Z.-Z. Yu, Y.W. Mai, Toughening polypropylene and its nanocomposites with submicrometer voids, *Macromolecules* 43 (2010) 5734–5739.
- [105] A. Lazzeri, C.B. Bucknall, Applications of a dilatational yielding model to rubber-toughened polymers, *Polymer* 36 (1995) 2895–2902.
- [106] A. Lazzeri, C.B. Bucknall, Recent development in the modelling of dilatational yielding, in *Toughening Plastics*, in: R.A. Pearson, H.J. Sue, A.F. Yee (Eds.), *Advances in Modeling and Experiments* 759, ACS Symposium Series, ACS, Washington, DC, 2000, p. 14.
- [107] R.J. Gaymans, J.W. Van der werff, Blends of polyamide-6 with acrylic core-shell impact modifiers, *Polymer* 35 (1994) 3658–3664.
- [108] R.J. Gaymans, Toughening of semicrystalline thermoplastics, in: D.R. Paul, C. B. Bucknall (Eds.), *Polymer Blends, 2*, Wiley-Interscience, New York, 2000, pp. 177–224. Performance.
- [109] W. Jiang, D. Yu, B. Jiang, Brittle-ductile transition of particle toughened polymers: influence of the matrix properties, *Polymer* 45 (2004) 6427–6430.
- [110] W. Jiang, D.H. Yu, L.J. An, B.Z. Jiang, Brittle–ductile transition of polypropylene/ethylene–propylene–diene monomer blends induced by size, temperature, and time, *J. Polym. Sci. B* 42 (2004) 1433–1440.
- [111] W. Jiang, Y.X. Hu, J.H. Yin, Critical behavior of brittle-ductile transition of polymers, *J. Polym. Sci. B* 46 (2008) 766–769.

- [112] G. Liu, X. Zhang, Y. Liu, X. Li, H. Chen, K. Walton, et al., Effect of elastomer on crystalline transition and deformation behavior of isotactic polypropylene, *Polymer* 54 (2013) 1440–1447.
- [113] B. Cioni, A. Lazzeri, The role of interfacial interactions in the toughening of precipitated calcium carbonate–polypropylene nanocomposites, *Compos. Interfac.* 17 (2010) 533–549.
- [114] S. Wu, Phase structure and adhesion in polymer blends: a criterion for rubber toughening, *Polymer* 26 (1985) 1855–1863.
- [115] S. Wu, Chain structure, phase morphology, and toughness relationships in polymers and blends, *Polym. Eng. Sci.* 30 (1990) 753–761.
- [116] A. Margolina, S.H. Wu, Percolation model for brittle-tough transition in nylon/rubber blends, *Polymer* 29 (1988) 2170–2173.
- [117] R.J.M. Borggreve, R.J. Gaymans, A.R. Luttmer, Influence of structure on the impact behaviour of nylon-rubber blends, *Macromol. Symp.* 16 (1988) 195–207.
- [118] R.J.M. Borggreve, R.J. Gaymans, H.M. Eichenwald, Impact behaviour of nylon-rubber blends: 6. Influence of structure on voiding processes; toughening mechanism, *Polymer* 30 (1989) 78–83.
- [119] R.J.M. Borggreve, R.J. Gaymans, J. Schuijjer, Impact behaviour of nylon-rubber blends: 5. Influence of the mechanical properties of the elastomer, *Polymer* 30 (1989) 71–77.
- [120] F. Ramsteiner, Influence of the morphology of polypropylene with propylene/ethylene copolymers on low-temperature impact strength and stress whitening, *Acta Polym.* 42 (1991) 584–589.
- [121] G.M. Kim, G.H. Michler, M. Gahleitner, J. Fiebig, Relationship between morphology and micromechanical toughening mechanisms in modified polypropylenes, *J. Appl. Polym. Sci.* 60 (1996) 1391–1403.
- [122] G.M. Kim, Martin Luther University, Ph.D. Thesis, Halle-Wit-tenberg, Germany, 1996.
- [123] C. Cheng, A. Hiltner, E. Baer, P.R. Soskey, S.G. Mylonakis, Cooperative cavitation in rubber-toughened polycarbonate, *J. Mater. Sci.* 30 (1995) 587–595.
- [124] R. Bagheri, R.A. Pearson, Role of blend morphology in rubber-toughened polymers, *J. Mater. Sci.* 31 (1996) 3945–3954.
- [125] R.J.M. Borggreve, R.J. Gaymans, Impact modification of poly(caprolactam) by copolymerization with a low molecular weight polybutadiene, *Polymer* 29 (1988) 1441–1446.
- [126] E.A. Flexman, D.D. Huang, H.L. Snyder, in: C.K. Riew, A.J. Kinloch (Eds.), *Polymer Preprints*, No. 29, ACS, Washington, DC, 1988, p. 189.
- [127] K. Yamanaka, Y. Tagagi, T. Inoue, Reaction-induced phase separation in rubber-modified epoxy resins, *Polymer* 30 (1989) 1839–1844.
- [128] R.A. Pearson, A.F. Yee, Influence of particle size and particle size distribution on toughening mechanisms in rubber-modified epoxies, *J. Mater. Sci.* 26 (1991) 3828–3844.
- [129] Y. Huang, A.J. Kinloch, The role of plastic void growth in the fracture of rubber-toughened epoxy polymers, *J. Mater. Sci. Lett.* 11 (1992) 484–487.
- [130] H.J. Sue, E.I. Garcia-Meitin, D.M. Piclelman, P.C. Yang, Optimization of mode-I fracture toughness of high-performance epoxies by using designed core-shell rubber particles, in: C.K. Riew, A.J. Kinloch (Eds.), *Toughened Plastics I*, American Chemical Society, Washington, DC, 1993, pp. 259–291.
- [131] H. Li, T. Chiba, N. Higashida, Y. Yang, T. Inoue, Polymer-polymer interface in polypropylene/polyamide blends by reactive processing, *Polymer* 38 (1997) 3921–3925.
- [132] R. Holsti-Miettinen, J. Seppala, O.T. Ikkala, Effects of compatibilizers on the properties of polyamide/polypropylene blends, *Polym. Eng. Sci.* 32 13 (1992) 868–877.
- [133] R. Mulhaupt, T. Duschek, J. Rosch, Reactive blending of polypropylene/polyamide-6 in the presence of tailor-made succinic anhydride-terminated oligopropene compatibilizers, *Polym. Adv. Technol.* 4 (1993) 465–474.
- [134] J. Rosch, R. Mulhaupt, Comparison of maleic anhydride-grafted poly(propylene) with maleic anhydride-grafted polystyrene-block-poly(ethylene-co-but-1-ene)-block-polystyrene as blend compatibilizers of poly(propylene)/polyamide-6 blends *Makromol. Chem. Rapid Commun.* 14 (1993) 503–509.
- [135] J. Rosch, R. Mulhaupt, The role of core/shell-microparticle dispersions in polypropylene/polyamide-6 blends, *Polym. Bull.* 32 (1994) 697–704.
- [136] J. Rosch, R. Mulhaupt, Deformation behavior of polypropylene/polyamide blends, *J. Appl. Polym. Sci.* 56 (1995) 1607–1613.
- [137] J. Rosch, R. Mulhaupt, G.H. Michler, Controlled architectures and property synergisms of polypropylene/polyamide6 blends prepared via reactive processing, *Macromol. Symp.* 112 (1996) 141–150.
- [138] A. Gonzalez-Montiel, H. Keskkula, D.R. Paul, Impact-modified nylon 6/polypropylene blends: 2. Effect of reactive functionality on morphology and mechanical properties, *Polymer* 36 (24) (1995) 4605–4620.
- [139] A. Gonzalez-Montiel, H. Keskkula, D.R. Paul, Impact-modified nylon 6/polypropylene blends: 1. Morphology-property relationships, *Polymer* 36 (24) (1995) 4587–4603.
- [140] S. Horiuchi, N. Matchariyakult, K. Yase, T. Kitano, K. Choi, Y.M. Lee, Compatibilizing effect of a maleic anhydride functionalized SEBS triblock elastomer through a reaction induced phase formation in the blends of polyamide 6 and polycarbonate: 1. Morphology and interfacial situation, *Polymer* 37 (1996) 3065–3078.
- [141] B. Ohlsson, H. Hassander, B. Tornell, Improved compatibility between polyamide and polypropylene by the use of maleic anhydride grafted SEBS, *Polymer* 39 (1998) 6705–6714.
- [142] B. Ohlsson, Morphology and Properties of Polymer Blends -Polypropylene and a Thermoplastic Elastomer -Polypropylene/Polyamide and a Modified Thermoplastic Elastomer, Lund University Publications, Lund, Sweden, 1998.
- [143] R.J.M. Borggreve, R.J. Gaymans, Impact behavior of nylon-rubber blends: 4. Effect of the coupling agent, maleic anhydride, *Polymer* 30 (1989) 63–70.
- [144] R.J.M. Borggreve, R.J. Gaymans, J. Schuijjer, Impact behavior of nylon-rubber blends: 5. Influence of the mechanical properties of the elastomer, *Polymer* 30 (1989) 71–77.
- [145] R.J.M. Borggreve, R.J. Gaymans, H.M. Eichenwald, Impact behavior of nylon-rubber blends: 6. Influence of structure on voiding processes; toughening mechanism, *Polymer* 30 (1989) 78.
- [146] K. Dijkstra, J.T. Laak, R.J. Gaymans, Nylon-6/rubber blends: 6. Notched tensile impact testing of nylon-6/(ethylene-propylene rubber) blends, *Polymer* 35 (1994) 315–322.
- [147] K. Dijkstra, H.H. Wevers, R.J. Gaymans, Nylon-6/rubber blends: 7. Temperature-time effects in the impact behaviour of nylon/rubber blends, *Polymer* 35 (1994) 323–331.
- [148] G.M. Kim, G.H. Michler, M. Gahleitner, R. Mulhaupt, Influence of morphology on the toughening mechanisms of polypropylene modified with core-shell particles derived from thermoplastic elastomers, *Polym. Adv. Technol.* 9 (1998) 709–715.
- [149] G.M. Kim, G.H. Michler, R. Rosch, R. Mulhaupt, Micromechanical deformation processes in toughened PP/PA/SEBS-g-MA blends prepared by reactive processing, *Acta Polym.* 49 (1998) 88–95.
- [150] Z.Z. Yu, Y.C. Ou, Z.N. Qi, G.H. Hu, Toughening of nylon 6 with a maleated core-shell impact modifier, *J. Polym. Sci., Part B: Polym. Phys.* 36 (1998) 1987–1994.
- [151] A.N. Wilkinson, L. Laugel, M.L. Clemens, V.M. Harding, M. Marin, Phase structure in polypropylene/PA6/SEBS blends, *Polymer* 40 (1999) 4971–4975.
- [152] J.D. Tucker, S. Lee, R.L. Einsporn, A study of the effect of PP-g-MA and SEBS-g-MA on the mechanical and morphological properties of polypropylene/nylon 6 blends, *Polym. Eng. Sci.* 40 (2000) 2577–2589.
- [153] N. Zeng, S.L. Bai, C. G'Sell, J.M. Hiver, Y.W. Mai, Study on the microstructures and mechanical behaviour of compatibilized polypropylene/polyamide-6 blends, *Polym. Int.* 51 (2002) 1439–1447.
- [154] S.L. Bai, G.T. Wang, J.M. Hiver, C. G'Sell, Microstructures and mechanical properties of polypropylene/polyamide 6/polyethylene-octene elastomer blends, *Polymer* 45 (2004) 3063–3071.
- [155] Y. Ou, Y. Lei, X. Fang, G. Yang, Maleic anhydride grafted thermoplastic elastomer as an interfacial modifier for polypropylene/polyamide 6 blends, *J. Appl. Polym. Sci.* 91 (2004) 1806–1815.
- [156] R. Krache, D. Benachour, P. Potschke, Binary and ternary blends of polyethylene, polypropylene, and polyamide 6,6: the effect of compatibilization on the morphology and rheology, *J. Appl. Polym. Sci.* 94 (2004) 1976–1985.
- [157] H. Liu, T. Xie, Y. Zhang, Y. Ou, G. Yang, Phase morphology development in PP/PA6 blends induced by a maleated thermoplastic elastomer, *J. Polym. Sci., Part B: Polym. Phys.* 44 (2006) 1050–1061.
- [158] H. Liu, T. Xie, Y. Zhang, L.Y. Hou, G. Yang, Toughening and compatibilization of polypropylene/polyamide-6 blends with a maleated-grafted ethylene-co-vinyl acetate, *J. Appl. Polym. Sci.* 99 (2006) 3300–3307.
- [159] Z. Ke, D. Shi, J. Yin, R. Li, Y.W. Mai, Facile method of preparing supertough polyamide 6 with low rubber content, *Macromolecules* 41 (2008) 7264–7267.
- [160] D. Yan, G. Li, M. Huang, C. Wang, Tough polyamide 6/core-shell blends prepared via in situ anionic polymerization of ϵ -caprolactam by reactive extrusion, *Polym. Eng. Sci.* 53 (2013) 2705–2710.
- [161] L.F. Ma, X.F. Wei, Q. Zhang, W.K. Wang, L. Gu, W. Yang, et al., Toughening of polyamide 6 with β -nucleated thermoplastic vulcanizates based on polypropylene/ethylene-propylene-diene rubber grafted with maleic anhydride blends, *Mater. Des.* 33 (2012) 104–110.
- [162] K. Zhang, A.K. Mohanty, M. Misra, Fully biodegradable and biorenewable ternary blends from polylactide, poly(3-hydroxybutyrate-co-hydroxyvalerate) and poly(butylene succinate) with balanced properties, *ACS Appl. Mater. Interfaces* 4 (2012) 3091–3101.
- [163] K. Zhang, V. Nagarajan, M. Misra, A.K. Mohanty, Supertoughened renewable PLA reactive multiphase blends system: phase morphology and performance, *ACS Appl. Mater. Interfaces* 6 (2014) 12436–12448.
- [164] H. Rastin, M.R. Saeb, S.H. Jafari, H.A. Khonakdar, et al., Reactive compatibilization of ternary polymer blends with core-shell type morphology, *Macromol. Mater. Eng.* 300 (2014) 86–98.
- [165] Y. Wu, H. Zhang, B. Shentu, Z. Weng, Preparation of poly(phenylene oxide)/polyamide - 6 nanocomposites with high tensile strength and excellent impact performance, *Ind. Eng. Chem. Res.* 54 (2015) 5870–5875.
- [166] H. Li, X.M. Xie, Morphology development and superior mechanical properties of PP/PA6/SEBS ternary blends compatibilized by using a highly efficient multiphase compatibilizer, *Polymer* (2016), <https://doi.org/10.1016/j.polymer.2016.11.044>.
- [167] Y. Wu, H. Zhang, B. Shentu, Z. Weng, Relationship between structure and properties in high-performance PA6/SEBS-g-MA/(PPO/PS) blends: the role of PPO and PS, *J. Appl. Polym. Sci.* 134 (2017), 45281.
- [168] B. Wang, D. Wu, L. Zhu, Z. Jin, K. Zhao, High-density polyethylene based ternary blends toughened by PA6/PBT core-shell particles, *Polym.-Plast. Technol. Eng.* 56 (2017) 1908–1915.
- [169] A.M. Zolali, B.D. Favis, Compatibilization and toughening of cocontinuous ternary blends via partially wet droplets at the interface, *Polymer* 114 (2017) 277–288.
- [170] A.M. Zolali, B.D. Favis, Toughening of cocontinuous polylactide/polyethylene blends via an interfacially percolated intermediate phase, *Macromolecules* 51 10 (2018) 3572–3581.
- [171] L. Zhu, H. Wang, M. Liu, Z. Jin, K. Zhao, Effect of core-shell morphology on the mechanical properties and crystallization behavior of HDPE/HDPE-g-MA/PA6 ternary blends, *Polymers* 10 (2018) 1040.

- [172] Y. Wang, D. Mi, L. Delva, L. Cardon, J. Zhang, K. Ragaert, New approach to optimize mechanical properties of the immiscible polypropylene/poly (ethylene terephthalate) blend: effect of shish-kebab and core-shell structure, *Polymers* 10 (2018) 1094.
- [173] Y. Chen, W. Wang, D. Yuan, C. Xu, et al., Bio-based PLA/NR-PMMA/NR ternary thermoplastic vulcanizates with balanced stiffness and toughness: “soft–hard” core–shell continuous rubber phase, in situ compatibilization, and properties, *ACS Sustainable Chem. Eng.* 65 (2018) 6488–6496.
- [174] X. Sui, X.M. Xie, Creating super-tough and strong PA6/ABS blends using multi-phase compatibilizers, *Chin. Chem. Lett.* 30 (2019) 149–152.
- [175] A. Ishigami, S. Nishitsuiji, T. Kurose, H. Ito, Evaluation of toughness and failure mode of PA6/mSEBS/PS ternary blends with an oil-extended viscoelastic controlled interface, *Polymer* 177 (2019) 57–64.
- [176] K. Hu, D. Huang, H. Jiang, S. Sun, Z. Ma, et al., Toughening biosourced poly(lactic acid) and poly(3-hydroxybutyrate-co-4-hydroxybutyrate) blends by a renewable poly(epichlorohydrin-co-ethylene oxide) elastomer, *ACS Omega* 4 (2019) 19777–19786.
- [177] M. Hasanpour, M.K. Razavi Aghjeh, M. Mehrabi Mazidi, B. Afsari, Effect of morphology alteration on mechanical properties and fracture toughness of polypropylene/polyamide 6/ethylene polypropylene diene monomer graft maleic anhydride (PP/PA6/EPDM-g-MA) reactive ternary blends, *Polym. Bull.* 77 (2020) 3767–3794.
- [178] G. Wang, S. Li, Y. Feng, Y. Hu, et al., Effectively toughening polypropylene with in situ formation of core-shell starch-based particles, *Carbohydrate Polym.* 249 (2020), 116795.
- [179] M. Mehrabi Mazidi, M.K. Razavi Aghjeh, Microscopic deformation behavior and crack resistance mechanism of core-shell structures in highly-toughened PP/PA6/EPDM-g-MA ternary blends, *Macromol. Mater. Eng.* 306 (2021), 2100174.
- [180] Z. Wei, R. Wang, J. Wang, Y. Yang, Y. Liu, W. Wang, Y. Cao, Highly toughened PA6 using residue of plasticized PVB film via two-step reactive melt blending, *Polymer* 186 (2020), 122052.
- [181] Z. Wei, R. Wang, C. Zhang, J. Wang, Y. Yang, et al., Preparation and characterization of super-toughened PA6/r-PVB blends with “transplanted” multicore morphology by reactive compatibilization, *Eur. Polym. J.* 143 (2021), 110173.
- [182] Y. Chen, Y. Wang, C. Xu, Y. Wang, C. Jiang, New approach to fabricate novel fluorosilicone thermoplastic vulcanizate with crosslinked silicone rubber-core/fluororubber-shell particles dispersed in poly(vinylidene fluoride): structure and property, *Ind. Eng. Chem. Res.* 55 (2016) 1701–1709.
- [183] F. Lv, J. Fan, J. Huang, L. Cao, X. Yan, et al., Preparation of polypropylene/ethylene-propylene-diene terpolymer/nitrile rubber ternary thermoplastics vulcanizates with good mechanical properties and oil resistance by core-shell dynamic vulcanization, *Polym. Adv. Technol.* 3 (2020) 2161–2171.
- [184] T. Peng, F. Lv, Z. Gong, L. Cao, X. Yan, L. Ge, et al., Design of PP/EPDM/NBR TPVs with tunable mechanical properties via regulating the core-shell structure, *Polym. Test.* 90 (2020), 106767, <https://doi.org/10.1016/j.polymertesting.2020.106767>.
- [185] J. Rosch, Modeling the mechanical properties in polypropylene/polyamide-6 blends with core shell morphology, *Polym. Eng. Sci.* 35 (24) (1995) 1917–1922.
- [186] M. Takayanagi, S. Nemura, S. Minami, Application of equivalent model method to dynamic rheo-optical properties of crystalline polymer, *J. Polym. Sci. Part: Chimia* 5 (1964) 113–122.
- [187] C. Poel, On the rheology of concentrated dispersions, *Rheol. Acta* 1 (1958) 198–205.
- [188] S. Shtrikman Hashin, A variational approach to the theory of the elastic behaviour of multiphase materials, *J. Mech. Phys. Solid.* 11 (1963) 127–140.
- [189] R.M. Christensen, *Mechanics of Composite Materials*, Wiley, New York, 1979.
- [190] E.H. Kerner, The elastic and thermo-elastic properties of composite media, *Proc. Phys. Soc. B* 69 (1956) 808.
- [191] J. Kolarik, L. Fambri, A. Pegoretti, A. Penati, Ternary polymer blends: prediction of mechanical properties for various phase structures, *Polym. Adv. Technol.* 11 (2) (2000) 75–81.
- [192] J. Kolarik, J. Velek, G.L. Agrawal, I. Fortelny, Dynamic mechanical behavior and structure of ternary blends of polypropylene/EPDM rubber/polyethylene, *Polym. Composer* 7 (1986) 472–479.
- [193] M.R. Saeb, H.A. Khonakdar, S.H. Jafari, H. Rastin, et al., Towards quantifying interfacial adhesion in the ternary blends with matrix/shell/core-type morphology, *Polym.-Plast. Technol. Eng.* 54 (2) (2015) 223–232.
- [194] R. Khalili, S.H. Jafari, M.R. Saeb, H.A. Khonakdar, et al., Toward in situ compatibilization of polyolefin ternary blends through morphological manipulations, *Macromol. Mater. Eng.* 299 (2014) 1197–1212.
- [195] W.M. Barentsen, Ph.D. Thesis, Eindhoven University of Technology, The Netherlands, 1972.
- [196] F. Li, Y. Gao, Y. Zhang, W. Jiang, Design of high impact thermal plastic polymer composites with balanced toughness and rigidity: toughening with core-shell rubber modifier, *Polymer* 191 (2020), 122237.
- [197] X.L. Ji, J.K. Jing, W. Jiang, B.Z. Jiang, Tensile modulus of polymer nanocomposites, *Polym. Eng. Sci.* 42 (5) (2002) 983–993.
- [198] W. Jiang, L.J. An, B.Z. Jiang, Brittle-tough transition in elastomer toughening thermoplastics: effects of the elastomer stiffness, *Polymer* 42 (10) (2001) 4777–4780.
- [199] X.H. Li, Y.D. He, X.F. Li, F. An, D.Z. Yang, Z.Z. Yu, Simultaneous enhancements in toughness and electrical conductivity of polypropylene/carbon nanotube nanocomposites by incorporation of electrically inert calcium carbonate nanoparticles, *Ind. Eng. Chem. Res.* 56 (10) (2017) 2783–2788.
- [200] US Patent, 4 174 358.
- [201] GB Patent, 998 439.
- [202] J. Rosch, R. Mulhaupt, Deformation behavior of polypropylene/polyamide blends, *J. Appl. Polym. Sci.* 56 (1995) 1607–1613.
- [203] G.M. Kim, G.H. Michler, Micromechanical deformation processes in toughened and particle-filled semicrystalline polymers: Part 1. Characterization of deformation processes in dependence on phase morphology, *Polymer* 39 (23) (1998) 5689–5697.
- [204] G.M. Kim, G.H. Michler, Micromechanical deformation processes in toughened and particle filled semicrystalline polymers. Part 2: model representation for micromechanical deformation processes, *Polymer* 39 (23) (1998) 5699–5703.
- [205] S.Y. Hobbs, M.E.J. Dekkers, V.H. Watkins, Toughened blends of poly(butylene terephthalate) and BPA polycarbonate, *J. Mater. Sci.* 23 (1988) 1219–1224.
- [206] W.J. Coumans, D. Heikens, S.D. Sjoerdsma, Dilatometric investigation of deformation mechanisms in polystyrene-polyethylene block copolymer blends: correlation between Poisson ratio and adhesion, *Polymer* 21 (1980) 103–108.
- [207] M.E.J. Dekkers, S.Y. Hobbs, V.H. Watkins, Toughened blends of poly(butylene terephthalate) and BPA polycarbonate, *J. Mater. Sci.* 23 (1988) 1225–1230.
- [208] M.C. Schwarz, H. Keskkula, J.W. Barlow, D.R. Paul, Deformation behavior of HDPE/(PEC/PS)/SEBS blends, *J. Appl. Polym. Sci.* 35 (1988) 653–677.
- [209] A.F. Yee, R.A. Pearson, Toughening mechanisms in elastomer-modified epoxies, *J. Mater. Sci.* 21 (1986) 2462–2474.
- [210] M.A. Maxwell, A.F. Yee, The effect of strain rate on the toughening mechanisms of rubber-modified plastics, *Polym. Eng. Sci.* 21 (1981) 205–211.
- [211] F. Ramsteiner, G. Kanig, W. Heckmann, W. Gruber, Improved low temperature impact strength of polypropylene by modification with polyethylene, *Polymer* 24 (1983) 365–370.
- [212] E.A.A. Hartingsveldt, J.J. Aartsen, Strain-rate dependence of interfacial adhesion in particle-reinforced polymers, *Polymer* 32 (1991) 1482–1487.
- [213] C. G'Sell, J.J. Jonas, Determination of the plastic behaviour of solid polymers at a constant true strain rate, *J. Mater. Sci.* 14 (1979) 583–591.
- [214] C. G'Sell, J.M. Hiver, A. Dahoun, Experimental characterization of deformation damage in solid polymers under tension, and its interrelation with necking, *Int. J. Solid Struct.* 39 (2002) 3857–3872.
- [215] C. G'Sell, A. Dahoun, J.M. Hiver, in: *Proceedings of Conf. Materials 2002*, 2002, pp. 1–4. Tours, France, 21 – 25 October CM 03003.
- [216] S. Elkoun, C. G'Sell, L. Cangemi, Y. Meimon, Characterization of volume strain of poly(vinylidene fluoride) under creep test, *J. Polym. Sci. Part B: Polym. Phys.* Ed 40 (2002) 1754–1759.
- [217] A. Gonzalez-Montiel, H. Keskkula, D.R. Paul, Impact-modified nylon G/polypropylene blends: 3. Deformation mechanisms, *Polymer* 36 (1995) 4621–4637.
- [218] S. Bai, M. Wang, Plastic damage mechanisms of polypropylene/polyamide 6/polyethylene-octene elastomer blends under cyclic tension, *Polymer* 44 (2003) 6537–6547.
- [219] S.L. Bai, C. G'Sell, J.M. Hiver, C. Mathieu, Polypropylene/polyamide 6/polyethylene-octene elastomer blends. Part 3. Mechanisms of volume dilatation during plastic deformation under uniaxial tension, *Polymer* 46 (2005) 6437–6446.
- [220] C. G'Sell, S.L. Bai, J.M. Hiver, Polypropylene/polyamide 6/polyethylene-octene elastomer blends. Part 2: volume dilatation during plastic deformation under uniaxial tension, *Polymer* 45 (2004) 5785–5792.
- [221] H.N. Matchariyakult, K. Yase, T. Kitano, H.K. Choi, Y.M. Lee, Compatibilizing effect of a maleic anhydride functionalized SEBS triblock elastomer through a reaction induced phase formation in the blends of polyamide6 and polycarbonate— ill. Microscopic the deformation mechanisms, *Polymer* 38 (1997) 6317–6326.
- [222] S.C. Wong, Y.W. Mai, Effect of rubber functionality on microstructures and fracture toughness of impact-modified nylon 6,6/polypropylene blends: 1. Structure–property relationships, *Polymer* 40 (1999) 1553–1566.
- [223] S.C. Wong, Y.W. Mai, Effect of rubber functionality on microstructures and fracture toughness of impact-modified nylon 6,6/polypropylene blends. Part II. Toughening mechanisms, *Polymer* 41 (2000) 5471–5483.
- [224] A.N. Wilkinson, M.L. Clemens, V.M. Harding, The effects of SEBS-g-maleic anhydride reaction on the morphology and properties of polypropylene/PA6/SEBS ternary blends, *Polymer* 45 (2004) 5239–5249.
- [225] O. Moini Jazani, A. Arefazari, S.H. Jafari, M.H. Beheshty, A.A. Ghaemi, Study on the effects of SEBS-g-MAH on the phase morphology and mechanical properties of polypropylene/polycarbonate/SEBS ternary polymer blends, *J. Appl. Polym. Sci.* 121 (2011) 2680–2687.
- [226] M. Mehrabi Mazidi, M. Hasanpour, M.K. Razavi Aghjeh, The effect of rubber functionality on the phase morphology, mechanical performance and toughening mechanisms of highly toughened PP/PA6/EPDM ternary blends, *Polym. Test.* 79 (2019), 106018.
- [227] I. Jeon, M. Lee, S.W. Lee, J.Y. Jho, Morphology and mechanical properties of polyketone/polycarbonate blends compatibilized with SEBS and polyamide, *Macromol. Res.* 27 (2019) 827–832.
- [228] L. Zare, A. Arefazari, O. Moini Jazani, Study on phase structure and properties of the toughened blends of polypropylene–polybutylene terephthalate (PP/PBT), *Iran. Polym. J. (Engl. Ed.)* (2021), <https://doi.org/10.1007/s13726-021-00978-x>.
- [229] B. Ohlsson, H. Hassander, B. Tornell, Effect of the mixing procedure on the morphology and properties of compatibilized polypropylene/polyamide blends, *Polymer* 39 (20) (1998) 4715–4721.
- [230] S. Shokoohi, A. Arefazari, G. Naderi, Compatibilized Polypropylene/Ethylene–Propylene–Diene–Monomer/Polyamide6 ternary blends: effect of twin screw extruder processing parameters, *Mater. Des.* 32 (2011) 1697–1703.

- [231] S. Shokoohi, A. Arefazar, G. Naderi, Compatibilized PP/EPDM/PA6 ternary blends: extended morphological studies, *Polym. Adv. Technol.* 23 (2012) 418–424.
- [232] L. Li, B. Yin, Y. Zhou, L. Gong, M. Yang, et al., Characterization of PA6/EPDM-g-MA/HDPE ternary blends: the role of core-shell structure, *Polymer* 53 (2012) 3043–3051.
- [233] B. Yin, L. Li, Y. Zhou, L. Gong, et al., Largely improved impact toughness of PA6/EPDM-g-MA/HDPE ternary blends: the role of core-shell particles formed in melt processing on preventing micro-crack propagation, *Polymer* 54 (2013) 1938–1947.
- [234] M. Mehrabi Mazidi, M.K. Razavi Aghjeh, M. Hasanpour, Fracture resistance and micromechanical deformations in PP/PA6/EPDM ternary blends: effect of rubber functionality, dispersion state and loading conditions, *Eng. Fract. Mech.* 191 (2018) 65–81.
- [235] L. Zare, A. Arefazar, O.M. Jazani, Effects of processing conditions on the phase morphology and mechanical properties of highly toughened polypropylene/polybutylene terephthalate (PP/PBT) blends, *Iran. Polym. J. (Engl. Ed.)* 30 (2021) 1181–1200.
- [236] D. Shi, E. Liu, T. Tan, H. Shi, T. Jiang, et al., Core/shell rubber toughened polyamide 6: an effective way to get good balance between toughness and yield strength, *RSC Adv.* 3 (2013) 21563–21569.
- [237] L. Corte, L. Leibler, A model for toughening of semicrystalline polymers, *Macromolecules* 40 (2007) 5606–5611.
- [238] O.T. Ikkala, R.M. Holsti-Miettinen, J. Seppälä, Effects of compatibilization on fractionated crystallization of PA6/PP blends, *J. Appl. Polym. Sci.* 49 (1993) 1165–1174.
- [239] H.S. Moon, B.K. Ryoo, J.K. Park, Concurrent crystallization in polypropylene/nylon-6 blends using maleic anhydride grafted polypropylene as a compatibilizing agent, *J. Appl. Polym. Sci.* 32 (1994) 1427–1435.
- [240] C. Shen, Y. Zhou, R. Dou, W. Wang, B. Yin, M. Yang, Effect of the core-forming polymer on phase morphology and mechanical properties of PA6/EPDM-g-MA/HDPE ternary blends, *Polymer* (2014), <https://doi.org/10.1016/j.polymer.2014.11.027>.
- [241] R. Dou, C. Shen, B. Yin, M. Yang, B. Xie, Tailoring the impact behavior of polyamide 6 ternary blends via a hierarchical core-shell structure in situ formed in melt mixing, *RSC Adv.* 5 (2015) 14592.
- [242] M. Shang, H. Cheng, B. Shentu, Z. Weng, Preparation of PBT/POE-g-GMA/PP ternary blends with good rigidity-toughness balance by core-shell particles, *J. Appl. Polym. Sci.* 137 (2019), 48872.
- [243] Y. Zhou, W. Wang, R. Dou, L. Li, B. Yin, M. Yang, Effect of EPDM-g-MAH on the morphology and properties of PA6/EPDM/HDPE ternary blends, *Polym. Eng. Sci.* 53 (9) (2013) 1845–1855.
- [244] R. Dou, Y. Zhou, C. Shen, L. Li, B. Yin, M. Yang, Toughening of PA6/EPDM-g-MAH/HDPE ternary blends via controlling EPDM-g-MAH grafting degree: the role of core-shell particle size and shell thickness, *Polym. Bull.* 72 (2015) 177–193.
- [245] Y. Wu, H. Zhang, B. Shentu, Z. Weng, In situ formation of the “core-shell” particles and its function in toughening PA6/SEBS-g-GMA/PP blends, *Ind. Eng. Chem. Res.* 56 41 (2017) 11657–11663.
- [246] R. Dou, Y. Zhou, C. Shen, L. Li, B. Yin, M. Yang, Effect of core-shell morphology evolution on the rheology, crystallization, and mechanical properties of PA6/EPDM-g-MA/HDPE ternary blend, *J. Appl. Polym. Sci.* 129 (2013) 253–262.
- PB-g-MA*: maleic anhydride-grafted polybutadiene
PS: polystyrene
PS-g-MA: Maleic anhydride-grafted polystyrene
PBE: poly(ethylene-co-butene)
PEO-g-MA: maleic anhydride-grafted polyolefin (polyethylene-octene) elastomer
TPE-g-MA: maleic anhydride-grafted thermoplastic elastomer
DMA (DMTA): dynamic mechanical (thermal) analysis
EVA-g-MA: maleic anhydride-grafted ethylene-co-vinyl acetate
DCP: dicumyl peroxide
TPV: thermoplastic vulcanizate
EPDM-g-MAH: maleic anhydride-grafted ethylene-propylene-diene monomer
CL: ϵ -caprolactam
HDPE-g-MA: maleic anhydride-grafted high density polyethylene
EVOH: ethylene-vinyl alcohol
EVA: ethylene-vinyl acetate
PBT: poly(butylene terephthalate)
SMA: styrene-maleic anhydride copolymer
PPO: poly(phenylene oxide)
St: styrene
ABS: acrylonitrile butadiene styrene
DN-4PB: double-notch four-point bending
 d_w : weight average particle size
 d_n : number average particle size
 G_c : critical strain energy
SIS: styrene-isoprene-styrene
SEPS: styrene-ethylene-propylene-styrene
IPC: impact polypropylene copolymer
EPC: ethylene-propylene copolymer
aEPC: amorphous ethylene propylene copolymer
cEPC: crystallizable ethylene-propylene copolymer
SSC: single site catalyst
ZNC: Ziegler-Natta catalyst
MFR (MFI): melt flow rate (index)
PET: poly(ethylene terephthalate)
PLA: polylactide, polylactic acid
NR: natural rubber
PMMA: poly(methyl methacrylate)
SEBS-g-(MAH-co-St): styrene-ethylene/butylene-styrene grafted with styrene and maleic anhydride
ABS-g-(MAH-co-St): acrylonitrile butadiene styrene grafted with styrene and maleic anhydride
Jc: J-integral fracture toughness
PK: polyketone
 w_c : essential work of fracture
 βw_p : non-essential (plastic) work of fracture
 $w_{e,y}$ & $\beta w_{p,y}$: yielding component of work of fractures
 $w_{e,t}$ & $\beta w_{p,t}$: tearing component of work of fractures
PHBV: poly(3-hydroxybutyrate-co-hydroxyvalerate)
LLDPE: linear low density polyethylene
PBS: poly(butylene succinate)
EMA: poly(ethylene-methyl acrylate)
EMA-GMA: ethylene methyl acrylate-glycidyl methacrylate
PCL: poly(ϵ -caprolactone)
PEBA: poly(ether-b-amide)
TPAS: thermoplastic starch acetate
ECO: poly(epichlorohydrin-co-ethylene oxide)
P_{3,4}HB: poly(3-hydroxybutyrate-co-4-hydroxybutyrate)
SR: silicone rubber
FKM: Fluororubber
PVDF: poly(vinylidene fluoride)
NBR: acrylonitrile butadiene rubber

Abbreviations

HIPS: high impact polystyrene
PB, PBD: polybutadiene
PP-g-MA: maleic anhydride-grafted polypropylene
EBA-g-FA: fumaric acid-grafted ethylene-butylene acrylate
SEBS-g-MA: maleic anhydride-grafted styrene-ethylene/butylene-styrene
EAE-GMA: ethylene-ethyl acrylate-glycidyl methacrylate
MA, MAH: maleic anhydride
AA: acrylic acid
GMA: glycidyle methacrylate
MAA: methacrylic acid
PA: polyamide (nylon)
PA6: polyamide (nylon) 6
PA11: polyamide (nylon) 11
PA66: polyamide (nylon) 66
PA36,6: polyamide (nylon) 36,6
PA12: polyamide (nylon) 12
iPP, PP: isotactic polypropylene
SEBS: styrene-ethylene/butylene-styrene
NAMW: number-average molecular weight
NCIS: notched Charpy impact strength
NIIS: notched Izod impact strength
EPM: ethylene-propylene rubber
EPM-g-MA: maleic anhydride-grafted ethylene-polypropylene rubber
EPDM: ethylene-propylene-diene monomer rubber
EPR: ethylene-propylene rubber
EP: ethylene-propylene copolymer
DBTT: ductile brittle transition temperature
TEM: transmission electron microscopy
HVEM: high voltage electron microscopy
PC: polycarbonate
LDPE: low density polyethylene



Majid Mehrabi Mazidi earned his Ph.D. in polymer engineering and science at Sahand University of Technology in 2016. Majid graduated with a Master's degree from Sahand University of Technology in 2010. Currently he works as a researcher and consultant with both industry and university in the field of polymeric materials, property modification, product development, recycling and upcycling. Majid's research interests are polymer structure and properties. His primary focus is on the processing-microstructure-micromechanics-macroscopic behavior relationships in bio-based and petro-based polymers as well as multicomponent polymeric systems such as alloys, blends, composites and nanocomposites. He has published over 30 peer reviewed journal articles on subjects in polymer blends and composites science and engineering.



Alessandro Pegoretti graduated in Materials Engineering at the University of Trento, Italy, in 1988. After a professional experience in industry, he joined the University of Trento as an Assistant Professor in 1992. Between 1995 and 1997 he has been Visiting Research Scientist at the Institute of Materials Science of the University of Connecticut (USA). Between 1997 and 2001 he has been Aggregate Professor at the University of Modena (Italy) and then Associate Professor and Full Professor of Materials Science and Technology at the University of Trento (Italy) in 2002 and 2012, respectively. From 2012 to 2018 he has been the Director of the Doctoral School in Materials, Mechatronics and System Engineering of the University of Trento and since 2021 he is the Head of the Department of Industrial Engineering of the University of Trento.

He has authored over 290 refereed publications, 2 books, 15 book chapters and 3 patents on various subjects in polymer and composites science and engineering. Currently, he is the editor-in-chief of polymer composites journal.



Mir Karim Razavi Aghjeh is professor of Polymer Science and Engineering at the Sahand University of Technology. He received his Ph.D. in polymer science and engineering from the Amirkabir University of Technology, Tehran, Iran in 2005 and joined the Faculty of Polymer Engineering, in Sahand University of Technology. He currently leads a research group involved in Rheology, Morphology, Mechanical Properties and Fracture behavior of Multicomponent Polymeric Systems. His current research topics include, structure-properties relationship in toughened bio-based and petro-based plastics, synthesis of vitrimers and vitrimerization of crosslinked polymeric materials and MXene-based polymeric strain sensors. He is the author or coauthor of more than 60 papers in international refereed journals and more than 50 conference contributions and has completed more than 10 industrially funded research projects. He is now the editor-in-chief of a newly established international journal of "Surface and Interface Science and Engineering (SISE)".